Universidade do Minho
Escola de Engenharia

Pedro António Veiga Rodrigues

Development of Polymeric Systems for Safety Footwear

October 2020

Development of Polymeric Systems for Safety Footwear
Pedro António Veiga Rodrigues

UMinho | 2020

Universidade do Minho
Escola de Engenharia

Pedro António Veiga Rodrigues

Development of Polymeric Systems for Safety Footwear

Doctoral Thesis in

Science and Engineering of Polymers and Composites

Work accomplished under the supervision of

Professor Ana Vera Machado

October 2020

DECLARAÇÃO

DIREITOS DE AUTOR E CONDIÇÕES DE UTILIZAÇÃO DO TRABALHO POR TERCEIROS

Este é um trabalho académico que pode ser utilizado por terceiros desde que respeitadas as regras e boas práticas internacionalmente aceites, no que concerne aos direitos de autor e direitos conexos.
Assim, o presente trabalho pode ser utilizado nos termos previstos na licença abaixo indicada.
Caso o utilizador necessite de permissão para poder fazer um uso do trabalho em condições não previstas no licenciamento indicado, deverá contactar o autor, através do RepositóriUM da Universidade do Minho.

Licença concedida aos utilizadores deste trabalho

Atribuição-NãoComercial-SemDerivações
CC BY-NC-ND
https://creativecommons.org/licenses/by-nc-nd/4.0/

ACKNOWLEDGEMENTS

Este documento reflete o fim de um ciclo de aprendizagem, não só a nível académico, mas fundamentalmente a nível de crescimento pessoal, decorrido ao longo de 3 anos na Universidade do Minho. Dedico esta página a todas as pessoas e instituições que, de alguma forma, me ajudaram a seguir em frente e que nunca deixaram de acreditar em mim, contribuindo para o sucesso deste trabalho.

À minha Orientadora, Professora Doutora Ana Vera Machado, o meu mais sincero agradecimento por aceitar ser minha orientadora e por nunca ter duvidado das minhas capacidades, pelo acompanhamento e aconselhamento prestado, e por me ter ajudado a dar o salto nos momentos mais difíceis. Ao Professor Doutor João Miguel Costa Nóbrega, pela disponibilidade, paciência e conhecimentos partilhados na área da modelação e simulação computacional. Ao projeto IMPULSE - Polímeros e Compósitos: Drivers da inovação tecnológica e da competitividade industrial (NORTE-08-5369–FSE-000034), cofinanciado pelo Programa Operacional Regional do NORTE (NORTE 2020) através do Portugal 2020 e do Fundo Social Europeu (FSE), pela atribuição da bolsa de doutoramento que permitiu iniciar este projeto.

A todos os meus colegas e amigos que trabalharam comigo no Departamento de Engenharia de Polímeros – Universidade do Minho, um sincero agradecimento: à Ana Soares, ao Arsénio Sá, ao Bruno Ramoa, à Cidália Castro, à Cláudia Peixoto, à Dalila Vieira, ao Duarte Moura, ao Hector Nunes, à Isabel Moura, ao João Paulo, à Liliana Melro, ao Mohammadreza Aali, ao Nuno Ramos e ao Ricardo Costa. A vossa presença, incentivo, compreensão e apoio foram essenciais para a realização deste projeto.

Aos meus amigos de sempre, que sempre estiveram lá para me apoiar, para me ouvir, para me aconselhar e para me dar força a nunca deixar de seguir em frente, um profundo agradecimento.

Por fim, e não menos importante, um especial agradecimento à minha família que sempre esteve presente desde o início, que acompanhou as minhas dificuldades, as minhas vitórias, as minhas conquistas e, sobretudo, toda a caminhada nesta etapa da minha vida..: aos meus pais (José e Maria), irmãos (Sandra e Sérgio), ao meu afilhado (Guilherme) e à sua mãe (Fátima), à minha avó (Rosa), à restante família, ao Benny, ao Scout e ao Kiko. Sempre que precisei, vocês estavam lá...

A todos, o meu sincero obrigado!

STATEMENT OF INTEGRITY

I hereby declare having conducted this academic work with integrity. I confirm that I have not used plagiarism or any form of undue use of information or falsification of results along the process leading to its elaboration.

I further declare that I have fully acknowledged the Code of Ethical Conduct of the University of Minho.

University of Minho, 31st October 2020

Pedro António Veiga Rodrigues

ABSTRACT

Development of Polymeric Systems for Safety Footwear

In the recent years, the Portuguese Footwear industry seeks to affirm itself in a global competitive market, with high technical and innovative solutions able to offer high quality products. The Safety footwear market deserves special attention since the manufactured products are used to protect worker's feet from potential hazards. The toe cap is one of the key components in safety shoes and one of the main contributors to the overall weight since most safety shoes are built with steel toe caps due to their high mechanical performance. Efforts have been made to replace these toe caps by non-metallic solutions, because they are lighter, provide better thermal and electrical insolation, and are insensitive to magnetic fields. However, most of these toe caps require higher volume concept to achieve a comparable performance to their metallic counterparts, causing aesthetic and design problems.

This thesis aimed to foster new solutions based on the enhancement of polycarbonate (PC) mechanical properties and to establish a numerical methodology based on the OpenFOAM®. To this end, PC blends and PC (nano)composites were prepared by melt blending, with ABS, ABS-*g*MA, SEBS-*g*MA, COPE, nanoclay and natural fibers, and characterized in terms of morphology, topology, structure, tensile and impact behavior of each system. The results demonstrate that ductile to brittle transition mode is highly dependent on the polymeric system and that PC suffers extensive thermo-oxidative degradation during processing, which can be delayed by blending with the elastomeric materials. SEBS-*g*MA and COPE can improve toughness, while nanoclay and natural fiber slightly increases the elastic modulus, and ABS and ABS-*g*MA only show a marginal increase on both. For the numerical studies, a commercially available toe cap was characterized, and the corresponding tensile behavior was obtained to feed the numerical simulations. A toolbox developed within the OpenFOAM® for solid mechanics and fluid-solid interaction was used to simulate the EN 12568 tests (15 kN of compression force and 200 J of impact) required for safety footwear product approval, showing excellent agreement with the experimental data, with a maximum error of 6.8%.

Keywords: Elastomers, OpenFOAM, Polycarbonate, Safety footwear, Toe cap.

RESUMO

Desenvolvimento De Sistemas Poliméricos Para Calçado De Segurança

Nos últimos anos, a indústria Portuguesa do Calçado tenta afirmar-se num mercado global muito competitivo apresentando soluções inovadoras e de elevada qualidade. A área do calçado de segurança merece especial atenção devido à sua importância na fabricação de produtos de proteção para os pés dos trabalhadores. A biqueira é um dos componentes mais importantes nesta tipologia de calçado, sendo um dos maiores contribuidores para o peso, uma vez as biqueiras de aço são as mais utilizadas devido à sua elevada resistência mecânica. Vários esforços têm sido direcionados na sua substituição por materiais não-metálicos, porque são mais leves, são térmica e eletricamente isolantes, e não apresentam resposta magnética. Por outro lado, esta alternativa cria problemas estéticos e de design uma vez que requer uma maior espessura maior para obter a resistência comparável à das biqueiras metálicas.

Esta tese teve como objetivo apresentar novas soluções que impulsionem o desenvolvimento de novas biqueiras não-metálicas, através de um estudo sobre a manipulação das propriedades do policarbonato (PC) e do desenvolvendo de uma metodologia numérica baseada em OpenFOAM® que permita ajudar na conceção de novos designs. Desta forma, misturas de PC e (nano)compósitos de PC foram preparados por mistura no fundido, com ABS, ABS-*g*-MA, SEBS-*g*-MA, COPE, nanoargila e fibras naturais, e procedeu-se à caracterização da sua morfologia, topologia, estrutura e comportamento à tração e ao impacto. Os resultados mostraram que o modo de transição dúctil-frágil é dependente do sistema polimérico, e que o PC sofre extensa degradação termo-oxidativa durante o seu processamento, que pode ser amenizado com materiais elastoméricos. O SEBS-*g*-MA e o COPE promoveram tenacidade, a nanoargila e as fibras naturais aumentaram o módulo de elasticidade, e o ABS e o ABS-*g*-MA tiveram um impacto ligeiro em ambas as propriedades. Relativamente aos estudos numéricos, uma biqueira comercial foi caracterizada e a respetiva curva tensão-deformação do material foi usada para alimentar as simulações numéricas. A ferramenta numérica baseada em OpenFOAM® para mecânica de sólidos e interação de sólidos-fluidos foi utilizada para simular os ensaios da norma EN 12568 (15 kN de força de compressão e 200 J de energia de impacto) que são requeridos na validação de biqueiras para calçado de segurança, mostrando uma excelente concordância com os dados experimentais com um máximo de erro de 6.8%.

PALAVRAS-CHAVE: Biqueira, Calçado de segurança, Elastómeros, OpenFOAM, Policarbonato.

TABLE OF CONTENTS

LIST OF FIGURES

LIST OF TABLES

List of Abbreviations and Symbols

Abbreviations

ABS	Acrylonitrile-Butadiene-Styrene
ABS-*g*MA	Acrylonitrile-Butadiene-Styrene grafted with Maleic Anhydride
C15A	Cloisite 15A
COPE	Thermoplastic Copolyether Ester Elastomer
DCoF	Dynamic Coefficient of Friction
DCP	Dicumyl Peroxide
DMA	Dynamic Mechanical Analysis
DSC	Differential Scanning Calorimetry
EG	Expandable Graphite
EMA	Ethylene-methyl Acrylate Copolymer
FSI	Fluid-solid interaction
FT-IR	Fourier transform infrared spectroscopy
GD	Grafting Degree
GMA	Glycidyl Methacrylate
IR	Infrared
MA	Maleic Anhydride
MFI	Melt Flow Index
MVR	Melt Volume Rate
Na+-MMT	Sodium Montmorillonite
NCW	Natural Cotton Waste
OM	Optical Microscopy
PB	Polybutadiene
PC	Polycarbonate
PC_{Lr}	Polycarbonate Lexan 103r
PC_{Lux}	Polycarbonate Lexan LUX2180T
PC_{M}	Polycarbonate Makrolon ET3137
PPE	Personal Protective Equipment
PU	Polyurethane
R&D	Research and Development

RH	Relative Humidity
SBS	Styrene-Butadiene-Styrene
SCoF	Static Coefficient of Friction
SEBS	Styrene-Ethylene-Butylene-Styrene
SEBS-*g*-MA	Styrene-Ethylene-Butylene-Styrene grafted with Maleic Anhydride
SEM	Scanning Electron Microscopy
St	Styrene
TPU	Thermoplastic Polyurethane
U.S.A.	United States of America

Symbols

%	Percentage
$\overline{T_m}$	Average Melt Temperature
D_{yy}	Displacement along the y-axis
E'	Storage Modulus
E_C	Energy of Fracture
a_{CN}	Impact Strength
b_N	Width at the Impact Zone
l_0	Initial Distance
$\boldsymbol{D_{y\,plate}}$	Plate Displacement along the y-axis
$\boldsymbol{F_{y\,plate}}$	Plate Force along the y-axis
$\boldsymbol{U_{y\,striker}}$	Striker Velocity
$\boldsymbol{h_{clay}}$	Clay height
$\boldsymbol{h_i}$	Initial Inner High of the Toe Cap
ε_{Eng}	Engineering Strain
ε_r	Strain at Break
ε_y	Strain at Yield
σ_{Eng}	Engineering Stress
σ_{Eq}	Von Mises Stress
σ_r	Stress at Break
σ_y	Stress at Yield

$\boldsymbol{\Delta h_i}$	Toe Cap Clearance Variation
μm	Micrometer (1 x 10^{-6} m)
A_0	Initial Area
–C = O	Carbonyl Group
–C ≡ N	Nitrile Group
C = C	Carbon Double Bond
C–H	Carbon – Hydrogen bond
cm^{-1}	Wavenumber for IR analysis
cm^3	Cubic Centimeter
cm^3/10 min	Cubic centimeter (volume) per 10 minutes
C–O–C	Ether Group
F	Force
g/cm^3	Gram per cubic centimeter
GPa	Gigapascal
h	Hour
h	Specimen Thickness
Hz	Hertz (Frequency)
J	Joules
kg	Kilogram
Kg/h	Kilogram per Hour
kg/m^3	Kilogram per cubic meter
kJ/m^2	Kilojoules per square meter
kN	Kilonewtons
kV	Kilovolts
min	Minute
mm	Millimeter
mm/min	Millimeters per Minute
mm/s	Millimeter per second
mm^3	Cubic Millimeter
MoS_2	Molybdenum Disulfide
MPa	Megapascal
N	Newton

N/mm	Newton per Millimeter
NaLS	Sodium Lauryl Sulfate
nm	Nanometer (1 x 10^{-9} m)
°C	Celsius Degree
°C/min	Celsius Degree per minute
–OH	Hydroxyl Group
rpm	Rotations per minute
SiC	Silicon Carbide
SiO_2	Silicon Dioxide
T_g	Glass Transition Temperature
TiO_2	Titanium Dioxide
t_{mixing}	Mixing time
w/w	Weight per Weight
wt.%	Weight Percentage
ZrO_2	Zirconium Dioxide or Zirconia
E	Modulus of Elasticity or Elastic Modulus
U	Toughness
dl	Displacement
$tan\ \delta$	Damping Factor
ε	Elongation
$\sigma - \varepsilon$	Stress – Strain Curve
σ	Tensile strength or Stress

CHAPTER 1

1 GENERAL INTRODUCTION AND THESIS OVERVIEW

This chapter presents a brief introduction to the thesis theme and an explanation about the motivation and main objectives of the present work. After, the thesis structure outline is presented.

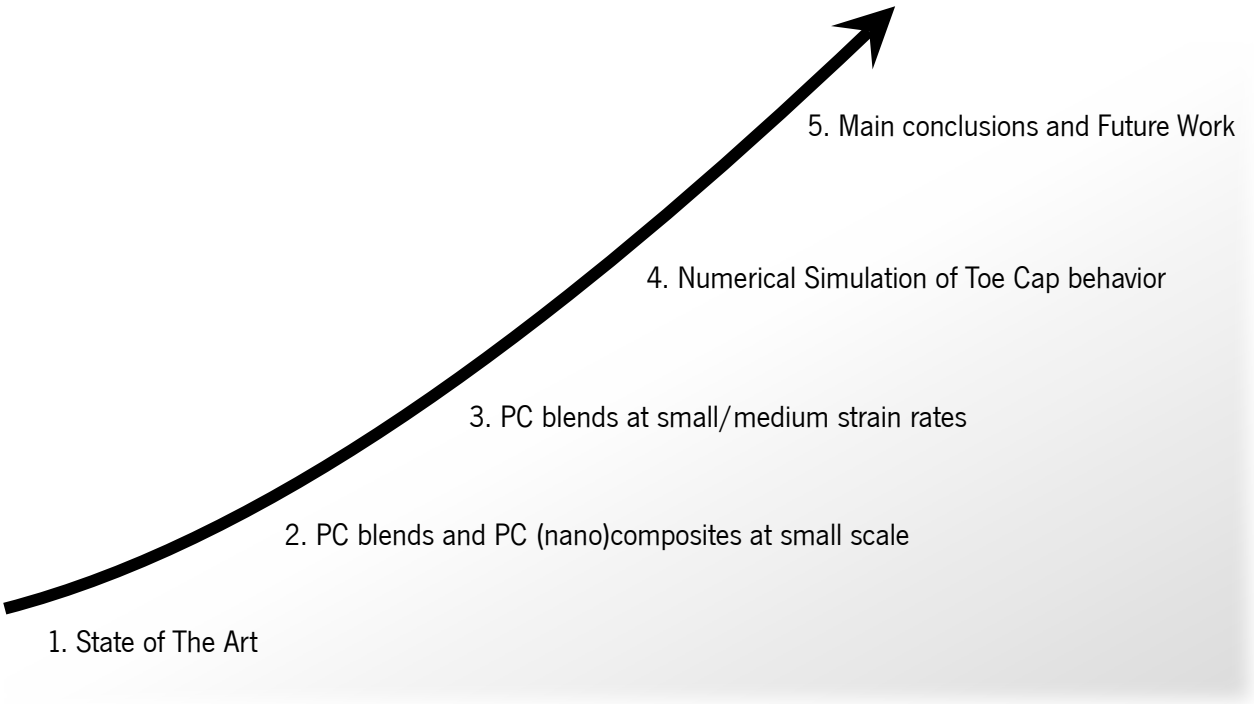

1.1 Motivation and Objectives

The Portuguese Footwear industry, one of the most important internationalized sectors of the Portuguese economy, has been investing in research and development in order to maintain its reference in the footwear industry. Safety footwear is a particular sector of this industry, it fits into personal protective equipment (PPE) category and is intended to protect the user's feet from hazards (e.g., falling objects) and prevent potential accidents (e.g., slippery floor). Safety shoes for safety footwear are built with special parts with higher performance, such as toe caps, shanks, overshoe protectors, penetration-resistant insert and anti-slip outsoles. Steel toe caps are one of the most important and used components in this type of footwear, they are mainly made of steel which confers superior mechanical resistance, but the higher density of steel contributes severely to the overall weight of the shoe. Also, they present a higher risk of electrocution and thermal issues due to their ability to conduct electricity and heat, and the magnetic sensitivity is also seen as an issue in security checkpoints like airports. Several studies have shown that the extra weight increases fatigue and discomfort to the wearer, and the temperature increase inside the shoes promotes sweating and biological proliferation (fungal infection), leading most of the users to neglect the PPEs in an industrial context, increasing the probability of an accident to happen. Non-metallic toe caps, such as toe caps made of thermoplastic or thermoset materials, have been used as an alternative to solve some of the issues of their steel counterparts, since they are lighter, prevents the risk of electrocution, are thermally insulator and does not present magnetic behavior. However, polymeric toe caps require larger volumes to achieve a comparable mechanical performance of metallic toe caps, which negatively impacting the overall aesthetics and design of the shoe. Regarding manufacturing and overall cost, steel toe caps are cheaper than non-metallic solutions due to higher production rate. Thermoplastic toe caps can be produced through injection molding with a lower cost, while thermoset toe caps require higher labor work, increasing the final cost. The latter is mechanically more resistant than thermoplastic materials, allowing the design of thinner solution.

In the last years, the interest in replacing steel toe caps with non-metallic ones have motivate efforts to develop new solutions. Thus, two investigation routes are presented in this work: a) material development, where ways to tailor polycarbonate properties by blending with elastomeric materials and compounding with additives are study, and b) new design methodologies, assessing the mechanical performance of toe caps through computational modelling. The knowledge build up with this work can be used to enhance the mechanical performance of thermoplastic toe caps.

1.2 Thesis Outline

This thesis is organized in six chapters:

Chapter 1 makes an overview about the main topic of this thesis, explaining the motivation and the main objectives.

Chapter 2 compiles a review regarding the state of the art on safety footwear, focusing on the historical development of toe caps and outsoles for safety shoes, their materials requirements to meet the European standards.

Chapter 3 presents the development of polycarbonate (PC) systems blended with elastomeric materials and additives prepared at a small scale on a Haake batch mixer. A systematic study was performed in order to evaluate the mechanical properties of PC blends with maleic anhydride (MA) grafted onto acrylonitrile-butadiene-styrene (ABS-*g*-MA) and styrene-ethylene-butylene-styrene rubber (SEBS-*g*-MA). Compositions with nanoclay and natural cotton waste were also studied.

Chapter 4 describes the fracture mode of PC systems blended with elastomeric materials at small to medium strain rate conditions. Blended PC with ABS, ABS-*g*-MA, SEBS-*g*-MA and thermoplastic copolyether ester elastomer (COPE) were prepared by melt blending on a twin-screw extruder. Quasi-static and high-speed tensile tests and impact were used to evaluate the mechanical properties, dynamic mechanical analysis and differential scanning analysis for thermomechanical behavior and glass transition temperature, electronic microscopy for blend morphology, and optical microscopy for fracture surface.

Chapter 5 depicts the development of a numerical methodology to simulate the mechanical tests (compression and impact) used to validate toe caps under the European standards, in order to further support the design of toe caps. For this purpose, the *solids4Foam* toolbox, a free and open-source code developed in the framework of the OpenFOAM® computational library, was used to assess stress distribution and deformation along the toe cap and compared with experimental results to validate the tool.

Chapter 6 gathers the general conclusions of this thesis and presents suggestions for future work.

Table 1.1: Thesis outline chart.

1	• General introduction and thesis overview
2	• A review on current issues of the safety footwear industry: toe cap and outsole, materials and requirements
3	• Structure-properties relationship for tailoring polycarbonate
4	• Tailoring the mechanical behavior of elastomeric PC blends at small and medium strain rates
5	• Assess the compressive and impact behavior of polymeric safety toe caps through computational modelling
6	• Conclusions and future work

CHAPTER 2

2 A REVIEW ON CURRENT ISSUES OF THE SAFETY FOOTWEAR INDUSTRY: TOE CAP AND OUTSOLE, MATERIALS AND REQUIREMENTS

Abstract: The use of personal protective equipment (PPE) is nowadays a mandatory policy at every company that wants to compete in today's manufacturing world. These are designed to protect its wearer from hazards and injuries. Footwear PPE is used to minimize injuries and thus loss of working days, from it toe caps and soles can be identified as key components for improving the safety of user's feet and to prevent potential accidents. This paper makes a review of the state-of-the-art regarding the evolution of toe caps and outsoles with focus on material development.

Keywords: safety, toe caps, outsoles, footwear

Submitted to Journal of Safety Science

2.1 Introduction

The footwear market is a key manufacturing sector within the European Union and has been rising throughout the last decades. This sector distinguishes itself by constant innovation in design, use of new materials and manufacturing technics, despite still being an intensive labor industry comprised mainly by small and medium companies with 10-15 workers [1]. However, in recent decades a lot of improvements in manufacturing occurred. Ames reported that in 2000 there was an estimated acquisition rate of 1.8 pairs of shoes per person per year worldwide. In 2004, he found information regarding a machine that was able to produce 10,000 pairs of shoes by one worker in a regular 8h shift [2]. This increase in production rate helped the Western European shoe market to directly compete with Asian manufactures, lowering the overall production cost.

In 2017, in a report by Statista, it was estimated that the footwear market was worth more than 400 billion US dollars and was projected to reach 513 billion by 2023 [3] (Figure 2.1).

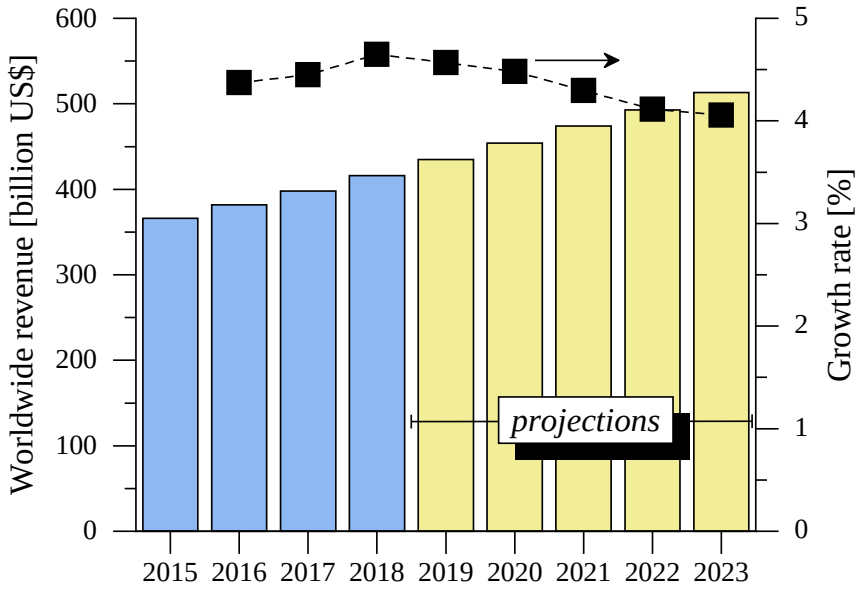

Figure 2.1: Revenue of the footwear market up to 2018 and estimation of growth until 2023 [3].

Regarding consumption, 60 % of the world's footwear consumption is located in just 10 Countries, Figure 2.2. Asia's supremacy on the international scene is based on an aggressive commercial strategy reflected by their low exportation prices, under 6 euros, whereas in Europe the average exportation price is 21.57 euros. However, in Europe there are wide variations among countries, for example Italy has the highest price (40 euros per pair) and Portugal comes in second place with an average price of 23.6 euros [4].

Despite the higher labor costs in Europe, the main difference is the quality, innovation, and personalization of the footwear.

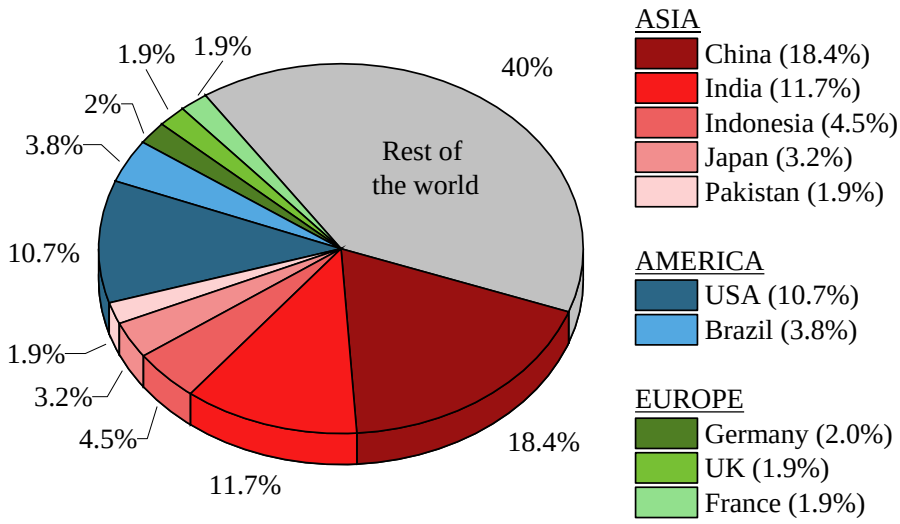

Figure 2.2: World's top 10 consumer countries regarding footwear share in 2018 [5].

Portuguese footwear industry is considered one of the most important internationalized sectors of the Portuguese economy. It has been growing steadily over the last decade, reaching a total of over 2,500 million euros in 2016. From this, about 1% is due to safety footwear, mainly toe cap and outsoles. This type of footwear fits into the category of personal protective equipment (PPE) and is intended to protect the user's feet from hazards (e.g., falling objects, slipping floor) and prevent potential accidents, thus the manufacturing of these products requires some high-performance materials capable of withstanding the most adverse and unpredictable situations. In recent years, this industry has been making efforts to claim itself in the world market with its outstanding quality, performance and unique product design [6]. To achieve this goal, the Portuguese footwear industry started to invest in research and technological development of new materials, products and processes that lead to revolutionary solutions, resulting in high value-added products [7]. These products are intended to compete directly with the crescent growing market all over the world.

Toe caps are reinforcements placed at the front of the footwear and one of the most important components in safety footwear and can represent a significant part of the total weight of the shoe. Occupations like military, construction workers, industrial workers, and others, where a potential for injury due to falling objects exists must use this safety footwear. Their purpose is to protect the wearer's toes from impact and compression loadings, which requires high mechanical resistance, depict at international

standards. Aside standard requirements, part weight, design/aesthetics, and electric/magnetic behavior are of extreme importance to its overall performance. Also, breathability is another concern that affects all toe caps due to microclimate footwear effect. Even though most safety shoes have steel toe caps, in the last decades, several attempts have been made to replace this material by a lighter one. Polymeric materials, with their specific strength, density, non-conductive and non-magnetic behavior have been at the forefront. Nevertheless, polymeric toe caps require a higher volume than their metallic counterparts, which can result in undesirable aesthetic and design adaptations.

Another crucial component in safety footwear able to prevent the user from falling due to slipping phenomenon or floor temperature is the outsole. Firefighters and miners are examples of critical occupations due to the unpredictable and rapidly changing environment. In the case of firefighter's, the outsole must have heat and flame resistant. For this purpose, vulcanized rubber is the material of excellence for outsoles but has disadvantages, like increase of the production price and recycling of the waste. In the last decade, nanomaterials have shown their great potential in enhancing the properties of polymers. Their high aspect ratio leads to a higher degree of interaction between filler and matrix, which requires only the use of small amounts of nanoparticles, bringing benefits to the final product cost and with negligible environmental impact.

This review paper intends to provide further insight into the safety footwear industry. It starts with historical development, followed by the description of the main components required in this type of footwear, namely toe caps and outsoles, their requirements and materials.

2.2 Safety Footwear

According to Eurostat, from 2010 until 2017 the number of accidents within the European Union has decreased from 2011 to 2012 and then increased reaching a value of 3,345,901 in 2017, Figure 2.3. In fact, some of these accidents could have been avoided or diminished with the proper use of PPE. Studies point out that unawareness and aversion to the usage of safety measures are some of the main reasons to disregard the use of PPE by workers. In fact, many industrial workers do not have a proper instruction training from their employer regarding its use. Also, PPE clothing can be heavy, tend to restrict the body motion and uncomfortable, leading workers to incorrect usage or the neglection of PPE [8–10].

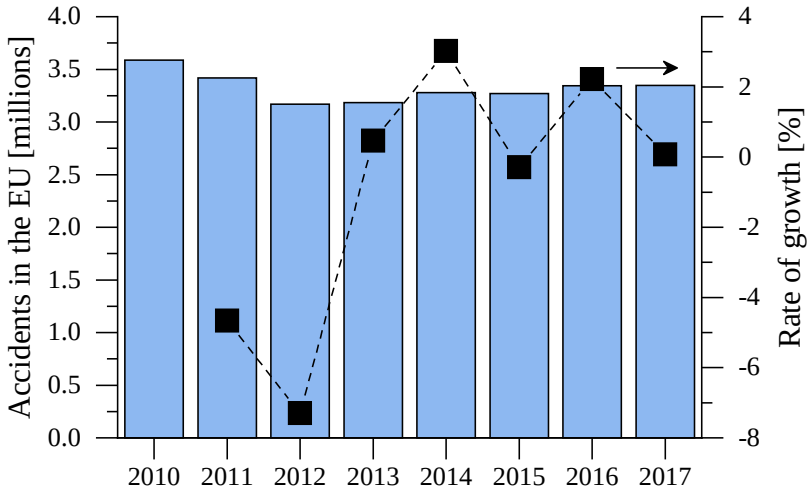

Figure 2.3: Total number of accidents in the EU between 2010 until 2017 [11].

From these, 28.4% of injuries were located in the lower extremities (encompassing hip, leg, ankle, foot, and toe), the second-highest value when considering the injuries by body part. The occupation related to the industrial sector (B-H as subdivided by Eurostat) has the highest percentage of lower extremity injuries, Figure 2.4. These numbers can be seen as a problem since an injury can result in loss of work time hence reducing the productivity of a company or worker incapacity. Therefore, personal protective equipment is important to help minimize the number of injuries at the workplace.

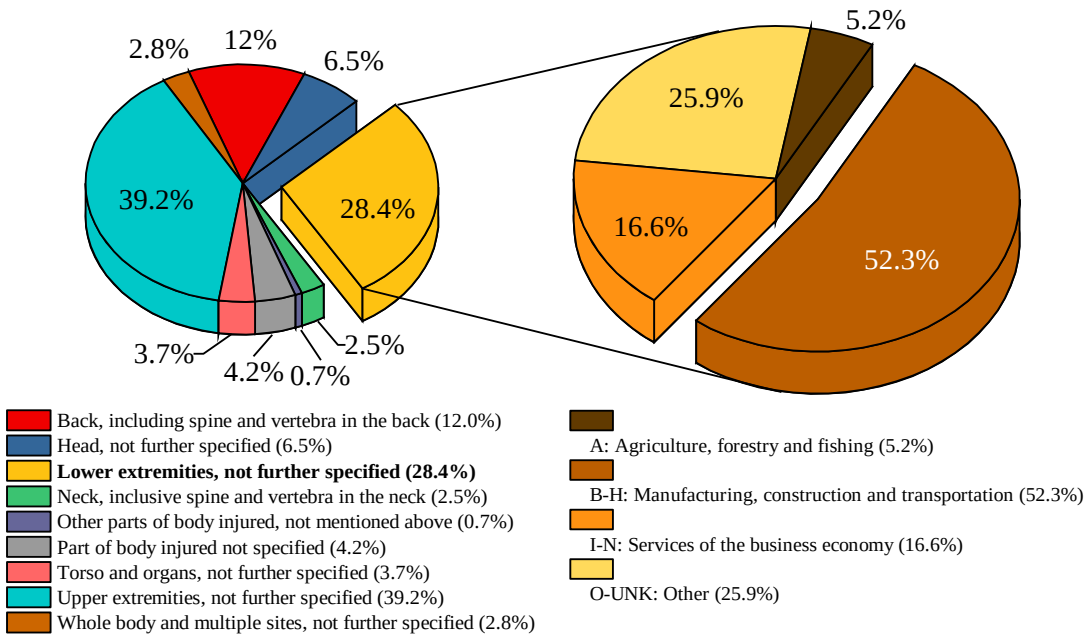

Figure 2.4: Percentage of accidents related to the part of body injured (left), and distribution of lower extremities injuries by occupation (right), in 2017 [11].

A particular sector of the footwear industry is related to safety footwear. This sector has become very important mostly due to regulations imposed by global economies such as China, the United States of

America, and the European Union. These regulations are intended to increase the protection and safety of workers from hazards that can occur at their workplace, and, therefore, decrease the number of accidents. Historically, in the 17th century there are records of various European workers using safety shoes called "sabots" which were made from wood. However, a generalized concern was not obtained until the beginning of the 20th century. In fact, the replacement of workers used to be cheaper and faster than the implementation of security measures (e.g., personal protective equipment) [12]. The shoes used were mainly made of wood or leather and did not provide any kind of protection. It was only in the 1920s and 1930s that the first prototypes of safety shoes started to emerge [13–16]. These patented devices were intended to protect the foot from falling objects and served as precursors for the modern toe caps that exist today, Figure 2.5.

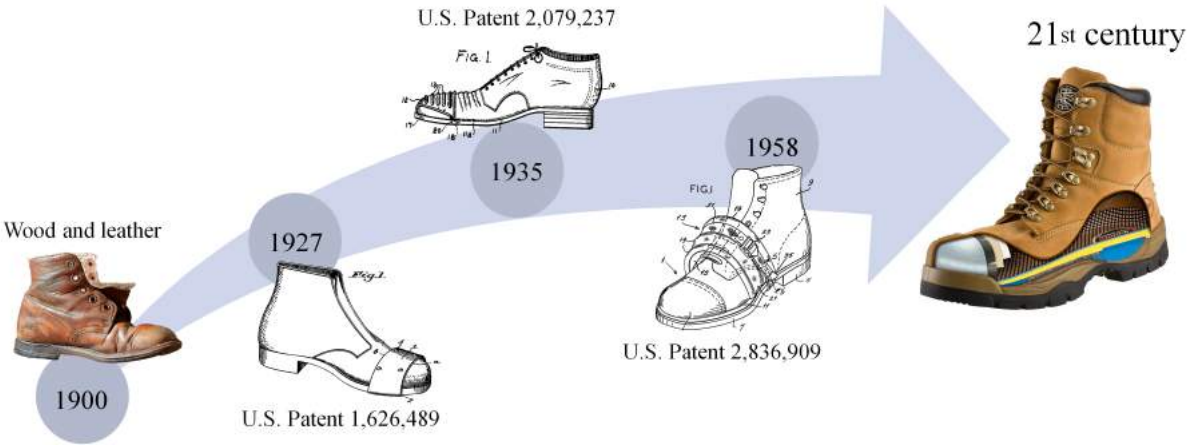

Figure 2.5: Evolution of protective footwear over the years [13–17].

The traditional safety shoes were heavy and bulky, this extra weight and inflexible design leads to a significant increase in oxygen consumption and could be easily correlated to discomfort and fatigue of the worker, resulting in less productivity [18, 19]. Therefore, it was very important to develop lighter solutions capable of providing protection and comfort to the user. Shoe attributes, such as protection, low weight, comfort, durability and design are important factors for users [20].

The footwear used for safety is intended to protect the user from potential and possible hazards, such as perforations, cuts and punctures, electrostatic buildup, metal and chemical splash, abrasion, exposure to thermal factors, falling objects, compression loadings, wet and slippery surfaces [21–24]. Unfortunately, a very significant percentage of workers still reject and neglect the use of this type of equipment. Some reasons that explain this behavior were presented by Goldcher and Acker and can be summed as: uncomfortable footwear; muscle pain and fatigue due to excessive weight; inflexible footwear

(due to base reinforcement); unsuited models for some feet morphology (could lead to internal injuries); lack of aesthetics and ergonomics; and inadequate ventilation (promoting sweating, maceration and fungal infection) [25]. Therefore, it became essential to develop solutions able to avoid these problems and make this kind of footwear more appealing and more user-friendly.

The construction of a protective shoe is very similar to an ordinary shoe (upper and sole), with the difference of technical parts included e.g., toe cap, penetration-resistant inserts and materials with higher performance designed to protect the user. Figure 2.6 shows some basic features of a commercial safety shoe. The upper comprises the external part that covers all the foot (toes, top, back and sides) except the bottom part, and is attached to the insole. Usually, an insock is inserted on top of the insole to provide better foot comfort. The toe cap is placed at the front of the shoe under the upper, fixed within the midsole and covered inside with some fabric to accommodate the user toes. The outsole is in direct contact with the floor, and therefore responsible for gripping, abrasion, flex and chemical resistance of the shoe. The midsole creates a bond between the outsole and the insole and must provide shock absorption and appropriate cushioning. A penetration-resistant insert is used at the interface midsole/insole to prevent sharp objects to injure the user foot [26].

Figure 2.6: Typical construction of a safety footwear and its components.

The ISO standards distinguish three different kinds of protective shoes: safety shoes, protection shoes and occupational shoes [27–29]. The main difference between the three types relies on the toe cap protection. Also, safety footwear is separated into two different classes: class I includes footwear with

upper "made from leather and other materials, excluding all-rubber or all-polymeric footwear"; and class II uppers made of all-rubber (i.e. entirely vulcanized) or all-polymeric (i.e. entirely molded) materials. Professional safety footwear is marked regarding its category (SB / PB / OB) and their basic properties, such as antistatic, penetration resistance, water resistance, where an extra designation is added (1 - 3 for class I, and to 4 - 5 for class II). Table 2.1, shows the difference between each type of safety footwear requirements and category. Both safety and protective footwear must comprise a 200 J / 15 kN and 100 J / 10 kN impact/compression resistance, respectively, while occupational category does not require the attachment of a toe cap.

Table 2.1: Categories of safety footwear: class I represents "footwear made from leather and other materials, excluding all-rubber or all-polymeric footwear"; and class II – "All-rubber (i.e. entirely vulcanized) or all-polymeric (i.e. entirely molded) footwear" [27–29].

	Category of footwear			**Class / or //**	**Requirement**
	Safety **SB** ISO 20345	Protective **PB** ISO 20346	Occupational **OB** ISO 20347		
Toe cap	200 J	100 J	-	/ or //	Impact resistance
	15 kN	10 kN	-		Compression resistance
Additional requirements	S1	P1	O1	/	Closed seat region Antistatic properties Energy absorption of seat region Resistance to fuel oil (only for SB/PB)
	S2	P2	O2	/	*As S1 / P1 / O1, plus:* Water penetration and absorption
	S3	P3	O3	/	*As S2 / P2 / O2, plus:* Penetration resistance Cleated outsole
	S4	P4	O4	//	Closed seat region Antistatic properties Energy absorption of seat region Resistance to fuel oil (only for SB/PB)
	S5	P5	O5	//	*As S4 / P4 / O4 plus:* Penetration resistance Cleated outsole

Slip resistance is of extreme importance in safety application, and is dependent on the tribological system, comprised by the outsole, the floor material and, in most cases, an interfacial medium (liquid, mud, e.g.). It is difficult to have a steady slip resistance in different situation when using the same outsole material. Therefore, marking is also used to differentiate the slip performance of safety footwear in distinct systems.

The dynamic coefficient of friction is determined for the heel site and for the flat zone under standardized systems with specific limits for each outsole zone. Table 2.2 presents the marking assigned for each system, as well as its coefficient limit: SRA is related to ceramic/surfactant, SRB to steel/glycerin, and SRC both SRA and SRB systems.

Table 2.2: Marking symbol of slip resistance performance for safety footwear, according to ISO 20345:2011 [27].

	Marking symbol for safety footwear regarding slip resistance (coefficient of friction)					
	SRA		**SRB**		**SRC**	
Test system	*heel*	*flat*	*heel*	*flat*	*heel*	*flat*
Ceramic tile + sodium lauryl sulphate solution	≥ 0.28	≥ 0.32	-	-	≥ 0.28	≥ 0.32
Steel floor + glycerin	-	-	≥ 0.13	≥ 0.18	≥ 0.13	≥ 0.18

2.2.1 Toe Caps

Toe caps are protective elements placed in front of the shoe, covering the frontal area, designed to protect the toes from potential hazards. Standards for assessing the performance of toe caps exist, like ANSI Standard Z41 and ISO 12568. The latter, regarding mechanical performance demands that toe caps for safety footwear must withstand a mechanical impact of 200 joules, a compression loading up to 15 kN and comply with the size-dependent specified clearance values, as displayed in Table 2.3 [30]. Nowadays, several commercial toe caps exist, which are metallic and non-metallic solutions.

Table 2.3: Clearance under toe cap for toe cap alone and toe cap placed inside safety shoes [27, 30].

Clearance under toe cap (mm)	**size**	**≤ 5**	**6**	**7**	**8**	**9**	**≥ 10**
	Toe cap alone [30]	19.5	20.0	20.5	21.0	21.5	22.0
	size	**≤ 36**	**37-38**	**39-40**	**41-42**	**43-44**	**≥ 45**
	Toe cap in safety shoes [27]	12.5	13.0	13.5	14.0	14.5	15.0

2.2.1.1 Metallic Toe Caps

As mentioned above, the first toe cap prototypes appeared in 1920-1950 mainly made of metal [13–16]. In fact, this component keeps under development to follow current fashion trends. The use of steel toe caps is obvious due to its known excellence in mechanical performance. Although with a small thickness,

this reinforcement is responsible for a high amount of the total weight of the shoe, around 35% [31]. According to literature, one way to manufacture this component is through stamping, where a single sheet of steel with a constant thickness is cut and stamped against a die [32, 33]. Afterward, a trimming process is applied and thermal treatment given. To conclude the process, a coating followed by painting is applied to protect it from corrosion [34]. Despite its excellent mechanical properties, steel toe caps are heavy and play an important contribution to user fatigue [35]. Over the years, some solutions have been investigated, for example, toe caps made of aluminum alloy, toe caps made of plastic and plastic composites [34, 36, 37]. All these materials have lower density than steel but require higher thickness to achieve the same performance, Figure 2.7.

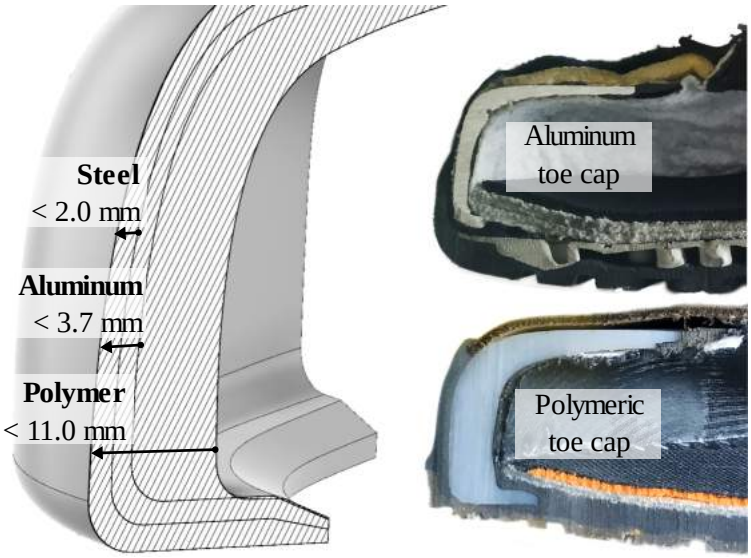

Figure 2.7: Illustration of toe cap thickness with different material selection [34, 38].

Aluminum alloy toe caps can also be produced through stamping, which is useful in case of reusing the steel toe cap molds [39, 40]. Casting and injection processes are also used to manufacture these products and allow the manufacture of geometries with variable thickness, which is important to optimize the shape through material distribution in zones with higher mechanical solicitation [34]. Moreover, toe caps made from aluminum alloy have several advantages, are lighter, less prone to corrosion and do not exhibit magnetic behavior.

2.2.1.2 Non-Metallic Toe Caps

Non-metallic solutions for toe caps are seen as an important trend in the global market. This type of products started to be considered in the 1980s, when innovation towards lightweight and esthetics/design began to be a topic of discussion [41]. The manufacturing process related to polymeric

materials, mainly injection molding, offers great freedom in part design, allowing to carry out engineering design in order to optimize the geometry to produce better and more stylish products. These materials are thermal and electrical insulators and have non-magnetic properties, which are not alerted by metal detectors [21, 42]. Contrary to metallic toe caps, when polymer/polymer composite materials are stressed beyond their elastic limit and before fracture, the deformation is not permanent due to the elastic energy stored internally (viscoelastic behavior). This means that when the load is removed from the safety shoe, the toes of the wearer are immediately freed from the stress since plastic toe cap will recover some of its original shape [43]. Some studies of toe caps made from thermoset and thermoplastic materials were reported in scientific articles as an alternative to their counterparts. For example, Lee *et al.* used a thermoset polyester resin impregnated with glass fibers with different stacking sequence, which showed a weight reduction of 40% with comparable static and impact resistance of steel toe caps [44]. The structural properties of fiber-reinforced composites are strongly dependent on the materials, like fiber orientation, fiber length and fiber/matrix interaction [44, 45]. More recently, Erden and Ertekin reported a 16 layer epoxy composite toe cap made of different layers of glass, aramid and carbon fiber that was 56% lighter than ordinary steel toe caps, with enough impact resistance to be applied in protective shoes [21]. Yang *et al.* [42] reported the production of a toe cap made of sisal-polypropylene thermoplastic composite thought compression molding able to withstand the 15kN force required for safety shoes without failure.

Polycarbonate (PC) has also been used to produce toe caps for safety footwear due to its outstanding mechanical properties. It has the highest impact resistance among all the engineering thermoplastics, despite having a brittle behavior under sharp impacts [46]. PC has been copolymerized with siloxane acting as a soft block in the polymer backbone, to provide better impact toughness at low temperature, good weatherability, improved ignition resistance, better hydrolytic stability, and slowed aging. The good performance of this type of material improves the use of toe caps under sub-zero temperature conditions [47]. The copolymerization of polydimethylsiloxane with polycarbonate is able to produce a material with elastomeric or rigid thermoplastic resin, resulting in a combination of properties from both materials, such as high flow characteristic from siloxane and high impact toughness from PC. The good flowability intrinsic of siloxane chain enables the injection of this composites into molds with complex geometry and thin-walled areas, which would be difficult with polycarbonate homopolymer due to its high melt viscosity [47–49]. It exhibits excellent release properties and enables shorter cycle times that improves production, which is very important in industrial production [47]. The addition of impact modifiers with rubber toughening mechanism is an alternative way to improve impact toughness of polymers at low

temperature, such as styrene-butadiene-styrene (SBS), styrene-ethylene-butylene-styrene (SEBS), acrylonitrile-butadiene-styrene (ABS) polymer or methacrylate-butadiene-styrene polymer [49, 50]. For PC systems rubber toughening mechanism occurs through rubber phase cavitation forming a void, followed by shear yielding of the polymer matrix where impact energy is dissipated [51, 52]. The addition of nanosized core-shell particles in the polymer matrix, such as poly(butylacrylate)-poly(methyl methacrylate), with controlled size is another solution [53, 54]. These particles have a rubbery core for impact energy absorption, which is surrounded by a shell designed to improve phase compatibility. The toughening mechanism is reported to occur through shell fibrillation which helps in the stabilization of the coalescent cavities [55]. In most cases, blend miscibility is poor due to lack of interfacial adhesion between different phases. To counter this issue, modification of the rubbery phase is performed with functional groups able to provide better chemical affinity or to bond covalently to the -OH terminal groups of PC, such as maleic anhydride groups, improving mechanical properties of the final blends [56–59]. The way rubber is dispersed (size, distribution) and the interaction with the matrix (affinity) will dictate the final properties of the polymer blend.

Recently, nanoparticles have been used to modify and enhance polymer properties as the amount of filler required to reinforce the matrix is significantly lower (0.1-8.0%) compared to microfillers (30-40%) [60–62]. The reason lies in the fact that nanoparticles have a much higher aspect ratio (length/thickness), which increases the interaction between the particles and matrix [63]. It is known that the final properties of nanocomposites have a high dependency on the dispersion of nanofillers within the polymer matrix, filler-polymer compatibility and interaction [60]. Several studies report the incorporation of nanoclays in polycarbonate matrix, increasing tensile strength and Young's modulus, but decreases the elongation at break and consequently the toughness of the material [64–66]. Chow *et al.* studied the effect of the addition of maleated styrene-ethylene-butylene-styrene (SEBS-*g*-MA) on the mechanical, morphological, and thermal properties of PC/ Na+-MMT nanocomposites produced through melt extrusion [67]. The addition of SEBS-*g*-MA has a toughening effect, which enhanced ductility and impact strength of the nanocomposite. In most of the studies reported in literature, it seems to be an inverse correlation between tensile strength and impact strength for thermoplastic systems. Therefore, a balance between these properties should be established to be used in applications that require both properties, such as toe caps. Zukas *et al.* [68] have incorporated different types of nanofiller into thermoset methyl methacrylate resin as reinforcement. They showed an improvement in stiffness and strength for natural bentonite and halloysite, while multiwalled carbon nanotubes have increased toughness. Overall, these nanofillers have a positive effect in impact resistance.

Figure 2.8 depicts the specific impact performance of conventional toe caps (clay clearance at an 200 J impact weighted by its mass and internal height), where current thermoplastic toe caps have better specific and compression performance over their counterparts.

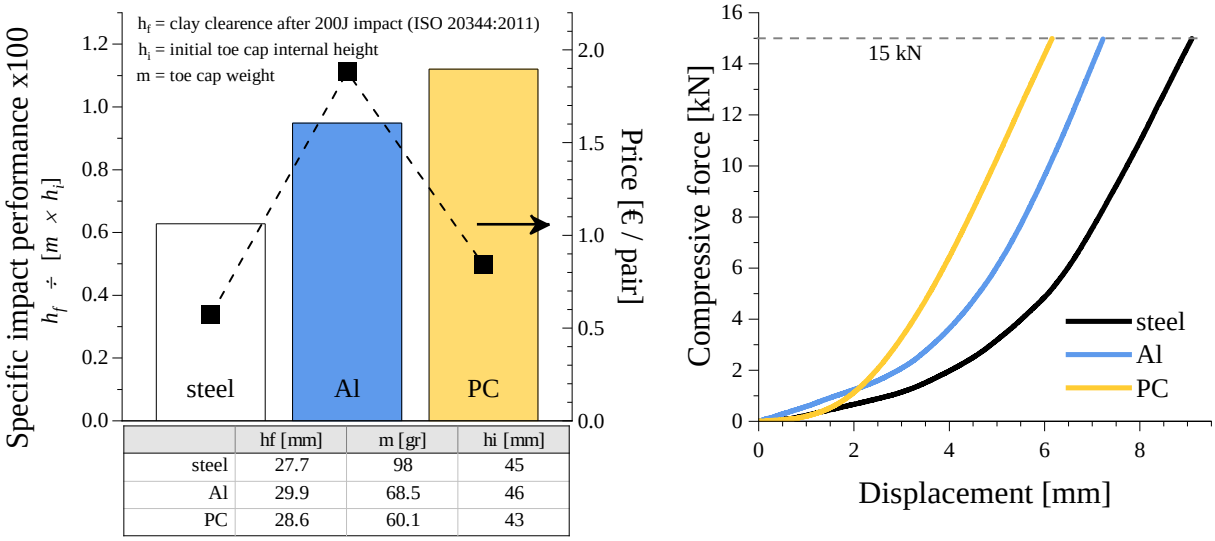

	hf [mm]	m [gr]	hi [mm]
steel	27.7	98	45
Al	29.9	68.5	46
PC	28.6	60.1	43

Figure 2.8: Conventional toe cap specific impact performance (clay clearance after 200 J impact test divided by mass and initial internal height of the toe cap), and compressive behavior for size 10 safety shoe made of steel, aluminum (Al) and thermoplastic polycarbonate (PC).

Despite its benefits, composite toe caps have some drawbacks compared to metallic ones. The main disadvantage relies on its mechanical performance, which requires a higher volume to achieve a comparable resistance, resulting in possible aesthetic and design problems [69]. Since composite materials are sensitive to low-velocity impact, damage tolerance should be considered carefully. Consequently, even if there is no visual damage on toe cap, it could fail due to this phenomenon [44]. Therefore, research in toe cap field regarding new material and design solutions is of utmost importance to the future of safety footwear, to enable the construction of safety shoes similar to ordinary shoes so the users feel it more natural and comfortable to use.

2.2.1.3 Manufacturing Process

Table 2.4 compares different materials, production processes, cost, design and physical characteristics regarding toe caps. Steel toe caps are mostly produced through stamping from steel sheets (Figure 2.9 a), and aluminum alloy counterparts can also be produced through casting (Figure 2.9 b). and injection. Compression molding is used for fiber reinforced thermoset and thermoplastic toe caps. The latter is firstly extruded as a fiber-reinforced composite sheet, cut with the required dimension and compression-

molded under certain pressure and temperature conditions into a mold [37]. This process is time-consuming and requires several processing steps. On the other hand, the remaining thermoplastic toe caps are produced through injection molding (Figure 2.9 c) using the reinforced materials as pellets [43]. Stamping and injection molding offer higher production rates, lowering overall cost production.

Overall, non-metallic solutions are lighter than their metallic counterparts, offering electrical/ thermal protection without magnetic behavior, but to compensate the lack of mechanical resistance they have to be thicker. These benefits are attractive to substitute traditional solutions, but design restrictions (bulky footwear) are preventing manufacturers to fully change the material base.

Table 2.4: Comparison between metallic and non-metallic toe caps.

Toe cap	Raw material	Production process	Product: cost / output	Design	Electric / magnetic conductivity, Thermal comfort
Metallic					
Steel					
	steel [70] stainless steel [71]	Stamping	$ fast	thin heavy	yes / yes poor
Aluminum					
	aluminum alloy aerospace alloy [38]	Stamping Casting [72] Injection	$$$ fast slow	thin light	yes / no poor
Non-metallic					
Thermoset					
	vinyl ester based reinforced with glass/ carbon fibers [73]	Compression molding	$$$$ slow	thin light	no / no better
Thermoplastic					
	laminated thermoplastic [74]	Compression molding	$$$ slow	thick light	no / no better
	polyamide polycarbonate [75]	Injection molding	$ fast		

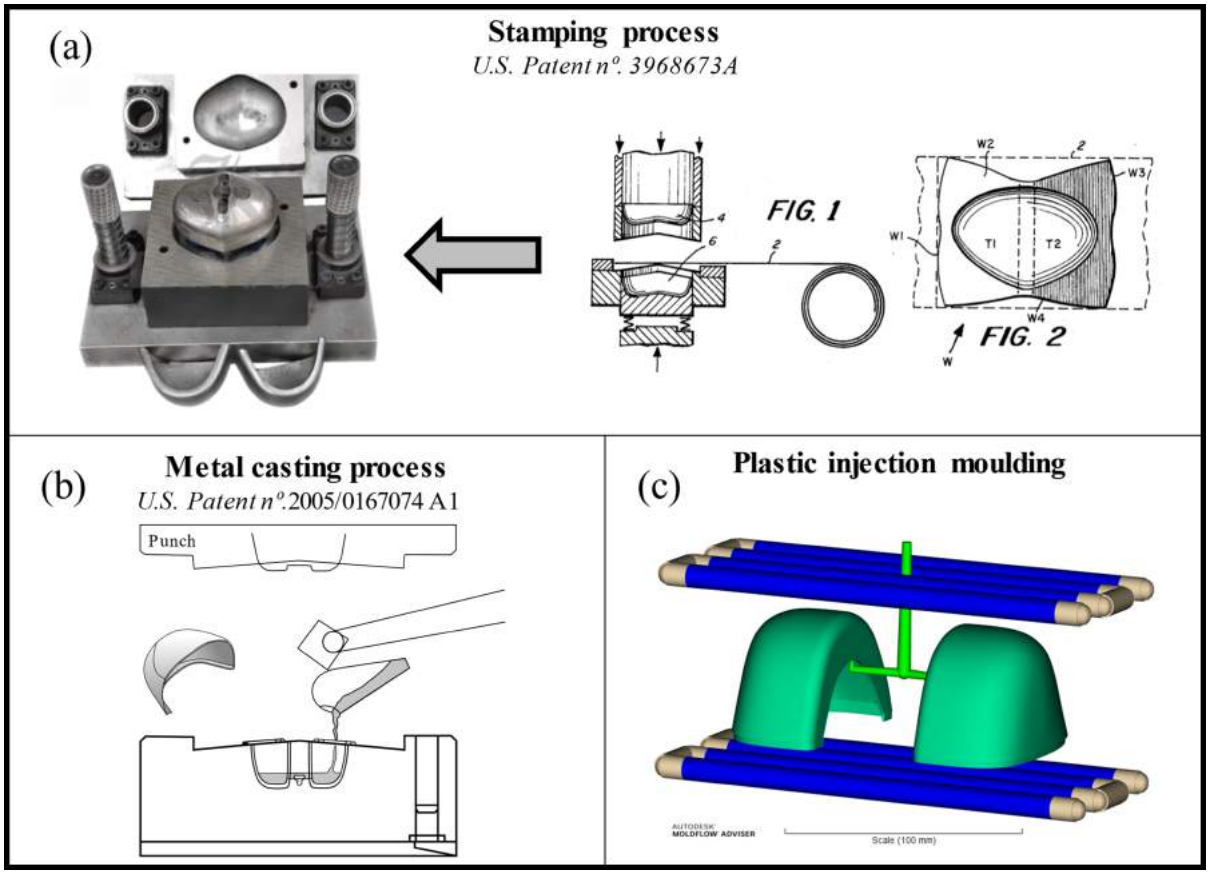

Figure 2.9: Industrial processes used to manufacture toe caps for safety footwear through (a) stamping and (b) casting for metallic toe caps, and (c) injection molding for thermoplastic [33, 76, 77].

2.2.1.4 Toe Cap breathability

Microclimate footwear complies the atmospheric conditions inside the shoe in terms of temperature, relative humidity and air flux between the inside and outside of the shoe [78]. As already mentioned, inadequate ventilation of safety shoes causes discomfort, which became one of the main reasons to neglect its use. Toe caps have this limitation due to the material nature since metals and plastics are non-breathable materials, promoting sweating. Some solutions have been patent and are commercially available that complies holes in the toe cap structure [79–81]. Irzmanska performed an experiment where the microclimate in protective footwear with a perforated vapor-permeable composite toe cap was compared to a shoe with steel toe cap [78]. Results showed better thermal comfort and lower humidity for the shoe with perforated toe cap. This characteristic is essential to maintain hygienic conditions to user's feet, preventing the development of pathogenic bacteria and fungi resulting in further problems. Hence, toe cap breathability is a currently issue in the safety footwear industry and requires a solid solution. Due to the wide variety of industries that need to use this kind of protective footwear, manufacturers have to adapt the geometry of the reinforcement in order to produce more stylish footwear to expand their products.

2.2.1.5 Design optimization using numerical simulation

Although several materials have been developed for toe caps to meet its requirements, the study for new solutions persists. Geometry optimization thought simulation is also another important way to improve toe caps performance. This approach relies on iterative design modifications to achieve the optimum relationship between thickness and performance. Numerical simulation software is a useful tool to study the stress distribution in the geometry during the compressive and the impact events, identifying critical regions such as weak or overdesigned sections of the toe cap. In this field, some authors reported a significant reduction in weight (40 - 50%) by using this approach. Changing from ordinary steel to hardened steel alongside design modification at the top of the part with ribs showed promising results in metallic toe caps [23, 31, 69, 82, 83]. During stamping process, the steel sheet is deformed at a higher degree at the ribs site, acting as local stiffeners due to plastic deformation. Hardened steel has superior mechanical properties, which improves overall mechanical resistance, and local reinforcements helps to better support the compressive force and the impact solicitation. Other studies focused on polymeric toe caps to access the fiber reinforcement effect of glass, sisal, or flax, manufactured through compression molding process of a pre-preg material with distinct stacking sequence of the fiber layers [42, 44, 84]. Good agreements with experimental results were observed, enabling the construction of a numerical tool able to create new polymeric solution. Also, the temperature behavior of a polymeric composite toe cap made of polyamide 66 and carbon fiber was reported, where the effect of fiber weight percentage was analyzed, showing that fiber incorporation improves thermal conductivity [85]. Most of these simulations make use of well-established commercial finite element analysis software, like ANSYS LS-Dyna solver, ANSYS explicit dynamics, SolidWorks Simulation, ABAQUS Standard and ABAQUS Explicit, with good agreement between simulation and experimental results. This kind of approach enables the prediction of different designs to optimize toe cap manufacture.

2.2.2 Outsoles

For safety footwear, a toe cap is not the only requirement for foot protection. The user must take into account, among others, metatarsal (upper foot) protection, heel protection, the use of adequate materials for electrical and chemical protection, puncture resistance and slip-resistant soles. The latter is of key importance in several occupations and can have a huge impact on the safety of the worker. In most footwear models the sole is comprised of 3 subcomponents: an insole, a midsole and an outsole. The insole sits underneath the foot and is responsible for comfort, while the outsole is in direct contact with the ground and should provide grip and durability. The midsole connects the outsole to the upper and

confers cushion and stability to the shoe.

According to Beschorner *et al.* walking movement is dependent of the frictional properties between footwear-floor interface and must be sufficient to counter the biomechanical requirement [86]. Slipping and tripping cause more industrial accidents than any other single cause [87, 88]. In the U.S.A. 40-60%, in Korea 57.3%, and in Italy 15% of the cases were reported to be related to slipping and falling occurred yearly, and in Finland 66.6% related to walking on surfaces covered in snow or ice [89–91].

Certain occupations are very prone to slip related accidents, among firefighters it has been estimated that falling, slipping and missed jump contributed with 23.5% of fire ground injuries [92]. The selection of a proper outsole for this occupation is quite challenging because firefighters can face a complex, unpredictable and rapidly changing environment (dry or wet floor, floor with debris or chemical contaminants, physical hazards, heat, noise). Adding to these, firefighter's equipment is heavy, leading to fatigue and exhaustion, which increases the probability of accidents [18, 92]. In 1972, Ramsay and Senneck reported that slipping plays an important role in men losing their balance in British coal mines [93]. The shoes made with rubber soles provided good grip on clean surfaces, but in the presence of oil and mud the grip was reduced. At that time, the solution to this problem was to equip the outsole with tungsten carbide tipped studs. However, the existence of metal parts is not desirable due to friction between metal and rock that can trigger a sparkle, causing explosion in this environment. From the above, it can be seen that slip resistance must be addressed and evaluated for consumers to select the more appropriated material.

2.2.2.1 Evolution in outsole materials

Nowadays, consumers are more self-aware about the benefits of using comfortable shoes, providing better life quality, well-being and injury prevention [87]. Chen *et al.* presented a guideline with the most important aspects to consider when selecting the proper slip resistance safety shoe, mainly, outsole material, outsole hardness, sole pattern shape, leading-edge and drainage channel, comfort and fitting [94].

Different types of materials have been used in the manufacture of soles. Historically, leather (derived from the skin of many animals) is the oldest material being used to produce soles. A great evolution was made through the appearance of unvulcanized natural rubber in the 1920s and vulcanized natural rubber in the 1930's [89]. Nowadays, vulcanized natural rubber is considered a material of excellence to produce

outsoles due to its properties and performance, especially in dry surfaces. The downside of this material is its high specific gravity (~1.5 g/cm^3), resulting in heavy soles and the labor associated with the processing technique to shape this material, where a formulation step is needed in order to incorporate additives, followed by a shaping procedure followed by final vulcanization stage.

In the 1960s, thermoplastic rubber, such as SBS, appeared with similar properties to vulcanized rubber but offering higher production rates, due to ease of processability through injection molding, resulting in a lower cost [2, 95]. Another advantage of thermoplastic materials is the use of recycled material into the process (about 20-30%), which cannot be performed with crosslinked polymer (e.g., vulcanized rubber).

Despite its inferior performance to rubber, polyvinyl chloride was the first thermoplastic material used in soles due to production advantages. Through the addition of plasticizers this material can be made into a rigid or soft plastic. Along with natural rubber, this material has a high specific gravity (~1.4 g/cm^3) and some environmental concerns [2].

Polyurethane (PU) appeared in the 60s and offered new possibilities. This material can be processed with blowing agents and thus have a wide range of densities (0.006- 1.2 g/cm^3). Outsoles made of PU can be lightweight, with good abrasion resistance and with good cushioning properties [2].

In the 1980s, the demand for lightweight shoes was achieved using crosslinked ethylene-vinyl acetate foams and polyolefin elastomers, both could be used in rubber blends as parts to improve outsole rubber performance.

Recently, thermoplastic polyurethane (TPU) outsoles production has increased, this material offers the possibility of tailoring its hardness, have great flexibility, abrasion resistance, high strength, good low-temperature performance, among others [2, 20, 95]. It was estimated a global production of almost half a million tons of TPU in 2015 with 34% used in the footwear industry [96]. The TPU based components represent about 60% of the European total production of footwear components [97]. It has a high specific gravity (~1.3 g/cm^3), which is comparable to vulcanized rubber, therefore, new solutions have been developed to promote TPU materials in soling, such as the use of blowing agents to achieve a reduction of 35% in weight, and the development of TPU grades with different hardness [2]. There seems to be a balance between slip resistance and wear resistance properties. For example, the copolymerization of TPU with poly(dimethyl siloxane) improves wear resistance due to the lowering of coefficient of friction [98].

New nanocomposite materials based on polyurethane systems have been developed to enhance its properties, with the incorporation of different nanofillers, such as clay, nanosilica, graphene-based (graphene, graphene oxide, reduced graphene oxide), SiC, ZrO_2, TiO_2, SiO_2 and MoS_2 particles, multi and single-walled carbon nanotubes, among others [99–103]. The use of clay and SiO_2 particles increases tensile strength, Young's Modulus and wear resistance of polyurethane, but affects negatively the coefficient of friction. Most friction tests, of these works, were conducted under a clean and dry surface (mostly metal), which is not the most critical scenario and not in accordance with the European Standards.

For specific occupations, e.g., firefighters, high quantities of halogen-based flame retardants (aliphatic or aromatic bromine or chlorine compounds) and halogen-free flame retardants (magnesium hydroxide, aluminum hydroxide) are used which have a negative effect on the mechanical properties [99, 104, 105]. The high toxicity of halogen-based materials lead Europe and other countries to prohibit its use, after reports indicating the presence of toxic components in humans, animals and environment resulting from combustion of these flame retardant and transported throughout the atmosphere [106, 107]. As alternative, nanoclay can be used as a flame-retardant filler in TPU systems, replacing other conventional filers with a small amount of nanoclay [99]. This enables the combination of both mechanical reinforcement and flame-retardant effect of nanoclay. Graphite-derived compounds have also been used as a flame retardant in TPU systems. Guler *et al.* studied the effect of expandable graphite (EG) on flame retardant properties of TPU composites filled with huntite and hydromagnesite mineral, and concluded that small EG particles with high expansion ratio performed better at flame retardancy [108].

Nitrile butadiene rubber, an elastomer quite used in the seal industry, has also been used in safety footwear to produce oil resistant outsoles with better slip resistance then PU when tested on dry ice (-5 and -20 °C) [109].

2.2.2.2 Slipping phenomena

Evidence of slip resistance mechanism was found to be influenced by microscopic roughness of floor surfaces and outsole, as well as wear evolution. First contact occurs when the highest asperities of the floor surface touches the outsole surface (Figure 2.10 a)). Due to the small area of contact, the pressure developed at the contact site can be high enough for the asperities to pierce the outsole material (Figure 2.10 b)). During continuous walking small amounts of outsole material are pull off due to mechanical failure, promoting wear and the presence of wear products between both surfaces (Figure 2.10 c)),

contributing even more to the wear phenomena [110, 111]. On a first stage, roughness allows some liquid drainage under wet conditions, preventing the user to squeeze the fluid, but its efficiency is quickly lost [88]. Outsole pattern allows the drainage of the fluid from the inner to the outer side of the outsole, avoiding the formation of a film with a lubricating effect underneath the shoe (Figure 2.10 d)).

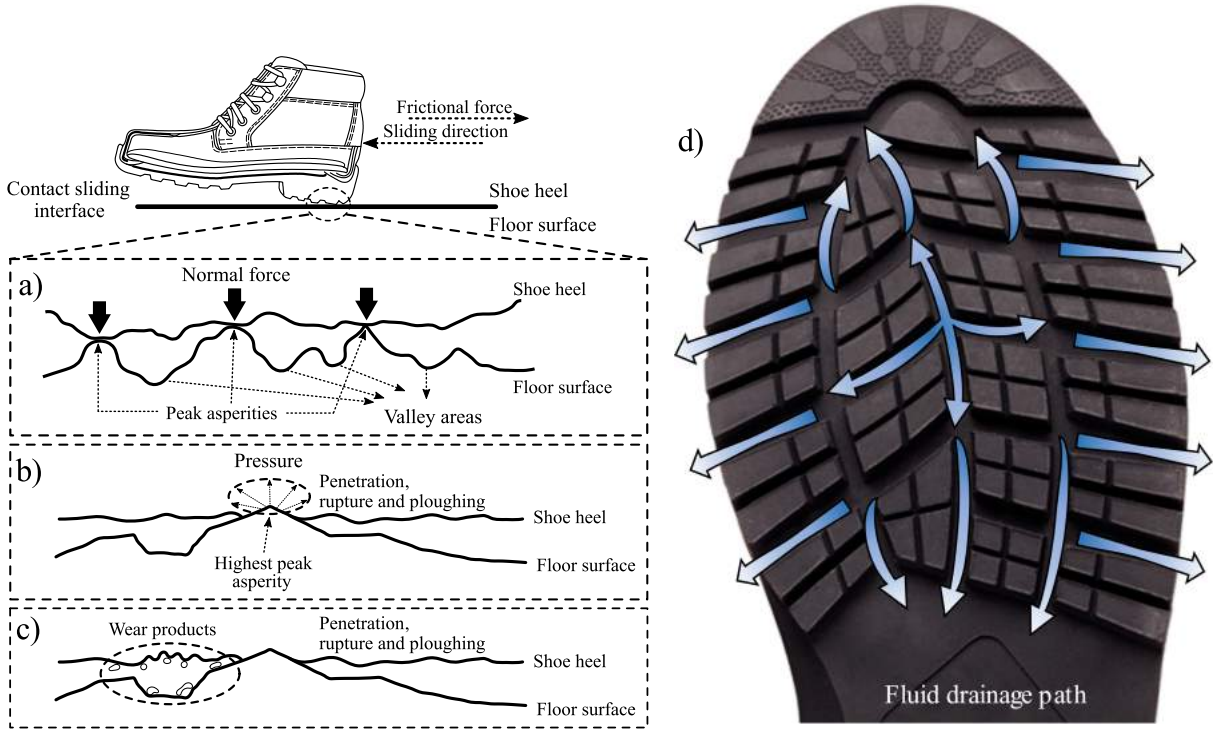

Figure 2.10: Interaction scheme between outsole and floor surface: a) initial contact, b) interlocked stage, c) wear development, and d) liquid drainage [111].

Recently, Bang *et al.* investigated the slip resistance of safety shoes available on the market with different properties (outsole pattern, roughness and hardness) to determine the major feature for grip improvement [90]. He found out that the friction coefficient was more affected by the outsole pattern design (higher values for outsoles with many small, raised blocks on the heel) and by the material property (lower hardness), rather than outsole roughness or contact area ratio between the outsole and the surface. Once more, drainage and damping properties of outsoles are important to improve gripping [87, 112, 113]. The evaluation and measurement of slip properties of shoes have been difficult to attain due to the high number of variables that govern the process. Friction is commonly used as an indicator of slipperiness, and there are two distinctive friction coefficients: the static coefficient of friction (SCoF) that indicates the minimum force required to initiate relative movement between two surfaces, and the dynamic coefficient of friction (DCoF) which is associated to keep the body in motion [113]. Some authors consider SCoF as

the most important parameter to evaluate slip resistance, since it determines the transition from static to initial slipping stage. On the other hand, others argue that in regular walking activity the contact time between sole and floor is too short for SCoF to be responsible for slip accidents. Therefore, the contact time is greater for DCoF providing a wider time window for the user's body to actively react in order to recover balance and prevent a possible injury [113, 114]. The European Standard ISO 20345 stands the first international method to evaluate slip resistance of safety footwear, which considers DCoF (ratio between frictional and normal forces) as an indicator of shoe performance on different soles, and the method is disclosed in ISO 13287 [27, 115]. The coefficient is determined for different floor conditions, shoes are tested in two different types of surfaces, metal and ceramic tile, with sodium lauryl sulfate (NaLS) solution and/ or glycerin at the surface. This standard is only proposed for conventional soled footwear not comprising special features like spikes, metal or similar, or special applications (footwear used on soft ground). These tests can be used as an indicator to help in the decision of selecting between different safety shoes. However, on icy surfaces there is no standard to access the slip resistance of footwear, which led some authors to create devices to quantify the coefficient of friction in different scenarios, such as in wet ice (0°C), dry ice (-5 to -20 °C) and on snow [109, 116, 117].

2.2.2.3 Outsole requirements

Slipping resistance are of outmost importance in safety shoes performance and vital for the professional daily life workers, but it is not the only requirement for outsoles. Table 2.5 compiles the outsole requirements for safety, protective and occupational footwear. Due to the diversity of outsole styles, ISO 20344:2011 distinguish two different outsoles construction on the shoe: direct injected, vulcanized and cemented outsoles (Figure 2.11 (a)); and all-rubber/all-polymeric footwear (Figure 2.11 (b)). In the first the outsole can be manufactured separately or directly injected into the bottom side of the shoe. In the latter the outsole material constitutes all of the shoe construction (upper and sole) [118]. Cleated outsole presents features on the sole surface for water drainage and grip performance. The parameters used to determine sole thickness limit (d_1, d_2, d_3) are dependent on the type of construction and class. Following this, it is of equal importance for the outsole attached to the boot to meet all the other requirements, such as tear strength, abrasion resistance, flexing resistance, hydrolysis and interlayer bond strength.

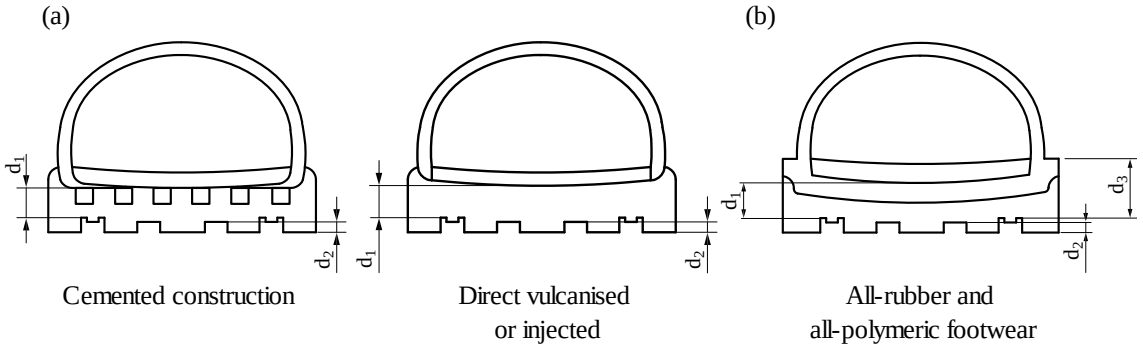

Figure 2.11: Example of cleated outsole construction for safety footwear as (a) cemented or directed injected or vulcanized outsoles, and (b) all-rubber and all-polymeric footwear [118].

Table 2.5: Requirements for tests of outsoles for safety, protective and occupational footwear [27–29].

Outsoles specifications	**Safety footwear ISO 20345**	**Protective footwear ISO 20346**	**Occupational footwear ISO 20347**
Thickness		**Class** (definition at Table 2.1)	
	Outsole type	**I**	**II**
	Non-cleated	$d_1 \geq 6$ mm	$d_1 \geq 6$ mm
	Cleated	$d_1 \geq 4$ mm $d_1 \geq 2.5$ mm	$d_1 \geq 3$ mm $d_1 \geq 4$ mm $d_1 \geq 6$ mm
Tear strength for non-leader outsoles	8 kN/m for a material with $\rho > 0.9$ g/cm³ 5 kN/m for a material with $\rho \leqslant 0.9$ g/cm³		
Abrasion resistance for other than non-leader, all-rubber, and all-polymer	volume loss $\leqslant$250 mm³ for materials with $\rho \leqslant 0.9$ g/cm³ volume loss $\leqslant$150 mm³ for materials with $\rho > 0.9$ g/cm³ * for all-rubber or all-plastic outsoles volume loss $\leqslant$250 mm³		
Flexing resistance for non-leader outsoles	cut growth $\leqslant$ 4mm before 30 000 flex cycles		
Hydrolysis for outsoles of polyurethane	the cut growth shall be not greater than 6 mm before 150 000 flex cycles.		
Interlayer bond strength between the outer or cleated layer and the adjacent layer	≥ 4.0 N/mm ≥ 3.0 N/mm if there is tearing of any part of the sole		
Resistance to fuel oil	Increase in volume $\leqslant$ 12%. * If the test piece shrinks by more than 1 % in volume or the shore hardness increases by more than 10 Shore A units, a test similar to the one performed to check hydrolysis must be performed		

2.2.2.4 Outsole attaching methods in safety footwear

Methods for safety footwear construction are described on Table 2.6, and are directly related to sole manufacturing techniques. On one way, the outsole can be manufactured and attached into the sole all at once (Direct method) throughout injection molding or vulcanization processes. On the other way, outsole is previously manufacture using compression or injection molding processes, to be further attached to the shoe by a cementation process (using an adhesive to bond both materials), or by a stitching process (Goodyear method).

Table 2.6: Common construction methods of safety footwear to attach the outsole to the upper [17, 119–122].

Method	Outsole process	Attaching process
Direct	In this process, the material used to shape the outsole is softened/molten and pressed against the upper, so the fibers of the upper are embedded by the sole material, creating a physical bond:	
	Injection molding	Melted plastic is poured or injected into a mold where it is held to the upper under pressure until the molding cavity is solidified and removed. In some cases, PU foam is used as midsole and.
	Vulcanization	Soften rubber is pressed against the upper under pressure and vulcanization process occurs with temperature (Direct Vulcanized Technology).
Cementation	In this process, a cement (adhesive) is used to glue the pre-made sole and the upper, allowing the fixation of different materials, whereas not all materials can be injection molded:	
	Compression molding	An aluminum/steel heated tool is used with the shape of the outsole. Slabs of rubber are introduced in a sufficient amount. After pressing and forming, the mold is closed for the vulcanization process to occur.
	PU casting	A polyol and polyisocyanate are mixed with catalysts, blowing agents and chain extenders are added to produce a foam within a wide range of densities [0.006 -1.2 g/cm^3].
Goodyear	Goodyear construction method attaches the upper to the outsole through a welt by a stitching process. The stitches maintain all components (upper, midsole and outsole) firmly attached, without using adhesives.	

2.3 Future Trends

On this manuscript it was shown that the enhancement of safety footwear properties is an ongoing effort and new solutions are presented every year to provide better protection and comfort to the wearer, such as new materials and new design components. On a recent article from Janson *et al.* it was presented a totally new concept for safety shoes, called "Safety-Smart Footwear", where custom-made shoes equipped with sensing capabilities are connected to the Industry 4.0 philosophy [123]. This approach

envisions the collection of individual data from the worker to an integrated cloud system, the analysis of the data as a whole to iteratively improve safety, comfort and design using the "Big data" knowledge. Also, improvements in the organization and working methodologies of the company can be deduced from this kind of approach, and, therefore, creating a united system that is actively acting to improve workers conditions and the efficiency.

2.4 Conclusions

The review regarding safety footwear panorama made for the main structural components of this type of footwear (toe caps and outsoles) demonstrate that:

- There is still a great concern regarding safety and comfort in the working place. Improvement of this characteristics will result in less worker down-time and less fatigue, leading to an improvement of overall worker satisfaction.
- Commercial toe cap typologies showed that non-metallic solutions have better benefits regarding their metallic counterparts, namely, lightweight, electric and thermally insulator, non-magnetic, non-corrosive. Despite the benefits, non-metallic solutions require higher volume design to achieve comparable mechanical performance.
- Some toe cap solutions were developed through numerical simulation, mainly metallic toe caps, achieving up to 50% mass reduction. This approach enables a faster and easier way to develop new toe cap designs. Due to non-metallic toe cap advantages, there is still a lot of work to be performed in this field.
- Rubber is the excellence material for outsoles. It provides great slip resistance and mechanical properties. Its high specific gravity, intensive labor work and non-recyclability are the main downside, driving the development of new solutions.
- For each situation there are different outsoles available, made of different materials, densities, additives and patterns.
- Even though the effort that has been put to improve current toe cap and outsole performance, throughout the last year, more research is essential to create new materials and design concepts to meet all the requirements.

2.5 Acknowledgements

The authors acknowledge the financial support by Portugal 2020, and Fundo Social Europeu (FSE) through Programa Operacional Regional do NORTE (NORTE-08-5369–FSE-000034), developed under the program "IMPULSE - Polímeros e Compósitos: Drivers da inovação tecnológica e da competitividade industrial".

2.6 References

[1] E. Schamp, P. Shaw, J. Vernon, E. Kantor, and H. Bertram, "In-depth assessment of the situation of the European footwear sector and prospects for its future development: Task 7 : synthesis report - Study," Revised Final Report, Risk & Policy Analysts Ltd, Publications Office of the European Union, 2012. Accessed: Feb. 21 2020. [Online]. Available: https://op.europa.eu/en/publication-detail/-/publication/daf8fc79-394f-4157-996d-829b63b916dc

[2] K. A. Ames, "Elastomers for shoe applications," *Rubber Chemistry and Technology*, vol. 77, no. 3, pp. 413–475, 2004, doi: 10.5254/1.3547832.

[3] S. Lüdemann, "Footwear Report 2019: Statista Consumer Market Outlook - Market Report," Statista did-55485-1, Apr. 2019.

[4] APICCAPS - Portuguese Footwear, Components, Leather Goods Manufacturers' Association, "Statistical Report: Portugal," Footwear cluster 2018, 2018.

[5] World Footwear by Portuguese Shoes, *The World Footwear 2019 Yearbook.* [Online]. Available: https://www.worldfootwear.com/world-footwear-yearbook.html (accessed: Feb. 24 2020).

[6] APICCAPS - Portuguese Footwear, Components, Leather Goods Manufacturers' Association, "Statistical Report Portugal: Footwear, Components and Leather Goods," 2017.

[7] I. P. Fernandes *et al., Eds., Newalk: Novos Materiais e Componentes para Calçado do Futuro*. I Encontro de Jovens Investigadores do Instituto Politécnico de Bragança, Livro de resumos, 2013.

[8] M. A. S. Hashim and E. J. May, "Effectiveness of Personal Protective Equipment (PPE) at Construction Site," *INTI Journal*, vol. 1, no. 12, 2018.

[9] V. Vitharana, G. De Silva, and S. De Silva, "Health hazards, risk and safety practices in construction sites – a review study," *Engineer: Journal of the Institution of Engineers*, vol. 48, no. 3, pp. 35–44, 2015.

[10] R. Sehsah, A.-H. El-Gilany, and A. M. Ibrahim, "Personal protective equipment (PPE) use and its relation to accidents among construction workers," *La Medicina del lavoro*, vol. 111, no. 4, pp. 285–295, 2020, doi: 10.23749/mdl.v111i4.9398.

[11] eurostat - Your key to European statistics, *Health and safety at work: Accidents at work by NACE Rev. 2 activity and part of body injured.* [Online]. Available: https://ec.europa.eu/eurostat/web/health/data/database (accessed: Feb. 24 2020).

[12] M. D. Silva, *The Origin of Safety Shoes: Because shoes are easier to replace than feet*. Health and Safety Middle East. [Online]. Available: https://www.hsmemagazine.com/article/the-origin-of-safety-shoes/ (accessed: Feb. 24 2020).

[13] F. J. Wojcik, "Foot shield," U.S. Patent 1,626,489, Apr 26, 1927.

[14] A. W. Hauer, "Toe protector," U.S. Patent 2,002,662, May 28, 1935.

[15] A. R. Allard, "Safety shoe," U.S. Patent 2,079,237, May 4, 1937.

[16] W. J. Richards, "Safety show," U.S. Patent 2,836,909, Jun 3, 1958.

[17] Honeywell - Industrial Safety, *Industrial Safety Footwear: Spring 2015.* [Online]. Available: https://www.honeywellsafety.com/Supplementary/Documents_and_Downloads/Footwear/4294989532/1033.aspx (accessed: Nov. 9 2020).

[18] S. S. Chiou, N. Turner, J. Zwiener, D. L. Weaver, and W. E. Haskell, "Effect of boot weight and sole flexibility on gait and physiological responses of firefighters in stepping over obstacles," *Human factors*, vol. 54, no. 3, pp. 373–386, 2012, doi: 10.1177/0018720811433464.

[19] M. J. Abreu, P. Mendonça, C. S. Pereira, and A. Abreu, Eds., *Design of Innovative Protective Insoles for Safety Footwear*. International Conference on Engineering, Technology and Innovation (ICE/ITMC): IEEE, 2017.

[20] R. Dubois, S. Karande, D. P. Wright, and F. Martinez, "The Use of Ethylene/Styrene Interpolymers in Crosslinked Foams for the Footwear Industry," *Journal of Cellular Plastics*, vol. 38, no. 2, pp. 149–161, Mar. 2002, doi: 10.1106/002195502022246.

[21] S. Erden and M. Ertekin, "Mechanical Evaluation of a Composite Overshoe Protector," *TEKSTIL VE KONFEKSIYON*, vol. 27, pp. 414–420, 2017.

[22] W. Tyrrell and G. Carter, "Chapter 6: Shoes for special purposes," in *Therapeutic Footwear*, Elsevier, 2009, pp. 85–99.

[23] R. C. F. Soares, "Simulação numérica do comportamento ao impacto de componentes para calçado de segurança," Dissertação de mestrado integrado em Engenharia Mecânica, Universidade do Minho, Departamento de Engenharia Mecânica, 2015.

[24] R. M. Silva, A. I. Garcia, and A. Oliveira, *Novos Perfis de Calçado de Segurança Proteção e Ocupacional*: Guia do Empresário por Centro Tecnológico do Calçado de Portugal - Projecto imatec, 2012.

[25] A. Goldcher and D. Acker, "Chaussures de sécurité, de protection et de travail," *EMC - Podologie*, vol. 1, no. 1, pp. 12–23, 2005, doi: 10.1016/j.emcpol.2005.01.002.

[26] R. Hrynyk and E. Irzmańska, "Protective footwear: requirements selection and ergonomics," *OSHwiki - European Agency for Safety and Health at Work.* https://oshwiki.eu/wiki/Protective_footwear_%E2%80%93_requirements_selection_and_ergonomics (accessed: Aug. 8 2020).

[27] *Personal protective equipment - Safety footwear*, ISO 20345:2011(E), 2011.

[28] *Personal protective equipment - Protective footwear*, ISO 20346:2014, 2014.

[29] *Personal protective equipment - Occupational footwear*, ISO 20347:2012, 2012.

[30] *Foot and leg protectors - Requirements and test methods for toecaps and penetration resistant inserts*, EN 12568:2010, 2010.

[31] S. L. Costa, J. P. Mendonça, and N. Peixinho, "Numerical Simulation of Quasi-Static Compression Behavior of the Toe Cap Component for Safety Footwear," *International Journal of Computer Theory and Engineering*, vol. 6, no. 4, pp. 285–291, 2014, doi: 10.7763/IJCTE.2014.V6.876.

[32] C.-J. Ching, "Metal toecap for safety shoes," U.S. Patent 2006/0213086 A1, Sep 28, 2006.

[33] W. H. Ryan and N. H. Evers, "Method and apparatus for producing steel box toes to be used in safety shoes," U.S. Patent 3,968,673, Jul 13, 1976.

[34] C. Frulla, "Protective toecap, particularly for safety shoes," WO 03/037127 A1, May 8, 2003.

[35] S. Marr and S. Quine, "Shoe concerns and foot problems of wearers of safety footwear," *Occupational Medicine*, vol. 43, no. 2, pp. 73–77, 1993, doi: 10.1093/occmed/43.2.73.

[36] F. Fron, "Plastic foot protector," U.S. Patent 4,103,438, Aug 1, 1978.

[37] Y. Tanaka, M. Hirota, and T. Ishida, "Resin safety shoe toe cap," European Patent 1 380 221 A1, Jan 14, 2004.

[38] Safit S.r.l, *Comparison between steel and aluminum toe caps, who is the best?* [Online]. Available: http://www.safit.us/en/blog/comparison-between-steel-and-aluminum-toe-caps-who-best (accessed: Feb. 25 2020).

[39] Safit S.r.l, *The guidance to the safety toe caps for shoes: steel, aluminum, composite materials, fiber glass and carbon-fiber.* [Online]. Available: http://www.safit.us/en/blog/guidance-safety-toe-caps-shoes-steel-aluminum-composite-materials-fiber-glass-and-carbon-fiber (accessed: Feb. 25 2020).

[40] C. Frulla, "Apparatus and method for producing toe caps for safety shoes," WO Patent 02/089625 A2, Nov 14, 2002.

[41] D. A. Smith, "Protective toe caps for footwear," GB Patent 2,071,989 A, Nov 28, 1984.

[42] C. C. Yang, M. Duhovic, R. J. T. Lin, and D. Bhattacharyya, "Finite element modelling and analysis of composites toecaps," *IOP Conference Series: Materials Science and Engineering*, vol. 4, pp. 1–6, 2009, doi: 10.1088/1757-899X/4/1/012010.

[43] J. L. Dykeman, "Protective toe cap for footwear," U.S. Patent 4,735,003, Apr 5, 1988.

[44] S. M. Lee, T. S. Lim, and D. G. Lee, "Damage tolerance of composite toecap," *Composite Structures*, vol. 67, no. 2, pp. 167–174, 2005, doi: 10.1016/j.compstruct.2004.09.009.

[45] S. Patcharaphun and G. Menning, "Prediction of tensile strength for sandwich injection molded short-glass-fiber reinforced thermoplastics," *Journal of Metals, Materials and Minerals*, vol. 17, no. 2, pp. 9–16, 2007.

[46] K. Nevalainen *et al.,* "Characterization of twin-screw-extruder-compounded polycarbonate nanoclay composites," *Polymer Engineering & Science*, vol. 49, no. 4, pp. 631–640, 2009, doi: 10.1002/pen.21086.

[47] "PC toecap can withstand extreme temperatures," *Plastics, Additives and Compounding*, vol. 7, no. 1, p. 15, 2005, doi: 10.1016/S1464-391X(05)00328-4.

[48] W. Zhou and J. Osby, "Siloxane modification of polycarbonate for superior flow and impact toughness," *Polymer*, vol. 51, no. 9, pp. 1990–1999, 2010, doi: 10.1016/j.polymer.2010.02.051.

[49] H. Wang and H. Shi, "New impact-modified polycarbonate/polyester blends," *Plastics Research Online*, 2015, doi: 10.2417/spepro.005830.

[50] F. O. M. S. Abreu, M. M. C. Forte, and S. A. Liberman, "SBS and SEBS block copolymers as impact modifiers for polypropylene compounds," *J. Appl. Polym. Sci.*, vol. 95, no. 2, pp. 254–263, 2005, doi: 10.1002/app.21263.

[51] D. S. Parker, H.-J. Sue, J. Huang, and A. F. Yee, "Toughening mechanisms in core-shell rubber modified polycarbonate," *Polymer*, vol. 31, no. 12, pp. 2267–2277, 1990, doi: 10.1016/0032-3861(90)90312-M.

[52] J. Wang, X. Zhang, L. Jiang, and J. Qiao, "Advances in toughened polymer materials by structured rubber particles," *Progress in Polymer Science*, vol. 98, p. 101160, 2019, doi: 10.1016/j.progpolymsci.2019.101160.

[53] W. Yao, L. Wang, D. He, S. Jiang, L. An, and H. Zhang, "Toughening of polycarbonate with PBA-PMMA core-shell particles," *Chinese Journal of Polymer Science*, vol. 23, no. 3, pp. 337–340, 2005, doi: 10.1142/S0256767905000473.

[54] H. Xu, S. Tang, L. Yang, and W. Hou, "Toughening of polycarbonate by core-shell latex particles: Influence of particle size and spatial distribution on brittle-ductile transition," *Journal of Polymer Science Part B: Polymer Physics*, vol. 48, no. 18, pp. 1970–1977, 2010, doi: 10.1002/polb.22075.

[55] G. H. Michler and H.-H. K.-B. von Schmeling, "The physics and micro-mechanics of nano-voids and nano-particles in polymer combinations," *Polymer*, vol. 54, no. 13, pp. 3131–3144, 2013, doi: 10.1016/j.polymer.2013.03.035.

[56] S. Balakrishnan and N. R. Neelakantan, "Mechanical properties of blends of polycarbonate with unmodified and maleic anhydride grafted ABS," *Polymer International*, vol. 45, no. 4, 1998.

[57] X. Zhang, Y. Chen, Y. Zhang, Z. Peng, Y. Zhang, and W. Zhou, "Effects of ABS-g-MAH on mechanical properties and compatibility of ABS/PC alloy," *Journal of Applied Polymer Science*, vol. 81, no. 4, pp. 831–836, 2001, doi: 10.1002/app.1502.

[58] A. Garhwal and S. N. Maiti, "Fabrication of Super Tough Polycarbonate/Styrene-Etylene-Butylene-Styrene Grafted Maleic Anhydride (SEBS-g-MA) Blends: Morphological, Short Term Static Mechanical and Fracture Performance Interpretation," *Polymer-Plastics Technology and Materials*, vol. 58, no. 2, pp. 113–125, 2019, doi: 10.1080/03602559.2018.1466167.

[59] I. Debbah, R. Krache, N. Aranburu, M. Fernández, and A. Etxeberria, "Effect of SEBS-g-MAH addition on the mechanical, rheological, and morphological properties of polycarbonate/acrylonitrile–butadiene–styrene blends," *Journal of Elastomers & Plastics*, vol. 50, no. 7, pp. 611–633, 2018, doi: 10.1177/0095244317753652.

[60] M. Bera and P. K. Maji, "Effect of structural disparity of graphene-based materials on thermo-mechanical and surface properties of thermoplastic polyurethane nanocomposites," *Polymer*, vol. 119, pp. 118–133, 2017, doi: 10.1016/j.polymer.2017.05.019.

[61] S. Pavlidou and C. D. Papaspyrides, "A review on polymer-layered silicate nanocomposites," *Progress in Polymer Science*, vol. 33, no. 12, pp. 1119–1198, 2008, doi: 10.1016/j.progpolymsci.2008.07.008.

[62] S. Suin and B. B. Khatua, "Exfoliated and Optically Transparent Polycarbonate/Clay Nanocomposites Using Phosphonium Modified Organoclay: Preparation and Characterizations," *Industrial & Engineering Chemistry*, vol. 51, no. 46, pp. 15096–15108, 2012, doi: 10.1021/ie302209x.

[63] J.-I. Weon and H.-J. Sue, "Effects of clay orientation and aspect ratio on mechanical behavior of nylon-6 nanocomposite," *Polymer*, vol. 46, no. 17, pp. 6325–6334, 2005, doi: 10.1016/j.polymer.2005.05.094.

[64] A. J. Hsieh *et al.,* "Mechanical response and rheological properties of polycarbonate layered-silicate nanocomposites," *Polymer Engineering & Science*, vol. 44, no. 5, pp. 825–837, 2004, doi: 10.1002/pen.20074.

[65] P. J. Yoon, D. L. Hunter, and D. R. Paul, "Polycarbonate nanocomposites. Part 1. Effect of organoclay structure on morphology and properties," *Polymer*, vol. 44, no. 18, pp. 5323–5339, 2003, doi: 10.1016/S0032-3861(03)00528-7.

[66] P. J. Yoon, D. L. Hunter, and D. R. Paul, "Polycarbonate nanocomposites: Part 2. Degradation and color formation," *Polymer*, vol. 44, no. 18, pp. 5341–5354, 2003, doi: 10.1016/S0032-3861(03)00523-8.

[67] W. S. Chow and S. S. Neoh, "Mechanical, Morphological and Thermal Properties of Polycarbonate/SEBS-G-MA/Montmorillonite Nanocomposites," *Polymer-Plastics Technology and Engineering*, vol. 49, no. 1, pp. 62–68, 2009, doi: 10.1080/03602550903283034.

[68] V. Jankauskaitė, T. ŽUKAS, K. ŽUKIENĖ, and M. MALCIUS, "Low-weight Impact Behaviour of Carbon Fibre Reinforced Methyl Methacrylate Nanocomposites," *Materials Science*, vol. 21, no. 2, 2015, doi: 10.5755/j01.ms.21.2.7075.

[69] S. L. Costa, J. V. Silva, N. Peixinho, and J. P. Mendonça, "Advanced Metallic Solution for Toe Cap Component," *Proceedings of the ASME 2013 International Mechanical Engineering Congress and Exposition*, pp. 1–9, 2013.

[70] S. L. F. Costa, N. R. M. Peixinho, and J. P. M. A. Silva, "Metal toe cap for safety footwear," WO Patent 2015/015477 A1, Feb 5, 2015.

[71] X. Quan, "Rust-proof steel toecap," CN 203789267 U, Aug 27, 2014.

[72] L. Y. Henan, "Safety shoe aluminium alloy toe-cap production technology," CN 108866405 A, Nov 23, 2018.

[73] J. L. Williams, "Plastic toe cap and method of making," U.S. Patent 6,367,170 B1, Apr 9, 2002.

[74] D. K. Tailor, M. F. Lang, P. S. Hruska, and K. J. McConnell, "Fabric-faced thermoplastic composite panel," U.S. Patent 5,529,826, Jun 25, 1996.

[75] I. Ikegami, "Resin safety shoe toe cap," U.S. Patent 7,552,548 B2, Jun 30, 2009.

[76] Dalian Kancoo Die & Mould Technology Co.,Ltd, *Kancoo stamping die/transfer die for toe cap application.* [Online]. Available: https://kancoo.net/product/kancoo-stamping-die-transfer-die-for-toe-cap-application/ (accessed: Feb. 25 2020).

[77] M. Mongini, "Process and machine for producing metal alloy components," U.S. Patent 2005/0167074 A1, Aug 4, 2005.

[78] E. Irzmańska, "Case study of the impact of toecap type on the microclimate in protective footwear," *International Journal of Industrial Ergonomics*, vol. 44, no. 5, pp. 706–714, 2014, doi: 10.1016/j.ergon.2014.07.006.

[79] J. P. Riera, "Safety toe cap for footwear," European Patent 2 220 955 A1, Aug 25, 2010.

[80] K. P. Kurth, "Toe protection cap and footgear comprising toe protection cap," U.S. Patent 2011/0185602 A1, Aug 4, 2011.

[81] Paladin (Yangzhou) Footwear Co ., Ltd, *Safety Shoe Composite Toe Cap Model 604.* [Online]. Available: https://paladinyangzhou.en.ec21.com/Safety_Shoe_Composite_Toe_Cap–5358180_5358212.html (accessed: Feb. 25 2020).

[82] S. Costa, N. Peixinho, and J. P. Mendonça, "Design and Testing of a New Metallic Solution for Toecap Component on Safety Footwear," *Applied Mechanics and Materials*, 44-47, pp. 1460–1464, 2011, doi: 10.4028/www.scientific.net/AMM.44-47.1460.

[83] N. Peixinho, S. Costa, and J. Mendonça, "Impact Behaviour of Safety Shoe High Strength Steel Parts," *Engineering Transactions*, vol. 66, no. 2, pp. 175–185, 2018.

[84] C.-C. Yang, "Development of High Strength Composite Toecaps Using LS-DYNA," Master of Engineering, Centre for Advanced Composite Materials / Department of Mechanical Engineering, The University of Auckland, New Zealand, 2010.

[85] S. Gaur, "Thermal Analysis of Safety Shoe Toe Cap," *International Journal of Innovative Technology and Exploring Engineering*, vol. 8, 12S, 2019, doi: 10.35940/ijitee.L1060.10812S19.

[86] K. E. Beschorner, D. L. Albert, and M. S. Redfern, "Required coefficient of friction during level walking is predictive of slipping," *Gait & posture*, vol. 48, pp. 256–260, 2016, doi: 10.1016/j.gaitpost.2016.06.003.

[87] R. M. Silva, J. L. Rodrigues, V. V. Pinto, M. J. Ferreira, R. Russo, and C. M. Pereira, "Evaluation of shock absorption properties of rubber materials regarding footwear applications," *Polymer Testing*, vol. 28, no. 6, pp. 642–647, 2009, doi: 10.1016/j.polymertesting.2009.05.007.

[88] I.-J. Kim, "Identifying shoe wear mechanisms and associated tribological characteristics: Importance for slip resistance evaluation," *Wear*, 360-361, pp. 77–86, 2016, doi: 10.1016/j.wear.2016.04.020.

[89] T. Jones, A. Iraqi, and K. Beschorner, "Performance testing of work shoes labeled as slip resistant," *Applied ergonomics*, vol. 68, pp. 304–312, 2018, doi: 10.1016/j.apergo.2017.12.008.

[90] C. H. Bang, T. G. Kim, and J. S. Kim, "Evaluation of Slip Resistance of Safety Footwear Using Novel Equipment," *Key Engineering Materials*, vol. 627, pp. 461–464, 2015, doi: 10.4028/www.scientific.net/KEM.627.461.

[91] P. Caravaggi, A. Giangrande, G. Lullini, G. Padula, L. Berti, and A. Leardini, "In shoe pressure measurements during different motor tasks while wearing safety shoes: The effect of custom made insoles vs. prefabricated and off-the-shelf," *Gait & posture*, vol. 50, pp. 232–238, 2016, doi: 10.1016/j.gaitpost.2016.09.013.

[92] J. S. Kim, "A Comparison of Slip Resistance Between the Grinded Outsoles and New Ones of Fire Fighter's Shoes," *Procedia Engineering*, vol. 45, pp. 868–874, 2012, doi: 10.1016/j.proeng.2012.08.251.

[93] H. Ramsay and C. Senneck, "Anti-slip studs for safety footwear," *Applied ergonomics*, vol. 3, no. 4, pp. 219–223, 1972, doi: 10.1016/0003-6870(72)90104-4.

[94] S. Chen, J. Jin, and E. Lou, "Toward Slip and Fall Prevention: Exploring the Guidance and Challenges of Anti-slip Footwear," *Procedia Engineering*, vol. 43, pp. 364–368, 2012, doi: 10.1016/j.proeng.2012.08.063.

[95] R. M. Silva and A. Oliveira, "Evolução dos Materiais Termoplásticos na Indústria do Calçado," Guia do Empresário por Centro Tecnológico do Calçado de Portugal - Projecto imatec, 2012.

[96] IAL Consultants, *Global Overview of the Thermoplastic Polyurethane (Tpu) Market*. 2016. [Online]. Available: http://www.ialconsultants.com/uploads/CUBE_press_release/2016-01-22/TPU press release 2016.pdf (accessed: Feb. 25 2020).

[97] I. P. Fernandes *et al.,* "Biobased Additives as Biodegradability Enhancers with Application in TPU-Based Footwear Components," *Journal of Renewable Materials*, vol. 4, no. 1, pp. 47–56, 2016, doi: 10.7569/JRM.2015.634126.

[98] D. J. T. Hill, M. I. Killeen, J. H. O'Donnel, P. J. Pomery, D. St. John, and A. K. Whittaker, "Development of wear-resistant thermoplastic polyurethanes by blending with poly(dimethyl siloxane). I. Physical properties," *Journal of Applied Polymer Science*, vol. 61, no. 10, pp. 1757–1766, 1996, doi: 10.1002/(SICI)1097-4628(19960906)61:10<1757::AID-APP16>3.0.CO;2-#.

[99] M. Kannan, S. Thomas, and K. Joseph, "Flame-retardant properties of nanoclay-filled thermoplastic polyurethane/polypropylene nanocomposites," *Journal of Vinyl & Additive Technology*, vol. 23, S1, E72-E80, 2017, doi: 10.1002/vnl.21523.

[100] P. K. Maji and A. K. Bhowmick, "Structure-property correlation of polyurethane nanocomposites: Influence of loading and nature of nanosilica and microstructure of hyperbranched polyol," *Journal of Applied Polymer Science*, vol. 127, no. 6, pp. 4492–4504, 2013, doi: 10.1002/app.38063.

[101] V. B. Mohan, K. Lau, D. Hui, and D. Bhattacharyya, "Graphene-based materials and their composites: A review on production, applications and product limitations," *Composites Part B: Engineering*, vol. 142, pp. 200–220, 2018, doi: 10.1016/j.compositesb.2018.01.013.

[102] B. Golaz, S. Tetouani, N. Diomidis, V. Michaud, and S. Mischler, "Processing and tribology of thermoplastic polyurethane particulate composite materials," *Journal of Applied Polymer Science*, vol. 125, no. 5, pp. 3745–3754, 2012, doi: 10.1002/app.36543.

[103] G. Mittal, V. Dhand, K. Y. Rhee, S.-J. Park, and W. R. Lee, "A review on carbon nanotubes and graphene as fillers in reinforced polymer nanocomposites," *Journal of Industrial and Engineering Chemistry*, vol. 21, pp. 11–25, 2015, doi: 10.1016/j.jiec.2014.03.022.

[104] T. R. Hull, A. Witkowski, and L. Hollingbery, "Fire retardant action of mineral fillers," *Polymer Degradation and Stability*, vol. 96, no. 8, pp. 1462–1469, 2011, doi: 10.1016/j.polymdegradstab.2011.05.006.

[105] H. Pi, S. Guo, and Y. Ning, "Mechanochemical Improvement of the Flame-Retardant and Mechanical Properties of Zinc Borate and Zinc Borate-Aluminum Trihydrate-Filled Poly (vinyl chloride)," *Journal of Applied Polymer Science*, vol. 89, no. 3, pp. 753–762, 2003, doi: 10.1002/app.12202.

[106] S. D. Shaw *et al.,* "Halogenated flame retardants: do the fire safety benefits justify the risks?," *Reviews on environmental health*, vol. 25, no. 4, pp. 261–305, 2010, doi: 10.1515/reveh.2010.25.4.261.

[107] R. J. Law *et al.,* "Levels and trends of brominated flame retardants in the European environment," *Chemosphere*, vol. 64, no. 2, pp. 187–208, 2006, doi: 10.1016/j.chemosphere.2005.12.007.

[108] T. Guler, U. Tayfun, E. Bayramli, and M. Dogan, "Effect of expandable graphite on flame retardant, thermal and mechanical properties of thermoplastic polyurethane composites filled with huntite&hydromagnesite mineral," *Thermochimica Acta*, vol. 647, pp. 70–80, 2017, doi: 10.1016/j.tca.2016.12.001.

[109] C. Aschan, M. Hirvonen, E. Rajamäki, and T. Mannelin, "Slip resistance of oil resistant and non-oil resistant footwear outsoles in winter conditions," *Safety Science*, vol. 43, no. 7, pp. 373–389, 2005, doi: 10.1016/j.ssci.2005.08.001.

[110] D. P. Manning, C. Jones, F. J. Rowland, M. Roff, and D. P. Manning, "The Surface Roughness of a Rubber Soling Material Determines the Coefficient of Friction on Water-Lubricated Surfaces," *Journal of Safety Research*, vol. 29, no. 4, pp. 275–283, 1998, doi: 10.1016/S0022-4375(98)00053-X.

[111] I.-J. Kim, "Wear Observation of Shoe Surfaces: Application for Slip and Fall Safety Assessments," *Tribology Transactions*, vol. 58, no. 3, pp. 407–417, 2015, doi: 10.1080/10402004.2014.980593.

[112] R. Grönqvist, "Mechanisms of friction and assessment of slip resistance of new and used footwear soles on contaminated floors," *Ergonomics*, vol. 38, no. 2, pp. 224–241, 1995, doi: 10.1080/00140139508925100.

[113] K. W. Li, W.-R. Chang, T. B. Leamon, and C. J. Chen, "Floor slipperiness measurement: friction coefficient, roughness of floors, and subjective perception under spillage conditions," *Safety Science*, vol. 42, no. 6, pp. 547–565, 2004, doi: 10.1016/j.ssci.2003.08.006.

[114] R. Grönqvist *et al.,* "Human-centred approaches in slipperiness measurement," *Ergonomics*, vol. 44, no. 13, pp. 1167–1199, 2001, doi: 10.1080/00140130110085556.

[115] *Personal protective equipment - Footwear - Test method for slip resistance*, ISO 13287:2012, 2012.

[116] C. Aschan, M. Hirvonen, E. Rajamäki, T. Mannelin, J. Ruotsalainen, and R. Ruuhela, "Performance of slippery and slip-resistant footwear in different wintry weather conditions measured in situ," *Safety Science*, vol. 47, no. 8, pp. 1195–1200, 2009, doi: 10.1016/j.ssci.2009.01.006.

[117] Z. S. Bagheri, N. Patel, Y. Li, K. Morrone, G. Fernie, and T. Dutta, "Slip resistance and wearability of safety footwear used on icy surfaces for outdoor municipal workers," *Work*, vol. 62, no. 1, pp. 37–47, 2019, doi: 10.3233/WOR-182840.

[118] *Personal protective equipment - Test methods for footwear*, ISO 20344:2011(E), 2011.

[119] RHINO SHOE, *Rhino Shoe Safety Footwear.* [Online]. Available: https://rhinoshoe.com/images/RHINO%20SHOE%20Catalogue.pdf (accessed: Nov. 9 2020).

[120] J. W. Ludemann, J. Behnke, P. W. Brabson, A. Barker, and X. Tong, "Polyurethane injected boot assembly and associated manufacturing method," U.S. Patent 9,642,416, May 9, 2017.

[121] K. A. Thomas and R. G. Rinehart, "Rubber footwear with neoprene layer," U.S. Patent 2004/0,020,077 A1, Feb 5, 2004.

[122] M. Sagripanti, "Method for manufacturing shoe soles with composite structure and such shoe soles," WO 2009/095935 A1, Aug 6, 2009.

[123] D. Janson, S. T. Newman, and V. Dhokia, "Next Generation Safety Footwear," *Procedia Manufacturing*, vol. 38, pp. 1668–1677, 2019, doi: 10.1016/j.promfg.2020.01.117.

CHAPTER 3

3 STRUCTURE-PROPERTIES RELATIONSHIP FOR TAILORING POLYCARBONATE

Abstract: This chapter presents a systematic study of PC blends and PC (nano)composites to access its ductile to brittle transition mode. Different PC grades were blended with two elastomeric material grafted with maleic anhydride, namely acrylonitrile-butadiene-styrene (ABS-*g*MA) and styrene-ethylene-butylene-styrene rubber (SEBS-*g*MA). Nanoclay and natural cotton waste incorporation was also investigated. All materials were prepared in a batch mixer and specimen for mechanical tests were prepared through compression molding. Structural analysis was accessed using infrared spectroscopy, quasi-static and impact tests for mechanical performance evaluation, scanning electron microscopy to analyze morphology, and optical microscopy for impact fracture behavior. The results demonstrate that processing conditions (shear rate, temperature, mixing time) severely affects the mechanical performance of neat PC, changing its ductile fracture mode to brittle. Blending with the elastomeric polymers increase toughness. Stress whitening was mostly detected for PC/ABS-*g*MA blends, while for PC/SEBS-*g*MA toughening mechanism was due to cavitation and debonding phenomena. Also, blending both SEBS-*g*MA and ABS-*g*MA with PC prevented the modified ABS from fractured during cryogenic cleavage.

Keywords: polycarbonate, toughening, rubber, nanocomposites

Submitted to Journal of Materials & Design

3.1 Introduction

Polycarbonate (PC) is widely used in different application due to the combination of distinct properties. Good optical transparency and good thermal resistance combined with excellent impact performance makes PC suitable for shield protector applications, optics in automobile industry, protective glasses, food packaging, compact disks, structural components, or even astronaut helmets [1–3]. Despite these advantages, some drawbacks have driven many researchers to investigate ways to overcome, for example, its high melt viscosity which requires high pressures and temperatures for processing, improving the material's notch sensitivity. Additionally, PC has a tendency to suffer crazing from direct sun light, chemicals and organic solvent exposure, or even from hot water, influencing the notch sensitivity problem [4–6]. Also, hydrolysis degradation during processing can have an effect on optical application since it induces color (yellowing) and transparency change [7]. Therefore, PC systems with rubber materials or inorganic reinforcements are reported in literature to toughen and provide chemical and thermal resistance to PC [8–18].

Acrylonitrile-butadiene-styrene (ABS) polymer is often used to toughen PC. In fact, their blends are well known engineering polymers widely used in the industry. This polymer combination can substantially decrease the melt viscosity, improve thermal stability, improve notch sensitivity and enhances the resistance to hydrolysis [19, 20]. Due to the chemical nature of both polymers, there is no compatibility between phases, which compromises performance at higher loading contents [21]. One way to improve phase adhesion is by using core-shell particles that will work as a compatibilizer, the shell is surrounded by a crosslinked rubber, for example, methyl methacrylate, butadiene, styrene core-shell [22, 23]. Another way to improve compatibility is to modify one of the polymers by grafting functional groups that can improve affinity or react with the other polymer, thus decreasing the interfacial energy. ABS is reported to be grafted with glycidyl methacrylate (GMA) or with maleic anhydride (MA) [21, 24, 25]. Also, styrene-acrylonitrile based terpolymers with GMA or MA are reported to be used in PC/ABS alloys [26]. ABS-*g*-MA has been the subject of intensive study as a compatibilizer agent in immiscible systems. Balakrishnan and Neelakantan studied the mechanical properties of PC/ABS and PC/ABS-*g*-MA blends and noticed a drastic increase in impact strength (almost x10 more) in PC/ ABS-*g*-MA (75/25, w/w) blend, over unmodified ABS, and attributes this behavior to an improvement in interfacial adhesion due to the chemical reaction between MA and hydroxyl terminal groups of PC (-OH) [8]. Zhang *et al.* study the effect of ABS-*g*-MA as a compatibilizer of PC/ABS blends, showing that impact strength double with the incorporation of 10 wt.% ABS-*g*-MA on a blend of PC/ABS (70/30, w/w) [25].

Styrene-ethylene-butylene-styrene rubber grafted with MA (SEBS-*g*-MA) is also reported to be used as a toughening agent in PC systems. Horiuchi *et al.* observed a substantial improvement at the elongation at break of PC/polyamide blends with the incorporation of 10 wt.% SEBS-*g*-MA, but at the cost of the elastic modulus, decreasing the elastic modulus and yield stress [27]. Debbah *et al.* have used this rubber to enhance the mechanical properties of PC/20 wt.% ABS blends, increasing impact strength more than 33% with only 1 wt.% of SEBS-*g*-MA, alongside an increase in tensile strength, modulus and elongation at break, but all mechanical properties reduced at higher amounts of compatibilizer [28]. Garhwal and Maiti studied the incorporation of different amounts of SEBS-*g*-MA onto PC and noticed distinct fracture behavior from lower (cavitation) to higher (crazing) rubber content, which attribute to a substantial increase in impact strength [29]. Chow and Neoh investigated the effect of SEBS-*g*-MA as a toughening agent in PC/nanoclay systems and observed an increase in impact strength and elongation at break up to 260 and 240%, respectively [15]. This behavior was attributed to cavitation and debonding phenomena of rubber phase that helps to dissipate the impact energy. It is believed that higher melt viscosity in polymeric systems containing nanoclays results in higher mechanical properties, since higher hydrodynamical stresses developed during melt processing provides better nanoclay exfoliation [18]. Taşdemır *et al.* compared the reinforcement effect of natural fibers from textile waste industry, silk and cotton, onto recycled PC, and found out that the longest cotton fibers (5 mm) doubled toughness, while silk fibers did not improve mechanical properties of PC. These results were attributed to the better compatibility between the PC matrix and cotton which presented good wettability [30].

Fracture behavior of PC depends of several factors, such as molecular weight, thickness, aging, service temperature, strain-rate, processing conditions and notch radius [31, 32]. These parameters dictate the ductile to brittle transition failure mode of PC. Ductile fracture mode is a plane stress condition that mainly occurs in thin bodies, where all stresses are placed on the same plane and the normal stress is considered to be negligible ($\sigma_z = 0$). Moreover, in thicker bodies the brittle fracture mode is associated to a plane strain condition, characterized by zero strain at the normal direction of the crack path ($\varepsilon_z = 0$) caused by triaxial conditions [33]. Under normal conditions, PC presents a ductile behavior and may fail in a brittle mode under notches with smaller radius, at high speed deformations, in plain strain conditions or at low temperatures [31, 34]. Blending ductile polymers, like PC, with rubbery phases is one way to prevent brittle failure. Shear yielding of the matrix phase and cavitation of the rubber phase are the main toughening mechanisms of this kind of systems, providing a better way to dissipate the energy without a catastrophic failure [31]. In brittle polymers, such as polystyrene homopolymer, toughening with rubbery

particles is also performed, and the toughening mechanism associated is mostly crazing (appearance of crazes with crack initiation), with shear yielding and cavitation at a low extent [31, 32].

This work investigates ways to improve PC drawbacks (notch sensitivity and high melt viscosity), through blending with elastomeric polymers (ABS-*g*MA and SEBS-*g*MA), incorporation of nanoclay and natural cotton waste. A systematic study is presented to evaluate the influence of the rubbers and reinforcements on PC properties under the same conditions. Composition morphology and glass transition temperature were assessed by electronic microscopy and differential scanning calorimetry, respectively, and mechanical characterization performed through quasi-static and impact tests. Optical microscopy was used to study the impact fracture behavior of the tested samples.

3.2 Experimental

3.2.1 Material

Acrylonitrile Butadiene Styrene (ABS) Terluran GP-22 was purchased from BASF. Three different grades of Polycarbonate (PC): Lexan LUX2180T (PC_{Lux}) and Lexan 103r (PC_{Lr}) were obtained from Sabic co., and Makrolon ET3137 (PC_M) from Covestro (Table 3.1). Styrene-Ethylene-Butylene-Styrene thermoplastic elastomer grafted with maleic anhydride (SEBS-*g*MA) Taipol 7126 was kindly supplied by TER® AS Chemicals. Cloisite 15A (C15A) was obtained from BYK Additives. Maleic anhydride (MA) with a purity of 99% and extra pure styrene (St) with a purity of 99% were purchased from Acros Organics, and dicumyl peroxide with a purity of 98% (DCP) from Alfa Aesar. These materials were used to chemically modify ABS with grafted MA (ABS-*g*MA). Natural cotton waste (NCW) from textile industry was kindly provided by a Portuguese company.

Table 3.1: Properties of PC grades from technical data sheet.

				Properties					
			MVR*	E	σ [MPa]		ε [%]		Charpy v-notch
			300°C/	1 mm/s	50 mm/s				23°C ISO
Code name	PC grade	Producer	1.2kg [cm^3/10min]	[MPa]	yield	break	yield	break	179/1eA [kJ/m^2]
PC_{Lux}	Lexan LUX2180T	Sabic	18	2 350	62	69	6	100	65
PC_{Lr}	Lexan 103r	Sabic	6	2 350	63	70	6	120	75
PC_M	Makrolon ET3137	Covestro	6	2 400	66	70	6.3	125	78

*Melt Volume Rate

3.2.2 Sample preparation

3.2.2.1 Grafting ABS with MA

ABS modification took place on a Haake Rheometer batch mixer (Haake Rheomix Roller Roters R600, volume 69 cm^3) with counter-rotating rotors. ABS was modified with 5 wt % of MA and 1 wt.% DPC, using 3.3 wt.% St as comonomer. The reaction was performed using the following steps: first, ABS was introduced inside the mixer and left around 1 min, then MA, followed by DPC and St, were added. An average melt temperature of 190 °C, 60 rpm and 4 min reaction time was used for processing.

3.2.2.2 Materials preparation in the mixer

Firstly, all materials were dried overnight in a vacuum oven at 105°C (polycarbonates, NCW) and at 80°C (ABS, ABS-*g*MA, SEBS-*g*MA, C15A), to avoid the hydrolysis of polymers during processing. Blending of different PC grades (PC_{Lux}, PC_{Lr}, PC_M) with ABS, ABS-*g*MA, SEBS-*g*MA, and incorporation of nanoclay (C15A) and natural cotton (NCW), were prepared in the same equipment used for ABS grafting, with the processing conditions reported in Table 3.2. Processing parameters (temperature, rotors speed, and mixing time) were previously optimized in order to diminish the thermal-oxidative degradation effect experienced at high hydrodynamic conditions, which has a negative influence on optical and mechanical properties of PC [7]. The degradation was visible by the yellowing effect of PC. Regarding the PC_M/ABS-*g*MA systems, two approaches for ABS modification were tested. One was to previously graft MA onto ABS and afterwards proceeding with the blending process (two steps process). In the other, grafting and blending took sample at the same time (one step process).

After processing, all materials were recovered in a metallic plate and left to cool under ambient conditions. Following this, milling took place on a Grindo Granulator with a 5 mm diameter sieve.

Table 3.2: PC systems, processing conditions and respective nomenclature.

									Processing conditions		
									$\overline{T_m}$	**Screw**	t_{mixing}
	Sample code		**Weight [%]**						[°C]	[rpm]	[min]
			ABS	**MA**	**St**	**DCP**					
ABS	ABS		100						200	60	5
	ABS-*g*MA		90.7	5	3.3	1					
			PC	**C15A**	**SEBS-*g*-MA**		**NCW**				
PC_{Lux} or PC_M	PC_{Lux}	PC_M	100						230	80	5
	PC_{Lux}_00	PC_M_00	100								
	PC_{Lux}_01	PC_M_01	97	3							
	PC_{Lux}_02	PC_M_02	85		15						
	PC_{Lux}_03	PC_M_03	82	3	15						
	PC_{Lux}_04	PC_M_04	97				3				
			PC	**ABS-*g*-MA**	**ABS**	**MA**	**St**	**DCP**			
PC_M	PC_M_10%ABS-*g*MA		90	10					230	80	5
	PC_M_25%ABS-*g*MA		75	25							
	PC_M_25%ABS-react*		75		22.675	1.250	0.825	0.250			
			PC	**ABS-*g*-MA**	**SEBS-*g*-MA**		**NCW**				
PC_{Lr}	PC_{Lr}		100						230	80	5
	PC_{Lr}_00		100								
	PC_{Lr}_01		99		1						
	PC_{Lr}_02		90	10							
	PC_{Lr}_03		89	10	1						
	PC_{Lr}_04		87	10			3				
	PC_{Lr}_05		86	10	1		3				

*MA grafting onto ABS took place alongside blending with PC, with the same wt.% MA, St and DCP (5/3.3/1) relative to ABS

3.2.2.3 Specimens preparation

Prior to specimen manufacturing, the blends were dried at 90°C in a vacuum oven overnight. A rectangle sheet (230×90×3 mm) was prepared by compression molding with the processing conditions indicated in Table 3. Dumbbell and rectangle specimens for quasi-static and impact tests (Figure 3.1), respectively, were cut from the rectangular sheet using a high speed laser cut with the settings indicated in Table 3.3. All the specimens were stored and kept under laboratory conditions (21°C, 50% RH) for at least 48h prior to testing.

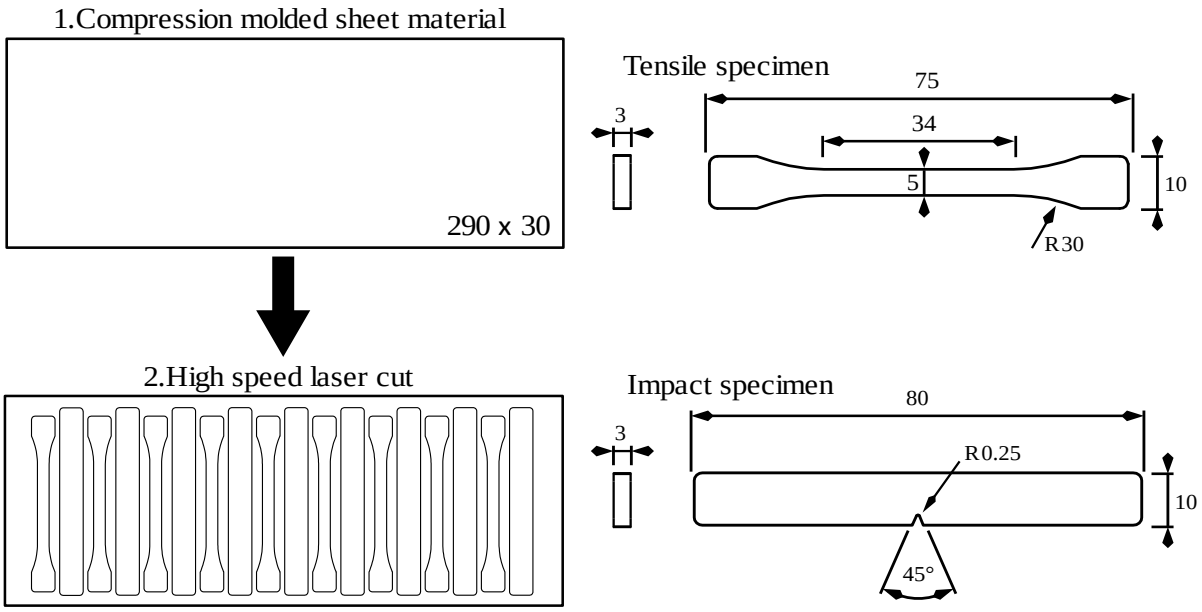

Figure 3.1: Specimen preparation through 1. compression molding and 2. laser cut, and tensile / impact specimen dimensions in mm.

Table 3.3: Compression molding cycle, and laser cut conditions used for specimen production.

	Compression cycle							Laser cut conditions	
Pressure [tons]	0 – 0	0 – 2	2 – 0	0 – 5	5 –0	0 – 10	10 – 10	Power [%]	v [mm/s]
Time [min]	5	2	0.5	2	0.5	1	colling	75	22

3.2.3 Characterization

3.2.3.1 Structural analysis and grafting degree

Fourier transform infrared (FT-IR) spectroscopy (Jasco FT/IR 4100) in transmission mode was used to access the chemical structure of the blends, and the MA grafting degree (GD) of purified grafted ABS, from a range of 400 – 4500 cm^{-1}. For the latter, purification of ABS-*g*-MA sample was performed by dissolution in acetone for unreacted MA removal, precipitation and washing several times in methanol. The recovered material was dried at 180°C during 1h under constant nitrogen flow. The grafting degree was calculated (wt.% MA) using a linear calibration curve was built with different ABS/MA content (m = 1.35), following Equation (3.1), correlating the absorption peaks at 1 780 and 2 237 cm^{-1} of carbonyl (-C = O) of MA and ABS nitrile groups (-C ≡ N), respectively [35].

$$GD\ (wt.\%MA) = m \times \frac{abs.CO_{1780}}{abs.CN_{2237}} \tag{3.1}$$

3.2.3.2 Mechanical characterization

3.2.3.2.1 Quasi-static tensile tests

A universal tensile testing machine Instron 5969 (Instron, EUA) with a load cell of 5 kN was used to test the quasi-static tensile behavior of the prepared materials, at 23 °C and 50% RH. The stress (σ) was evaluated using the engineering stress definition in ISO 527 [36], Equation (3.2), Where F is the force recorded by the load cell and A_o is the initial cross-sectional area.

$$\sigma = \frac{F}{A_0} \tag{3.2}$$

The strain (ε) was defined according to the engineering strain definition reported in ISO 527 [36], Equation (3.3), where dl is the displacement recorded by the tensile apparatus and l_0 is the initial distance between grips.

$$\varepsilon = \frac{dl}{l_0} \tag{3.3}$$

The tensile properties evaluated were the yield stress (σ_y) and strain (ε_y), elastic modulus (E), stress (σ_r) and strain at break (ε_r) and modulus of toughness (U). E was calculated using a cross-head velocity of 1 mm/min from the engineering stress- strain curve ($\sigma - \varepsilon$). Afterwards, the cross-head speed was changed to 50 mm/min to assess the remaining mechanical parameters. U was assessed by integrating the engineering stress over the engineering strain. At least 5 specimens of each composite were analyzed. The specimen dimension is displayed in Figure 3.1.

3.2.3.2.2 Impact Tests

Charpy impact characterization with a 2 mm v-notch was performed on an impact test CEAST, using rectangular shape 80 x 10 x 3 specimens, according to ISO 179-1. The tests were performed according to the procedure defined in ISO 179-1[37]. The geometry of the specimen is depicted in Figure 3.1. The impact strength was determined following Equation (3.4), where E_C is the fracture energy in Joules read from the equipment, h the specimen thickness, and b_N the width at the impact zone. At least 5 specimens of each composite were analyzed.

$$a_{CN} = \frac{E_C}{h \times b_N} \times 10^3 \ [kJ/m^2] \quad (3.4)$$

3.2.3.3 Thermal characterization

The thermal behavior of the samples was analyzed using a DSC Netzsch 200 Maya (Netzsch, Germany) equipment. The tests were performed under nitrogen atmosphere with a heating rate of 10°C/min from 30 to 180 °C. Even though two heating cycles were performed, only the second was used since the first was used to erase the thermal history of the material. Glass transition was determined following the midpoint method disclosed in ASTM D3418-15 [38].

3.2.3.4 Fracture surface and Morphological characterization

To analyze the morphology between the different blends, the samples were fractured in liquid nitrogen, coated with a gold thin film, and analyzed by Scanning Electron Microscope (SEM) using a FEI Quanta 400 (FEI, The Netherlands), operating at a voltage of 10 kV.

An optical microscope DMS 1000 (Leica, Germany) coupled with a light polarizer was used to access the fracture mechanic behavior that occurred during impact tests.

3.3 Results and Discussion

3.3.1 Grafting degree evaluation

The IR absorbance spectra of ABS, ABS-*g*-MA before and after purification, and the torque curves are shown in Figure 3.2. The torque curves (Figure 3.2-b), demonstrate the ABS introduction into the chamber at ~190 °C with continuous mixing during 1 min allowing it to became a viscous fluid. The introduction of cold polymeric granules is evidenced by a decrease on the average temperature and an increase in torque. After torque stabilization, MA, DCP and St were added, and the grafting reaction takes place. Since peroxide degradation is an exothermic process, the energy released during radical formation will increase the temperature of the system [39]. This is consistent with a rapidly increase in temperature around 1.6 – 2 min interval. The final torque of modified ABS is lower than its neat counterpart, which could be a result of polymeric chain degradation (scission) or the lubricant effect of the residual MA [40, 41]. The appearance of tree new bands at 1 859 and 1 781 cm^{-1} of asymmetric and symmetric C=O stretching, respectively, and 1 683 cm^{-1} of C=C stretching of styrene vinylic group, confirms a successful incorporation of MA [42, 43]. Calculated GD before purification was 4.5 wt.%, which is compatible with

the total wt.% of MA used. After ABS-*g*MA purification, the intensity of C=O decreases and C=C band disappears due to the removal of unreacted MA and St, lowering GD value to 3.8 wt.%.

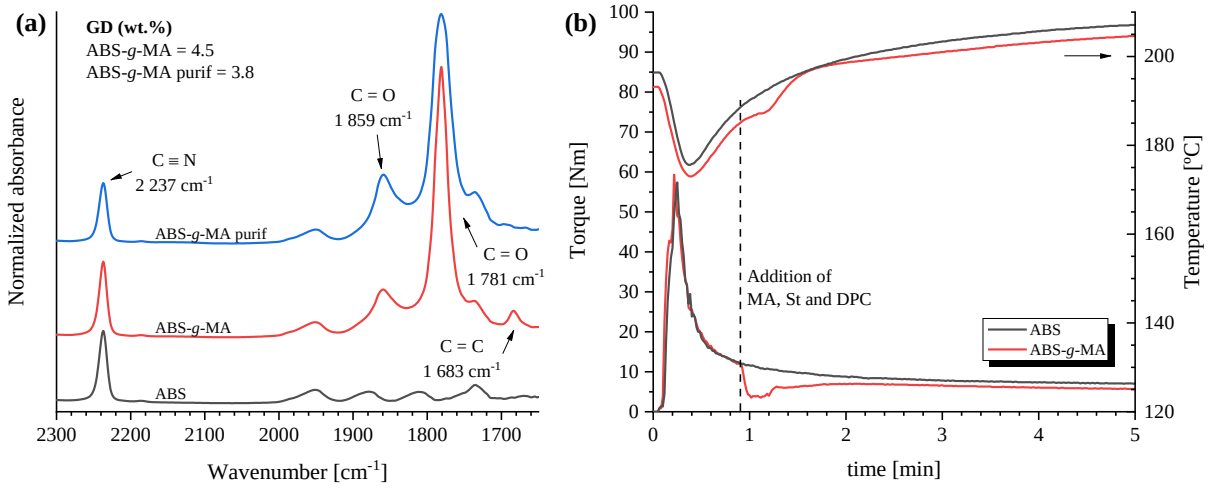

Figure 3.2: IR absorbance spectra of ABS, non-purified and purified ABS-g-MA (a), and Torque and Temperature curves of MA grafting reaction (b).

IR absorbance spectra of PC_{Lr} blended with SEBS-*g*MA, ABS-*g*MA and incorporating NCW are presented in Figure 3. Due to the intense band of PC carbonate groups at 1 770 cm^{-1} (C=O stretching) and between the range of 1 300 – 1 130 cm^{-1} (C-O-C stretching), it is difficult to observe the C=O band of MA for the PC/ABS-*g*MA blends [44, 45]. However, it is possible to observe the appearance of a sharp peak at 2 237 cm^{-1} related to the vibration of C≡N from the acrylonitrile branch of ABS, as well as new peak at 761 and 701 cm^{-1} from olefinic C-H out of plane bending vibration from polybutadiene branch [46]. The composites with NCW (PC_{Lr}_04 and PC_{Lr}_05), a -OH band is detected in the range of 3600 – 3100 cm^{-1} region, due to the -OH cellulose groups [47]. In the literature is reported that MA groups chemically react with the hydroxyl groups of cellulose [48]. The addition of only 1wt.% SEBS-*g*MA (PC_{Lr}_05) decreases substantially the concentration of -OH, which could indicate a better affinity between SEBS-*g*MA/NCW, than ABS-*g*MA/NCW.

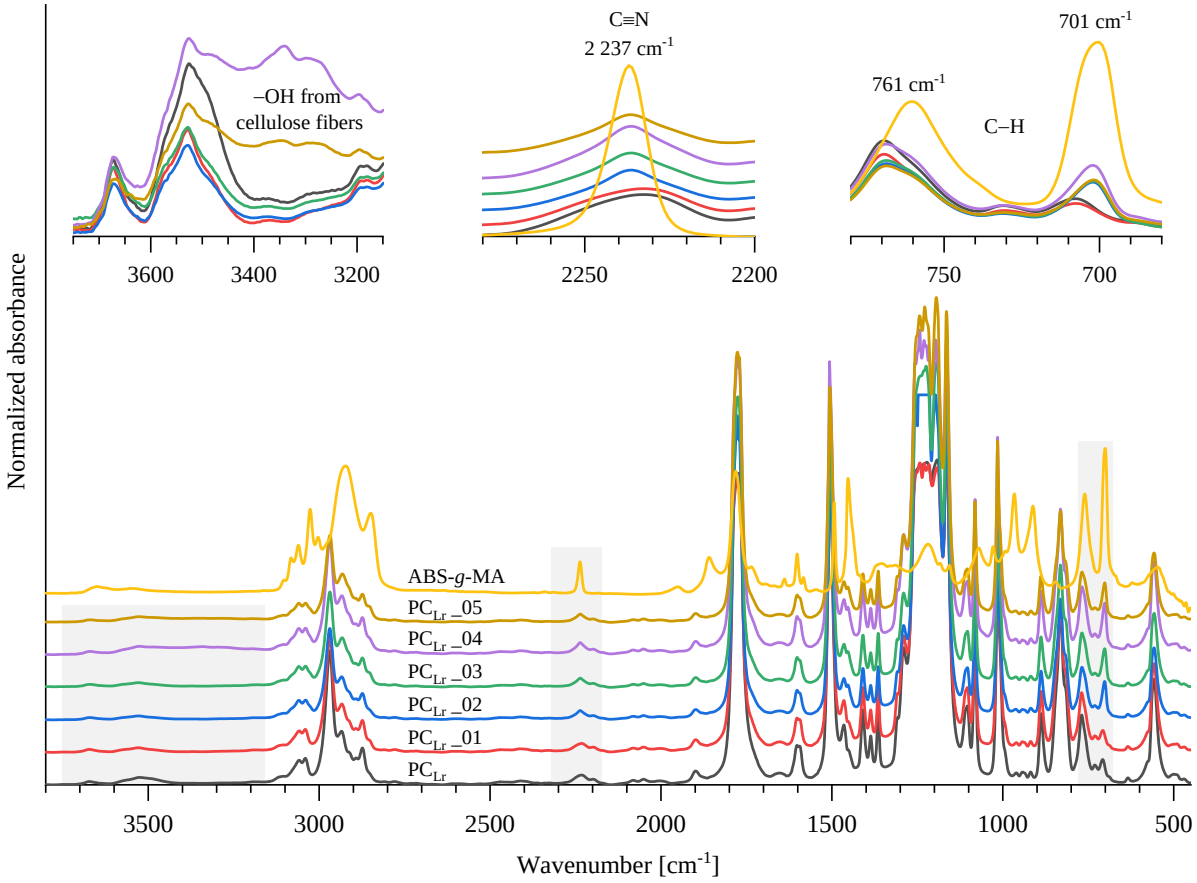

Figure 3.3: IR absorbance spectra of PC_{Lr} blends and ABS-g-MA.

3.3.2 Torque and structural analysis of blends

Torque and temperature plots as a function of time for the produced PC blends are displayed in Figure 3.4. PC torque is in accordance with respective MVR technical data sheet (Table 3.1), where PC_M and PC_{Lr} have similar MVR, and PC_{Lux} has a higher value. Comparing both PC_M and PC_{Lux} with the same systems (Figure 3.4 a-b), the incorporation of 3wt.% of nanoclay (PC_{Lux}_01 and PC_M_01), 1 min after adding PC, decreases the torque and temperature in a similar way. A different behavior has been described in literature, with clay content increasing the viscosity of polymeric systems due to polymeric chain entanglement between the layered clay [49, 50]. The use of 15wt.% SEBS-*g*MA (PC_{Lux}_02 and PC_M_02) also decreases the torque and is more pronounced for the PC with higher viscosity (PC_M). In the PC_M_03 system, the introduction of 3wt.% of nanoclay raises the torque of the PC/15wt.% SEBS-*g*MA blend. The addition of 3wt.% of NCW (PC_{Lux}_04 and PC_M_04) does not significantly impact the evolution of torque.

Blends of PC_M with ABS-*g*MA (Figure 3.4-c), show a decrease of the final torque value (Figure 3.5), and the average temperature curve lowers as the amount of ABS-*g*MA increases. This is to be expected since the ABS-g-MA has a lower viscosity. Moreover, the overall peroxide quantity is lower when comparing both ABS grafting routes (two steps and one step), the increase in temperature seconds after the addition of peroxide is not perceptible, and the variation in torque is higher for the one step process, which could be explained by the presence of unreacted MA acting as a lubricant.

While the blend containing 1wt.% SEBS-*g*MA (PC_{Lr}_01) increased the torque, the remaining materials had an opposite effect. The effect of blending or incorporation are more evident for both PC_{Lux} and P_M, PC_{Lr} shows a sightly change but its behavior is similar to the matrix it-self. This can be clearly noticed from Figure 3.5 that the final torque and temperature are similar for PC_{Lr}_02 to PC_{Lr}_05.

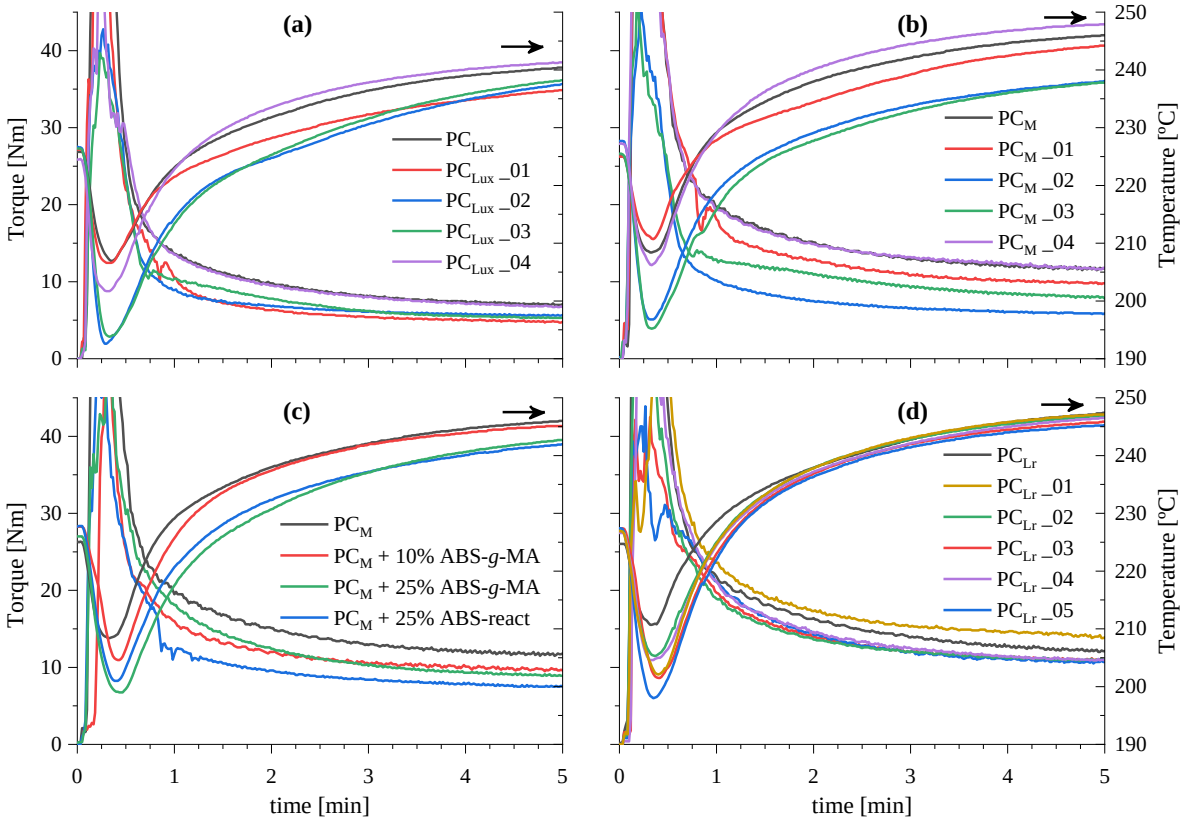

Figure 3.4: Torque and average temperature curves of (a) PC_{Lux}, (b and c) PC_M and (d) PC_{Lr} blends.

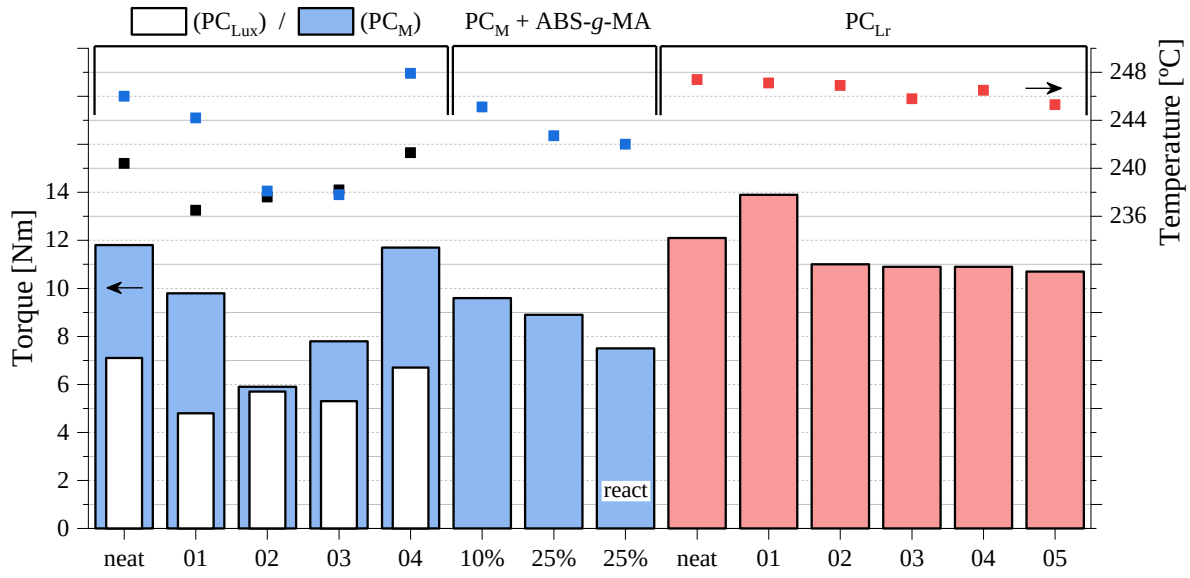

Figure 3.5:Torque and average temperature of blends, after 5 minutes mixture time.

3.3.3 Blends Morphology

The cross-section morphology of cryogenic fracture samples for PC_M and PC_{Lr} systems are displayed in Figure 3.6, Figure 3.7 and Figure 3.8 at different magnification scales. The morphology observed in both PCs is typical of a single polymer, with a clear and smooth surface (Figure 3.6-a and Figure 3.8-a). Despite the homogeneous dispersion of 3wt.% C15A in the matrix (Figure 3.6-b), it is possible to distinguish the reinforcement from the matrix at micro scale, however it is not possible to infer if the nanoclay are exfoliated or intercalated. Droplets of SEBS-*g*-MA with different sizes dispersed in the PC_M matrix are visible in Figure 3.6-c. However, even with the presence of MA groups the interfacial adhesion between both phases is not good, being easily detached from the PC matrix, and some elongated rubber particles are seen due to the coalescence of the surrounding rubber droplets, as reported by Garhwal and Maiti [29]. The addition of nanoclay clearly improves the compatibility between PC_M and SEBS-*g*-MA (Figure 3.6-d), providing better dispersion with smaller droplets, which is in accordance with the observations of Chow and Neoh[15]. Similarly, Tjong and Bao suggests that there is a chemical affinity between the SEBS-*g*-MA (disperse phase) and organoclay, allowing the rubber chain to penetrate and exfoliate its lamellar structure, which improves the dispersion and increases the polymers compatibility [51].

The hallow ring observed around the NCW (Figure 3.7-a) suggests poor adhesion between PC matrix and cotton fibers, nevertheless the nonlinear fiber morphology holds the cotton fiber to the matrix, and no pull-out fibers were found. Taşdemır *et al.* reported good adhesion between recycled PC and waste cotton

fiber from textile industry, possibly, due to fiber surface treatment or the presence of a higher amount of -OH groups in recycled PC resulting from thermal degradation [30, 52]. PC/ABS-*g*MA blends (Figure 3.7-b and Figure 3.7-c) at lower magnification seem to have only one phase, however, at higher magnification it is visible that compatibility increases as the amount of ABS-*g*MA increases and the blend that seems to have better compatibilization is the one where blending and modification took place in a single step. Contrary to what was observed in Figure 3.6-c, the cryogenic fracture also promotes the fracture of modified ABS phase, and no evidence of total debonding is observed. The halo ring around these rubber particles are related to cavitation mechanism, but in a less extent than the degree observed for SEBS-*g*MA system. This could be related to the less deformation ability of modified ABS phase and the tendency to fracture. Physical connections are observed between both phases, which can be related to the higher grafting degree obtained (GD=3.8), suggesting a chemical linkage between MA groups and -OH terminals of PC. SEM analysis does not exhibited any visible morphological difference between 25wt.% ABS-*g*MA (Figure 3.7-c) and the one step ABS grafting (Figure 3.7-d), but cavitation phenomena under both systems is smaller compared to the system with 10 wt.% ABS-*g*MA.

The addition of 1wt.% of SEBS-*g*MA changes the fracture morphology of PC_{Lr} to a wave-like surface, with visible small rubber droplets homogeneously dispersed (Figure 3.8-b). A massive halo around these particles evidences cavitation phenomena, which is one of the main mechanisms for polymer toughening [6]. The same wt.% of ABS-*g*MA resulted in similar morphology for both PC grades (Figure 3.7-b and Figure 3.8-c). PC/ABS-*g*MA/SEBS-*g*MA blend (Figure 3.8-d) show that SEBS-*g*MA is attached to the modified ABS phase, preventing ABS-*g*MA phase from breaking alongside the cryogenic fracture, increasing the halo sizes that result from cavitation. At higher magnifications, the blend systems with NCW (Figure 3.8-e and f) shows that PC_{Lr}_05 sample has more attached material at the surface of the cotton fiber, possibly due to the linkage between SEBS-*g*MA and hydroxyl groups of cellulose, which is in agreement with the IR spectra results, where -OH band intensity of cellulose decrease with the incorporation of SEBS-*g*MA phase.

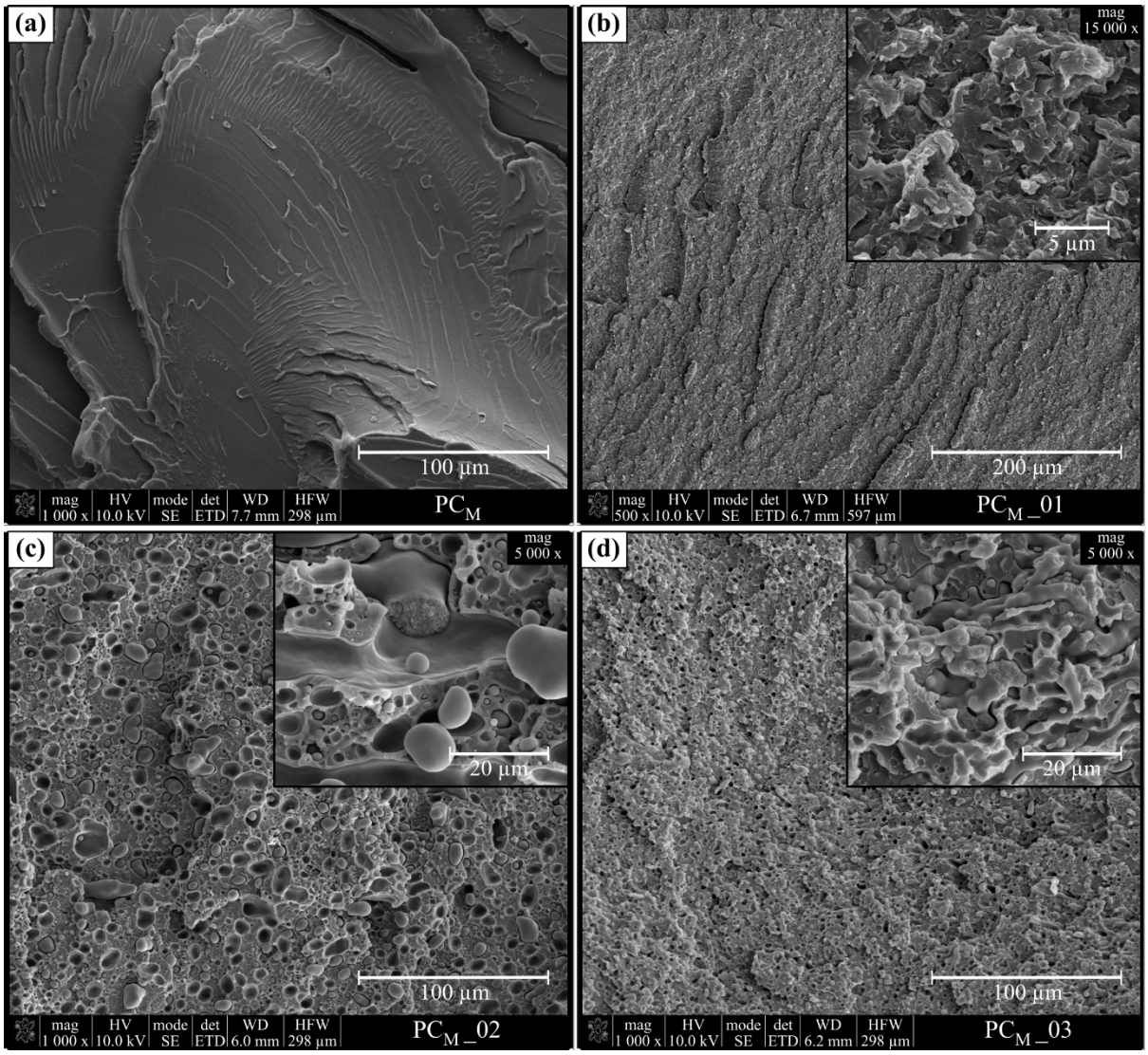

Figure 3.6: SEM (cross-section) of PC_M (a) and PC_M with 3wt.% C15A (b), 15wt.% SEBS-g-MA (c), and both (d) after cryogenic fracture.

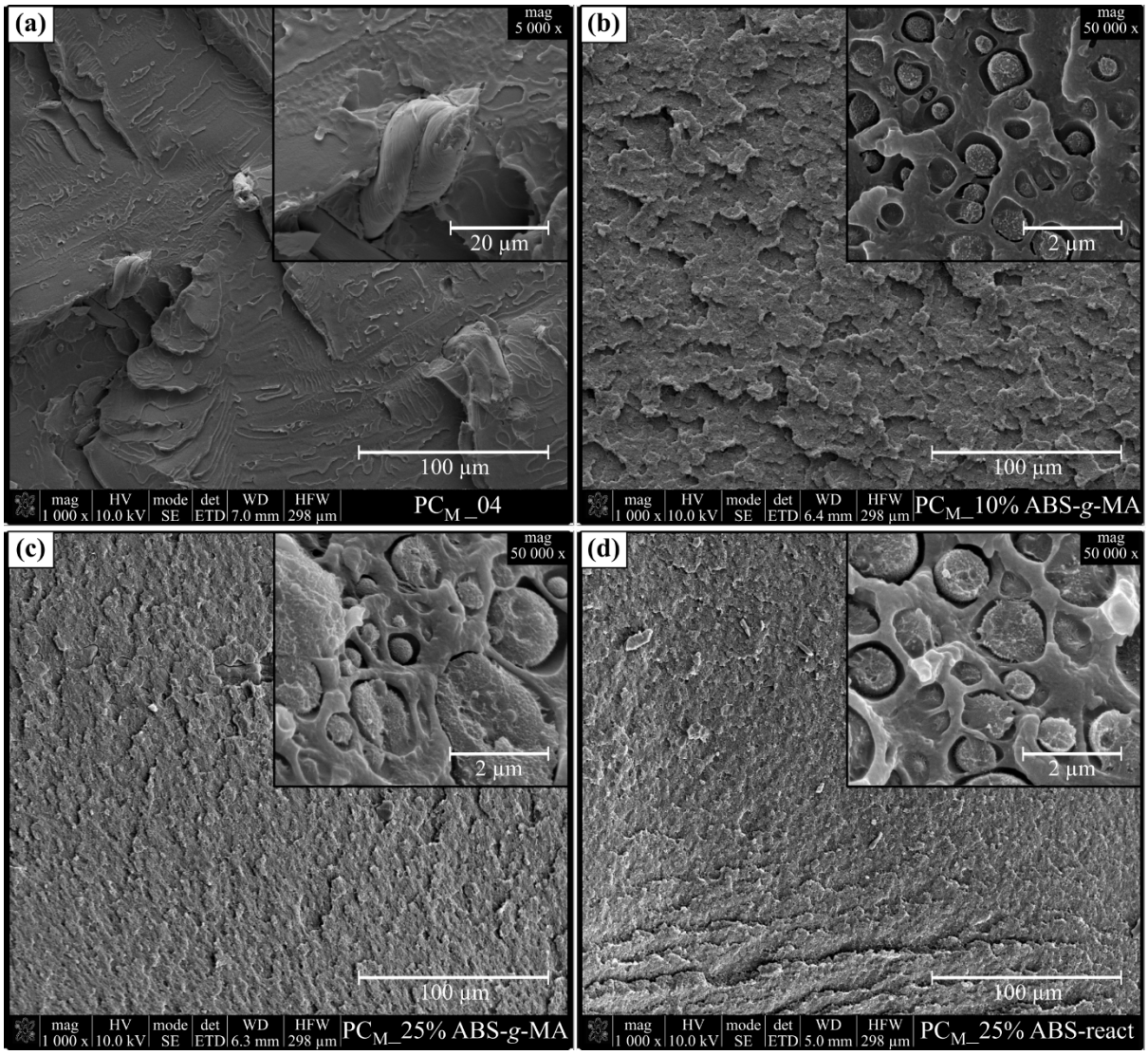

Figure 3.7: SEM (cross-section) of PC_M samples blended with NCW (a), and 10/15wt.% ABS-g-MA (b-c) and in-line MA grafting onto ABS (d) after cryogenic fracture.

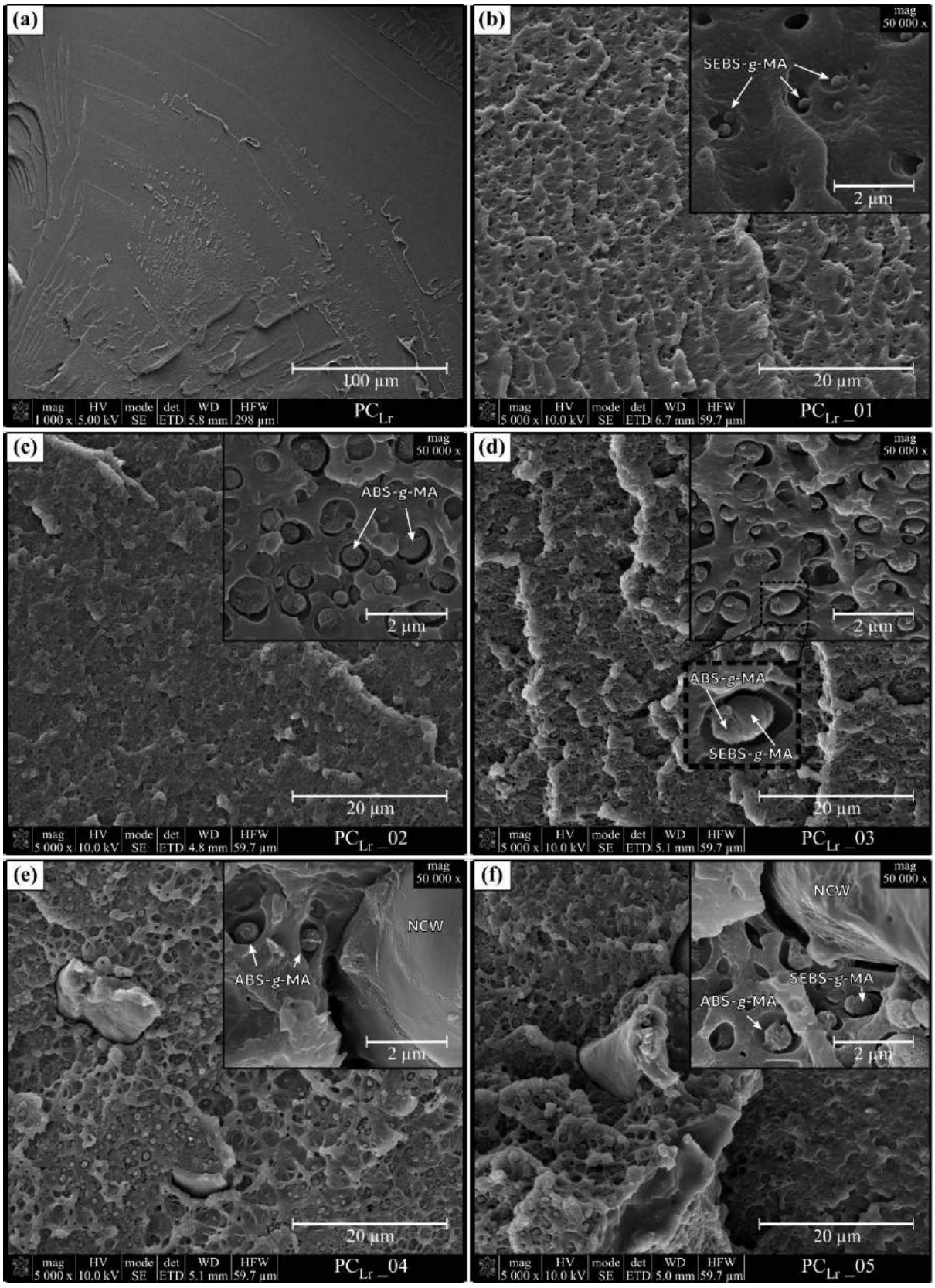

Figure 3.8: SEM (cross-section) of neat PC_{Lr} (a) and PC_{Lr} samples with 1wt.%SEBS-g-MA (b), 10wt.%ABS-g-MA (c), both (d), 10wt.%ABS-g-MA+3wt.%NCW (e), and 1wt.%SEBS-g-MA+10wt.%ABS-g-MA+3%NCW (f) after cryogenic fracture.

3.3.4 Thermal characterization results

DSC curves and characteristic thermal transition values of unmodified and modified ABS, and PC_{Lr} samples are depicted in Table 3.4 and Figure 3.9. Only PC_{Lr} blends were chosen to be tested since all blends were incorporated with elastomeric particles. The chemical structure of the polymeric materials used in this work does not allow the existence of crystalline structures and, as a result, only transitions associated to the change in molecular chain mobility are detected (glass transition, T_g).

The modification of ABS lowers its T_g from 106.1 °C to 103.9 °C due to MA groups, which is reported to be a consequence of the introduction of small chemical compounds onto the backbone of the polymer chain, increasing the free volume available for the chain to move [25]. The processing of neat PC does not influence its thermal property, but the introduction of 1wt.% SEBS-*g*-MA (PC_{Lr}_01) slightly increases the T_g of PC. Since the amount of SEBS-*g*-MA incorporated is small, DSC can not detect the transition temperature associated to the styrene segment (circa T_g = 95°C) [53]. Despite the small variation in Tg, it is visible the existence of two glass transitions for the PC/ABS-*g*-MA blends systems (PC_{Lr}_02 to PC_{Lr}_05) from modified ABS (T_{g1}) and PC_{Lr} matrix (T_{g2}), suggesting partial compatibility between both phases. The introduction of cotton fibers slightly decreases PC T_g.

Table 3.4: Thermal properties of ABS, ABS-g-MA, and PC_{Lr} blends from DSC.

	Tg_1			**Tg_2**		
Sample	**T_{onset}**	**$T_{midpoint}$**	**T_{endset}**	**T_{onset}**	**$T_{midpoint}$**	**T_{endset}**
ABS	103.8	106.3	110.0	-	-	-
ABS-*g*-MA	99.1	103.5	108.9	-	-	-
PC_{Lr}	-	-	-	142.9	145.7	149.0
PC_{Lr}_00	-	-	-	142.4	145.4	148.7
PC_{Lr}_01	-	-	-	143.6	146.5	149.7
PC_{Lr}_02	104.2	107.4	114.6	141.8	144.9	148.3
PC_{Lr}_03	108.2	110.7	114.1	143.1	145.8	148.7
PC_{Lr}_04	106.6	110.8	115.1	138.6	141.8	145.0
PC_{Lr}_05	106.0	109.9	114.5	138.9	141.7	144.8

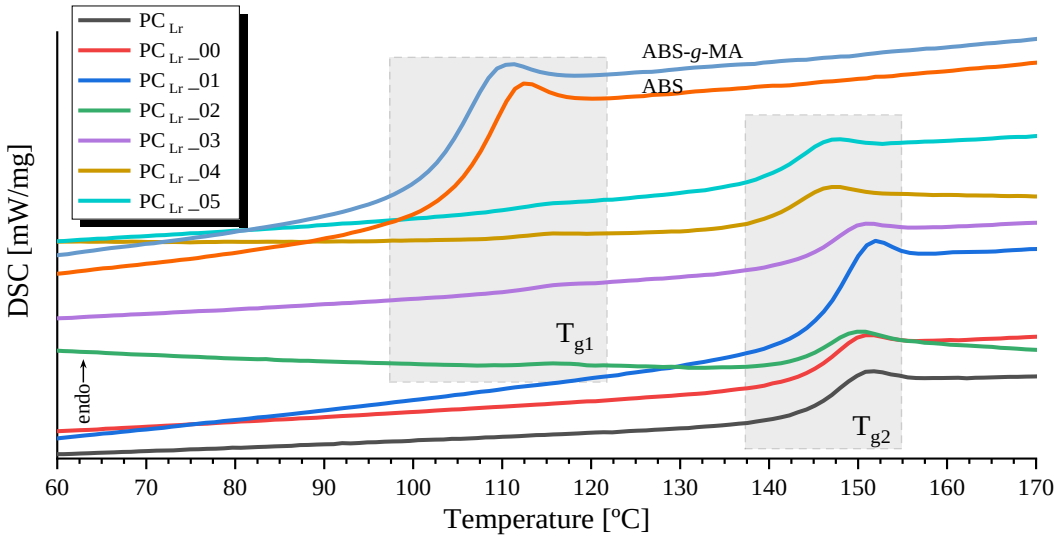

Figure 3.9: DSC thermograms for ABS, and ABS-g-MA and PC_{Lr} blends.

3.3.5 Mechanical characterization and MO

3.3.5.1 Quasi-static tensile behavior of PC and PC blends

The calculated mechanical properties are shown in Figure 3.10, where a deformation speed of 1 mm/min was used to determine E and 50 mm/min for the remaining values. The percentage variation of the average values in comparison with the values of processed PC (PC_{Lux}_00, PC_M_00 and PC_{Lr}_00) are displayed Figure 3.11. All values of neat polymer are in accordance with the technical data sheet (Table 3.1), excepting ε_r which is x10 times lower, and could be due to the specimen preparation and geometry used. The effect of processing is evident with a decrease in mechanical properties and toughness also being affected for both PC grades, presenting higher value variability, indicating that specimen failure occurs between fragile and ductile transition. The incorporation of nanoclay into PC (PC_{Lux}_01 and PC_M_01) increases E but has a negative impact on the plastic deformation (-71 to -90%). Although this behavior was expected, the loss in toughening was higher than what it is reported in literature, indicating that a low dispersion degree of nanoclay was achieved [17, 50]. Since PC_M has lower MVR and presented higher torque than PC_{Lux} (Figure 3.5), the higher shear-rate developed during compounding could induce better dispersion of nanoclay [18]. This could explain the higher values variation of E of PC_M_01 (+16%) in comparison with PC_{Lux}_01 (+7%). Blending PC with 15 wt.% SEBS-*g*MA slightly increases the overall plastic deformation of PC_{Lux}_02 blend (+3%), which was significant for PC_M_02 blend (+39%) severely affecting the modulus of elasticity (-26 to -30%). This can be attributed to the elastomeric nature of SEBS-*g*MA that has lower stiffness [16]. Adding both nanoclay and SEBS-*g*MA (PC_{Lux}_03 and PC_M_03) improves deformation at break but slightly decreases elastic modulus, compared to PC_{Luz}_01 and PC_M_01 systems. The use of 3wt.% NCW (PC_{Lux}_04 and PC_M_04) does not affect overall performance

of PC_{Lux}, but increases E and U of PC_M system (+11% and +59%). Regarding the PC_M / ABS-*g*MA systems, it is possible to infer that the addition of 10 wt.% has the best improvement in terms of elasticity (+10%) and toughening (+122%). Overall, PC_M_10%ABS-*g*MA has a better performance than PC_M, but increasing ABS-*g*MA content did not improve the mechanical properties and no significant difference between two steps and one step ABS modification was noticed. As observed in SEM (Figure 3.7 c-d), a higher amount of modified ABS in the blend (25 wt.%) resulted in higher particle size of elastomeric phase, which lead to a mediocre tensile reinforcement effect. Regarding PC_{Lr} samples, blending with 1 wt.% SEBS-*g*MA (PC_{Lr}_01) increased up to 24% the toughening, maintaining similar performance to neat PC_{Lr}. The addition of 10 wt.% ABS-*g*MA (PC_{Lr}_02) improved the elastic modulus of the blend (E increased almost +20%), but negatively affected toughening (-25%), indicating that toughening mechanism is dependent on the type of PC grade used. PC_{Lr}_03 system showed a synergetic effect when using both types of rubber together, increasing U by 40%. Adding 3 wt.% of NCW to PC_{Lr}_02 system slightly reduced the negative impact of ABS-g-MA. PC_{Lr}_05 system showed a significant improvement in toughening (from -18 to 1%) over PC_{Lr}_04 blends, and can be explained by the chemical affinity between SEBS-*g*MA and cotton, evidenced by the lowering of hydroxyl bands in IR spectra analysis (Figure 3.3) and by SEM analysis (Figure 3.8-f).

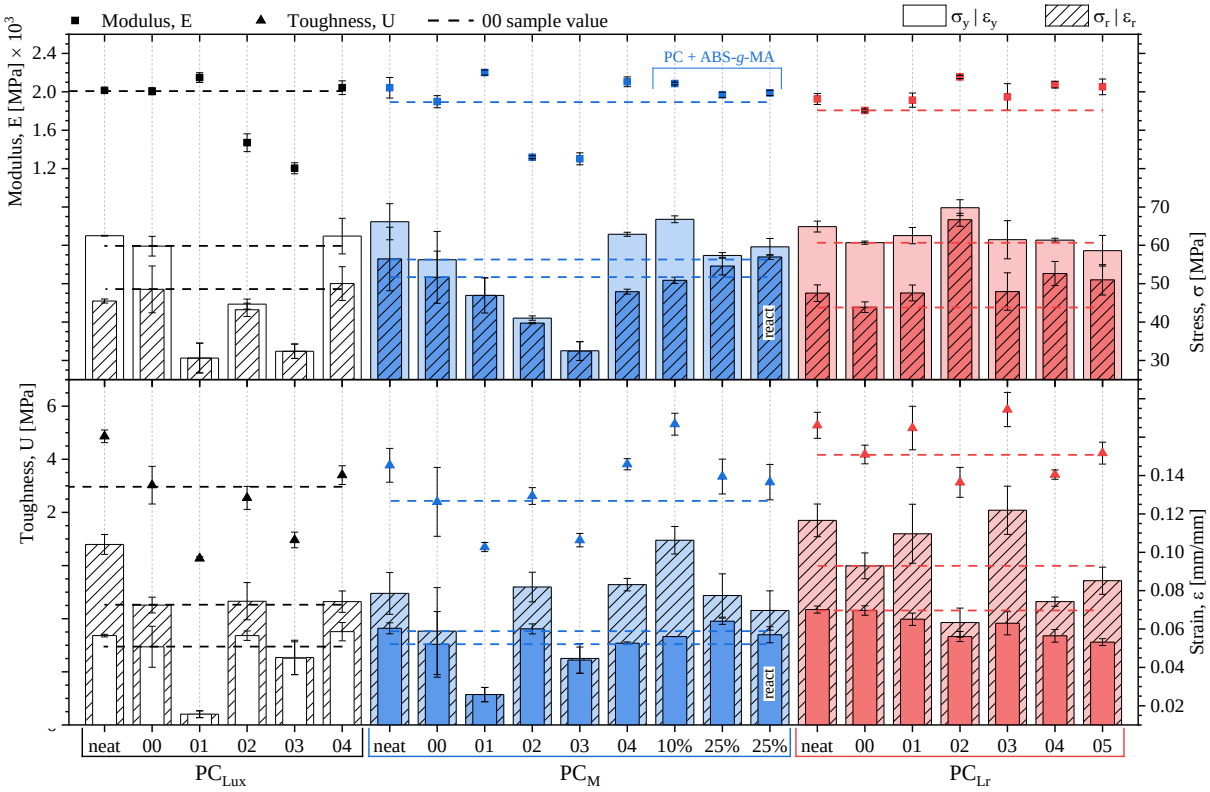

Figure 3.10: Average of stress (σ_y) and strain (ε_y) at yield, modulus (E), stress (σ_r) and strain (ε_r) at break, and toughness (U), of quasi-static tests on PC_{Lux}, PC_M and PC_{Lr} blends.

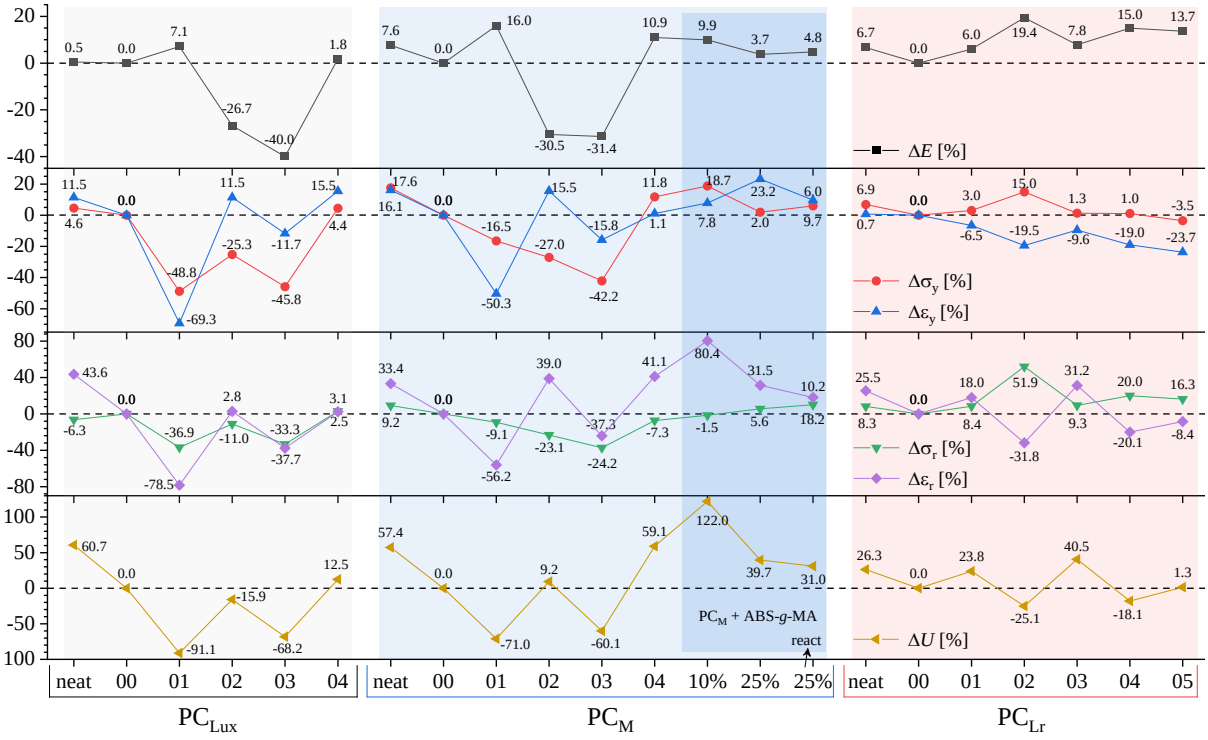

Figure 3.11: Percentage variation of the average values of stress (σ_y) and strain (ε_y) at yield, modulus (E), stress (σ_r) and strain (ε_r) at break, and toughness (U), of quasi-static tests on PC_{Lux}, PC_M and PC_{Lr} blends

3.3.5.2 Impact tests and morphology

The v-notched impact test results (Figure 3.12) are consistent with quasi-static tests, and toughness of PC matrix drops during melt processing, probably due to thermo-oxidative degradation. Regarding PC_{Lux} and PC_M systems, nanoclay severely impacts the ability to withstand impact loadings. PC_{Lux}_01 broke during demolding of specimen, proving the fragility of these samples. The incorporation of 15 wt.% SEBS-*g*MA (PC_{Lux}_02 and PC_M_02) improved the impact strength by 42 and 66%. No positive effect was observed for the incorporation of both nanoclay and SEBS-*g*MA (PC_{Lux}_03 and PC_M_03), which can be explained by absence of cavitation phenomena observed on SEM analysis (Figure 3.6-d). Also, no toughening effect was obtained with 3 wt.% NCW (PC_{Lux}_04 and PC_M_04), which might be associated to the poor adhesion between PC and cotton fiber (Figure 3.7-a), creating sharp notches (interface voids) that leads to catastrophic failure. Regarding the PC_M / ABS-*g*MA systems, no toughening effect was perceived, which can be related to the higher GD obtained. MA grafting occurs on the polybutadiene branch of ABS, increasing the elastic modulus at the cost of toughening, and therefore, impact strength is reduced.

The lost in impact strength of PC_{Lr} after processing was smaller, but it should be noticed that the neat value obtained (22.7 kJ/m^2) was lower compared to technical data sheet (75 kJ/m^2). Since most of

specimen are prepared through injection molding, the difference in the manufacturing procedure can explain these result deviations. Blending 1 wt.% SEBS-*g*MA (PC_{Lr}_01) improved the impact strength more than 460%, and similar results were obtained in PC_{Lr}_03 with the addition of 10 wt.% ABS-*g*MA and 1 wt.% SEBS-*g*MA (412%). It was detected that the incorporation of modified SEBS in PC_{Lr}_03 blend boosts the impact toughness. Superior toughening properties of SEBS-*g*MA over ABS-*g*MA can be explained by the ability for modified SEBS to cavitate, as noticed in blend morphology, while ABS phase did not present this behavior. Despite the improvement of NCW in PC_{Lr} elastic modulus, it affects negatively the toughening mechanism provided by the rubber phase (PC_{Lr}_04 and PC_{Lr}_05). Since it was detected that SEBS-*g*MA linked chemically with cotton fibers via FT-IR and SEM, it could also explain the non-toughening mechanism by the less rubber phase available for PC matrix.

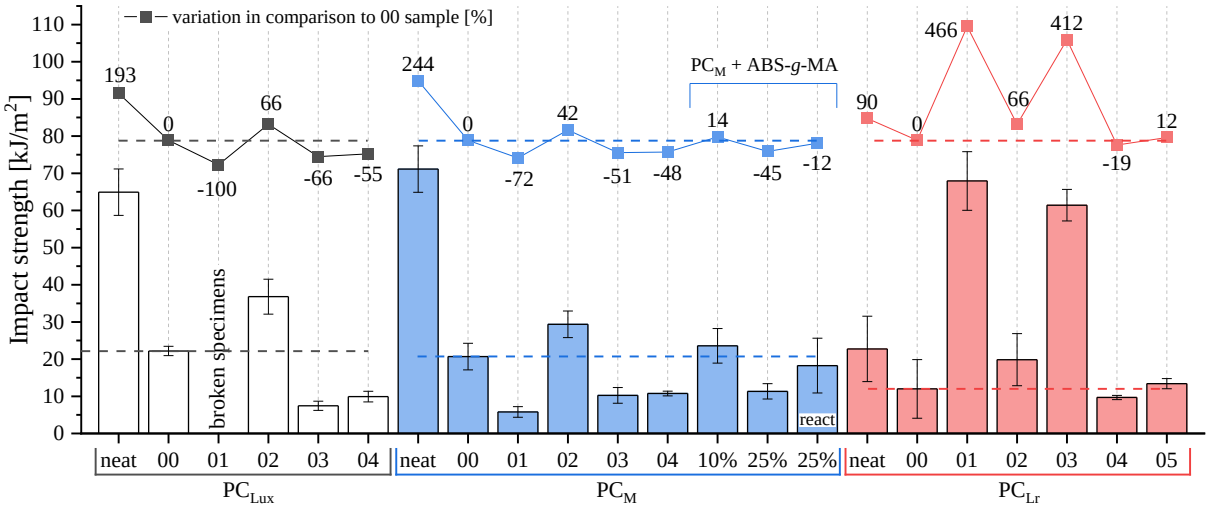

Figure 3.12: Impact strength of v-notched specimens.

The cross-section of the fractured impact specimens (Figure 3.13) demonstrates that in all neat PC a ductile mode of fracture is seen, which is proved by the thickness reduction of the cross-section of the specimen during deformation (red dash line) [32]. This reduction is smaller for the neat PC_{Lr} due to the less ability of this sample to absorb the impact energy and is in accordance with the impact strength values obtained. Ductile fracture mode is referred as a plane stress condition in thin bodies, where all stresses acting are placed on the same plane and the normal stress is negligible. On the other hand, brittle fracture mode is associated to plane strain in thick bodies, characterized by zero strain at the normal direction of the crack path caused by triaxial conditions [33]. After processing, the PC matrix loses the ability to dissipate the impact energy through plastic deformation, and no thickness reduction is observed for PC_{Lux}_00 and PC_{M}_00 specimens. The fracture surface shows the initiation of the crack

propagation from the notch tip side (nucleus), small size crack propagation lines (slow crack growth), following the increase in the size of the crack lines (fast crack growth), changing the propagation direction from the in-plane to the out-plane before reaching the border (chaotic fracture) [54]. PC_M_01 sample shows a clear surface fracture without plane changing direction of the crack propagation, which proves its fragile behavior (brittle mode, plane strain). For PC_{Lux}_02 and PC_M_02 systems, thickness reduction is small but presents shear bands due to fracture. For PC_{Lux}_03 and PC_M_03 systems, no plastic deformation is detected, the surface fracture is clear like in PC_01 specimens but with higher rugosity. PC_{Lux}_04 and PC_M_04 presents similar behavior to processed PC, but with smaller shear bands. Regarding PC_M / ABS-*g*MA systems, the incorporation of 10 wt.% ABS-*g*MA induces stress whitening phenomena, alongside with plastic deformation, perceived at the crack initiation site (notch tip), and can be related to the formation of voids at the microscale [55]. Increasing ABS-*g*MA content promotes a decrease on the stress whitening area and is in accordance with SEM results where cavitation degree was less extent for PC_M_25% ABS-*g*MA system. For the one step grafting and blending (PC_M_25%ABS-react), the stress whitening at the notch tip is negligible, but instead spreads along the whole fractured plane. Crack propagation was more even along the ABS-react specimens (in-plane), while for 10 and 25% ABS-*g*MA systems the impact energy was also dissipated with crack path propagation going outside the impact plane (out-plane).

Even though the impact strength energy of neat and processed PC_{Lr}, these samples present some ductile fracture behavior. PC_{Lr}_01 and PC_{Lr}_03 blend systems present ductile fracture mode with deep carved shear bands, which can explain the substantial increase in toughening (more than +400%). PC_{Lr}_02 also presents some shear bands but in a lesser extent, with lower ductile deformation and with a brittle fracture mode near the end of the crack path. Regarding PC_{Lr}_04 and PC_{Lr}_05, compounding with 3 wt.% NCW changed the fracture behavior from ductile to complete brittle fracture, with no thickness reduction but with some whitening along all plane.

Figure 3.13: Cross-section of v-notch specimens after Charpy impact tests, with red dash line indication ductile deformation along specimen, and circled area with arrows indicating fracture nucleus, initiation and propagation lines.

3.4 Conclusions

Three different PC grades with different MVR were used to blend with elastomeric materials (SEBS-*g*MA and ABS-*g*MA) and/or for the incorporation of nanoclay, cotton fibers.

The results of several characterization techniques demonstrate that melt processing has a significant impact on the mechanical properties of neat PC, changing from ductile fracture mode to brittle. The degradation phenomena can be delayed by blending with rubbery polymers, promoting an increment in toughening on quasi-static and impact tests. Melt viscosity promoted better nanoclay dispersion on PC_M system, rather for PC_{Lux}, and SEBS-*g*MA improved compatibility between nanoclay and PC matrix. Nanoclay and cotton fiber increase the modulus of elasticity, but no toughening was observed.

The use of 1wt.% SEBS-*g*MA improved the impact strength of PC_{Lr} up to +466%, while for quasi-static tests the values were similar to neat PC_{Lr}. PC / SEBS-*g*MA toughning mechanism is mainly due to cavitation phenomena, while stress whitening was more evident for ABS-*g*MA systems. In cryogenic fracture, ABS-*g*MA fractured alongside PC_{Lr} matrix, while for SEBS-*g*MA debond and cavitation phenomena were observed. Blending PC with both rubber material, SEBS-*g*MA sticked to the surface of ABS-*g*MA phase, preventing its fracture in cryogenic conditions, improving toughness compared to PC_{Lr} / ABS-*g*MA blends.

As general conclusion of this research work it is possible to state that materials properties can be tailored by blending with appropriated polymers, according to the required properties of the final material.

3.5 Acknowledgements

The authors acknowledge the financial support by Portugal 2020, and Fundo Social Europeu (FSE) through Programa Operacional Regional do NORTE (NORTE-08-5369–FSE-000034), developed under the program "IMPULSE - Polímeros e Compósitos: Drivers da inovação tecnológica e da competitividade industrial". The authors also acknowledge the Portuguese Foundation of Science and Technology (TSSiPRO - TECHNOLOGIES FOR SUSTAINABLE AND SMART INNOVATIVE PRODUCTS - NORTE-01-0145-FEDER-000015) and UID/CTM/50025/2013 for the financial support.

3.6 References

[1] H. Xu, S. Tang, L. Yang, and W. Hou, "Toughening of polycarbonate by core-shell latex particles: Influence of particle size and spatial distribution on brittle-ductile transition," *Journal of Polymer Science Part B: Polymer Physics*, vol. 48, no. 18, pp. 1970–1977, 2010, doi: 10.1002/polb.22075.

[2] R.-R. Ang *et al.,* "A review of copolymerization of green house gas carbon dioxide and oxiranes to produce polycarbonate," *Journal of Cleaner Production*, vol. 102, pp. 1–17, 2015, doi: 10.1016/j.jclepro.2015.04.026.

[3] E. V. Antonakou and D. S. Achilias, "Recent Advances in Polycarbonate Recycling: A Review of Degradation Methods and Their Mechanisms," *Waste and Biomass Valorization*, vol. 4, no. 1, pp. 9–21, 2013, doi: 10.1007/s12649-012-9159-x.

[4] B. S. Lombardo, H. Keskkula, and D. R. Paul, "Influence of ABS type on morphology and mechanical properties of PC/ABS blends," *J. Appl. Polym. Sci.*, vol. 54, no. 11, pp. 1697–1720, 1994, doi: 10.1002/app.1994.070541113.

[5] F. Elmaghor, L. Zhang, R. Fan, and H. Li, "Recycling of polycarbonate by blending with maleic anhydride grafted ABS," *Polymer*, vol. 45, no. 19, pp. 6719–6724, 2004, doi: 10.1016/j.polymer.2004.07.022.

[6] A. Garhwal and S. N. Maiti, "Influence of styrene–ethylene–butylene–styrene (SEBS) copolymer on the short-term static mechanical and fracture performance of polycarbonate (PC)/SEBS blends," *Polym. Bull.*, vol. 73, no. 6, pp. 1719–1740, 2016, doi: 10.1007/s00289-015-1573-3.

[7] H. de Brouwer, J. van den Bogerd, and J. Hoover, "Color stability of polycarbonate for optical applications," *European Polymer Journal*, vol. 71, pp. 558–566, 2015, doi: 10.1016/j.eurpolymj.2015.08.031.

[8] S. Balakrishnan and N. R. Neelakantan, "Mechanical properties of blends of polycarbonate with unmodified and maleic anhydride grafted ABS," *Polymer International*, vol. 45, no. 4, 1998.

[9] Q.-Z. Fang, T. J. Wang, and H. M. Li, "Overload effect on the fatigue crack propagation of PC/ABS alloy," *Polymer*, vol. 48, no. 22, pp. 6691–6706, 2007, doi: 10.1016/j.polymer.2007.08.048.

[10] Q.-Z. Fang, T. J. Wang, and H.-M. Li, "Large tensile deformation behavior of PC/ABS alloy," *Polymer*, vol. 47, no. 14, pp. 5174–5181, 2006, doi: 10.1016/j.polymer.2006.04.069.

[11] J.J. Herpels and L. Mascia, "Effects of Styrene-Acryonitrile/Butadiene ratio on the toughness of Polycarbonate/ABS blends," *Eur. Polym. J.*, vol. 26, no. 9, pp. 997–1003, 1990.

[12] Z. N. Yin and T. J. Wang, "Deformation of PC/ABS alloys at elevated temperatures and high strain rates," *Materials Science and Engineering: A*, vol. 494, 1-2, pp. 304–313, 2008, doi: 10.1016/j.msea.2008.05.039.

[13] Z. Yin and T. Wang, "Investigation of tensile deformation behavior of PC, ABS, and PC/ABS blends from low to high strain rates," *Applied Mathematics and Mechanics*, vol. 33, no. 4, pp. 455–464, 2012, doi: 10.1007/s10483-012-1563-x.

[14] F. O. M. S. Abreu, M. M. C. Forte, and S. A. Liberman, "SBS and SEBS block copolymers as impact modifiers for polypropylene compounds," *J. Appl. Polym. Sci.*, vol. 95, no. 2, pp. 254–263, 2005, doi: 10.1002/app.21263.

[15] W. S. Chow and S. S. Neoh, "Mechanical, Morphological and Thermal Properties of Polycarbonate/SEBS-G-MA/Montmorillonite Nanocomposites," *Polymer-Plastics Technology and Engineering*, vol. 49, no. 1, pp. 62–68, 2009, doi: 10.1080/03602550903283034.

[16] J. J. Huang, H. Keskkula, and D. R. Paul, "Rubber toughening of an amorphous polyamide by functionalized SEBS copolymers: morphology and Izod impact behavior," *Polymer*, vol. 45, no. 12, pp. 4203–4215, 2004, doi: 10.1016/j.polymer.2004.04.002.

[17] S. Suin, S. Maiti, N. K. Shrivastava, and B. B. Khatua, "Mechanically improved and optically transparent polycarbonate/clay nanocomposites using phosphonium modified organoclay," *Materials & Design (1980-2015)*, vol. 54, pp. 553–563, 2014, doi: 10.1016/j.matdes.2013.08.091.

[18] P. J. Yoon, D. L. Hunter, and D. R. Paul, "Polycarbonate nanocomposites. Part 1. Effect of organoclay structure on morphology and properties," *Polymer*, vol. 44, no. 18, pp. 5323–5339, 2003, doi: 10.1016/S0032-3861(03)00528-7.

[19] R. Greco, M. F. Astarita, L. Dong, and A. Sorrentino, "Polycarbonate/ABS blends: Processability, thermal properties, and mechanical and impact behavior," *Advances in Polymer Technology*, vol. 13, no. 4, pp. 259–274, 1994, doi: 10.1002/adv.1994.060130402.

[20] R. Greco and A. Sorrentino, "Polycarbonate/ABS blends: A literature review," *Advances in Polymer Technology*, vol. 13, no. 4, pp. 249–258, 1994, doi: 10.1002/adv.1994.060130401.

[21] S. Balakrishnan, N. Neelakantan, D. Saheb, and J. P. Jog, "Rheological and morphological behaviour of blends of polycarbonate with unmodified and maleic anhydride grafted ABS," *Polymer*, vol. 39, no. 23, pp. 5765–5771, 1998, doi: 10.1016/S0032-3861(98)00088-3.

[22] D. Debier, J. Devaux, R. Legras, and D. Leblanc, "Influence of a core/shell rubber phase on the morphology and the impact resistance of a PC/SAN blend (75/25)," *Polymer Engineering & Science*, vol. 34, no. 8, pp. 613–624, 1994, doi: 10.1002/pen.760340802.

[23] K. Yang, S.-H. Lee, and J.-M. Oh, "Effects of viscosity ratio and compatibilizers on the morphology and mechanical properties of polycarbonate/acrylonitrile-butadiene-styrene blends," *Polymer Engineering & Science*, vol. 39, no. 9, pp. 1667–1677, 1999, doi: 10.1002/pen.11561.

[24] Huiju Shao, Shuhao Qin, Jianbing Guo, and Bin Wu, "Melt grafting copolymerization of glycidyl methacrylate onto acrylonitrile-butadiene-styrene (ABS) terpolymer," *Science and Engineering of Composite Materials*, vol. 22, no. 4, pp. 391–398, 2015, doi: 10.1515/secm-2013-0121.

[25] X. Zhang, Y. Chen, Y. Zhang, Z. Peng, Y. Zhang, and W. Zhou, "Effects of ABS-g-MAH on mechanical properties and compatibility of ABS/PC alloy," *Journal of Applied Polymer Science*, vol. 81, no. 4, pp. 831–836, 2001, doi: 10.1002/app.1502.

[26] H. Duan, M.-Q. Xin, K.-Y. Kim, and J.-J. Tang, "The Role of Compatibilizers on the Properties of PC/ABS Alloy," *Journal of Materials Science and Chemical Engineering*, vol. 5, no. 6, pp. 21–30, 2017, doi: 10.4236/msce.2017.56003.

[27] S. Horiuchi, N. Matchariyakul, K. Yase, T. Kitano, H. K. Choi, and Y. M. Lee, "Compatibilizing effect of maleic anhydride functionalized SEBS triblock elastomer through a reaction induced phase formation in the blends of polyamide6 and polycarbonate: 2. Mechanical properties," *Polymer*, vol. 38, no. 1, pp. 59–78, 1997, doi: 10.1016/S0032-3861(96)00465-X.

[28] I. Debbah, R. Krache, N. Aranburu, M. Fernández, and A. Etxeberria, "Effect of SEBS-g-MAH addition on the mechanical, rheological, and morphological properties of polycarbonate/acrylonitrile–butadiene–styrene blends," *Journal of Elastomers & Plastics*, vol. 50, no. 7, pp. 611–633, 2018, doi: 10.1177/0095244317753652.

[29] A. Garhwal and S. N. Maiti, "Fabrication of Super Tough Polycarbonate/Styrene-Etylene-Butylene-Styrene Grafted Maleic Anhydride (SEBS-g-MA) Blends: Morphological, Short Term Static Mechanical and Fracture Performance Interpretation," *Polymer-Plastics Technology and Materials*, vol. 58, no. 2, pp. 113–125, 2019, doi: 10.1080/03602559.2018.1466167.

[30] M. Taşdemır, D. Koçak, İ. Usta, M. Akalin, and N. Merdan, "Properties of Recycled Polycarbonate/Waste Silk and Cotton Fiber Polymer Composites," *International Journal of Polymeric Materials and Polymeric Biomaterials*, vol. 57, no. 8, pp. 797–805, 2008, doi: 10.1080/00914030802089138.

[31] P. Sivaraman *et al.,* "Thermoplastic copolyether ester elastomer toughened polycarbonate blends: 1. Mechanical properties and morphology of the blends," *Polymer Testing*, vol. 23, no. 5, pp. 527–532, 2004, doi: 10.1016/j.polymertesting.2003.12.001.

[32] J. Aranda-Ruiz, K. Ravi-Chandar, and J. A. Loya, "On the double transition in the failure mode of polycarbonate," *Mechanics of Materials*, vol. 140, p. 103242, 2020, doi: 10.1016/j.mechmat.2019.103242.

[33] M.-P. Lee, A. Hiltner, and E. Baer, "Fractography of injection molded polycarbonate acrylonitrile-butadiene-styrene terpolymer blends," *Polymer Engineering & Science*, vol. 32, no. 13, pp. 909–919, 1992, doi: 10.1002/pen.760321311.

[34] F.-C. Chang, J.-S. Wu, and L.-H. Chu, "Fracture and impact properties of polycarbonates and MBS elastomer-modified polycarbonates," *Journal of Applied Polymer Science*, vol. 44, no. 3, pp. 491–504, 1992, doi: 10.1002/app.1992.070440314.

[35] R. Qi, Z. Chen, and C. Zhou, "Solvothermal preparation of maleic anhydride grafted onto acrylonitrile–butadiene–styrene terpolymer (ABS)," *Polymer*, vol. 46, no. 12, pp. 4098–4104, 2005, doi: 10.1016/j.polymer.2005.02.116.

[36] *Plastics — Determination of tensile properties — Part 1: General principles*, ISO 527-1:1996, 1996.

[37] *Plastics — Determination of Charpy impact properties — Part 1: Non-instrumented impact test*, ISO 179-1:2010, 2010.

[38] *Standard Test Method for Transition Temperatures and Enthalpies of Fusion and Crystallization of Polymers by Differential Scanning Calorimetry*, ASTM D3418 - 15, 2015.

[39] S.-H. Wu, M.-L. Shyu, Y.-P. I, J.-H. Chi, and C.-M. Shu, "Evaluation of runaway reaction for dicumyl peroxide in a batch reactor by DSC and VSP2," *Journal of Loss Prevention in the Process Industries*, vol. 22, no. 6, pp. 721–727, 2009, doi: 10.1016/j.jlp.2008.08.004.

[40] R. Qi, J. Qian, and C. Zhou, "Modification of acrylonitrile–butadiene–styrene terpolymer by grafting with maleic anhydride in the melt. I. Preparation and characterization," *Journal of Applied Polymer Science*, vol. 90, no. 5, pp. 1249–1254, 2003, doi: 10.1002/app.12679.

[41] R. Qi, J. Qian, Z. Chen, X. Jin, and C. Zhou, "Modification of acrylonitrile-butadiene-styrene terpolymer by graft copolymerization with maleic anhydride in the melt. II. Properties and phase behavior," *Journal of Applied Polymer Science*, vol. 91, no. 5, pp. 2834–2839, 2004, doi: 10.1002/app.13468.

[42] V. Hermán, H. Takacs, F. Duclairoir, O. Renault, J. H. Tortai, and B. Viala, "Core double–shell cobalt/graphene/polystyrene magnetic nanocomposites synthesized by in situ sonochemical polymerization," *RSC Advances*, vol. 5, no. 63, pp. 51371–51381, 2015, doi: 10.1039/C5RA06847A.

[43] R. Qi, Q. Yu, Y. Shen, Q. Liu, and C. Zhou, "Grafting copolymerization of maleic anhydride onto styrene-butadiene-styrene block copolymer through solvothermal process," *J. Appl. Polym. Sci.*, vol. 102, no. 6, pp. 5274–5279, 2006, doi: 10.1002/app.24780.

[44] O. C. S. Al-Hamouz, B. A. Sweileh, and H. A. Al-Salah, "Synthesis and characterization of polycarbonates by melt-phase interchange reactions with alkylene and arylene diphenyl dicarbonates," *Journal of Applied Polymer Science*, vol. 102, no. 4, pp. 3597–3609, 2006, doi: 10.1002/app.23996.

[45] P. Wang *et al.,* "Sustainable synthesis and characterization of a bisphenol A-free polycarbonate from a six-membered dicyclic carbonate," *Polymer Chemistry*, vol. 9, no. 27, pp. 3798–3807, 2018, doi: 10.1039/C8PY00676H.

[46] B. M. Rao, P. R. Rao, and B. Sreenivasulu, "Grafting of Maleic Anhydride onto Acrylonitrile-Butadiene-Styrene Terpolymer: Synthesis and Characterization," *Polymer-Plastics Technology and Engineering*, vol. 38, no. 5, pp. 967–977, 1999, doi: 10.1080/03602559909351625.

[47] S. Thambiraj and D. Ravi Shankaran, "Preparation and physicochemical characterization of cellulose nanocrystals from industrial waste cotton," *Applied Surface Science*, vol. 412, pp. 405–416, 2017, doi: 10.1016/j.apsusc.2017.03.272.

[48] B. Hermawan, S. Nikmatin, Sudaryanto, H. Alatas, and S. G. Sukaryo, "Effect of oil palm empty fruit bunches fibers reinforced polymer recycled," *IOP Conference Series: Materials Science and Engineering*, vol. 223, p. 12064, 2017, doi: 10.1088/1757-899X/223/1/012064.

[49] A. M. Rezadoust, M. Esfandeh, M. H. Beheshty, and G. Heinrich, "Effect of the nanoclay types on the rheological response of unsaturated polyester–clay nanocomposites," *Polymer Engineering & Science*, vol. 53, no. 4, pp. 809–817, 2013, doi: 10.1002/pen.23325.

[50] A. J. Hsieh *et al.,* "Mechanical response and rheological properties of polycarbonate layered-silicate nanocomposites," *Polymer Engineering & Science*, vol. 44, no. 5, pp. 825–837, 2004, doi: 10.1002/pen.20074.

[51] S. C. Tjong and S. P. Bao, "Fracture toughness of high density polyethylene/SEBS-g-MA/montmorillonite nanocomposites," *Composites Science and Technology*, vol. 67, no. 2, pp. 314–323, 2007, doi: 10.1016/j.compscitech.2006.08.006.

[52] J. Xiao, S. Wang, P. Lu, and Y. Hu, "Effect of Organically Modified Montmorillonite on Thermal Degradation Mechanism of Polycarbonate Nanocomposites," *Procedia Engineering*, vol. 62, pp. 791–796, 2013, doi: 10.1016/j.proeng.2013.08.127.

[53] F. You, D. Wang, J. Cao, X. Li, Z.-M. Dang, and G.-H. Hu, "In situ thermal reduction of graphene oxide in a styrene–ethylene/butylene–styrene triblock copolymer via melt blending," *Polymer International*, vol. 63, no. 1, pp. 93–99, 2014, doi: 10.1002/pi.4528.

[54] R. A. Pearson and A. F. Yee, "Toughening mechanisms in elastomer-modified epoxies," *Journal of Materials Science*, vol. 21, no. 7, pp. 2475–2488, 1986, doi: 10.1007/BF01114294.

[55] M. Ishikawa and I. Chiba, "Toughening mechanisms of blends of poly(acrylonitrile-butadiene-styrene) copolymer and BPA polycarbonate," *Polymer*, vol. 31, no. 7, pp. 1232–1238, 1990, doi: 10.1016/0032-3861(90)90213-I.

CHAPTER 4

4 TAILORING THE MECHANICAL BEHAVIOR OF ELASTOMERIC PC BLENDS AT SMALL AND MEDIUM STRAIN RATES

Abstract: Polycarbonate blended with different wt.% of elastomeric polymers, thermoplastic copolyether ester elastomer (COPE), acrylonitrile-butadiene-styrene (ABS), modified ABS and styrene-ethylene-butylene-styrene (SEBS) with maleic anhydride, were melt blended in a twin-screw extruder. Dumbbell and bar specimens were prepared through injection molding for mechanical characterization at quasi-static and high-speed conditions. Fracture behavior and morphology of the specimens were assessed by optical (OM) and electronic microscopy (SEM), and thermal properties by differential scanning calorimetry (DSC). At quasi-static and high-speed tests, elongation at break of PC was substantially improved with the addition of only 1wt.% of maleated SEBS by 18 and 46%, respectively, and the addition of 10wt.% COPE by 59 and 114%. SEM analysis showed better compatibility between PC and ABS phase after grafting with MA. Only one phase was detected in PC/COPE blend, demonstrating that both phases are highly compatible. DSC supported this observation by a shifting in 6.3 °C of T_g to lower values. OM allowed the identification of different fracture modes in PC blends, from ductile to brittle behavior.

Keywords: polycarbonate, COPE, ABS-*g*MA, SEBS-*g*MA, toughening

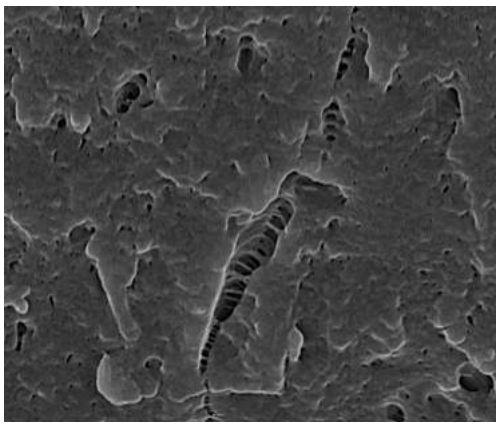

Submitted to Journal of Materials & Design

4.1 Introduction

Polycarbonate (PC) has been used in several engineering applications, most notably in automotive parts, due to its mechanical properties, as impact mitigators in energy absorbing applications and others due to its excellent transparency. It is known that many factors, such as temperature and strain rate, play an important role in the material mechanical performance [1]. The latter is of special importance since the mechanical properties of commercial thermoplastics are usually tested in eletromechanical machines that only covers small strain-rates. The extrapolation of the mechanical characterization to dynamic events will lead to erroneous results and thus it is recommended to characterize the material properties in similar conditions to those used in service application to improve the results accuracy. Additionally, analyzing a material at high strain rates explores aspects of response that might not be visible in quasi-static analysis, allowing insight into physical characteristics of the material structure and properties [2, 3].

When a polymer has some desired characteristics but lacks in performance, one approach to improve its behavior is through blending. One polymer has usually properties that overcome the undesired properties of the other, depending on the polymer blend, compatibilization might be necessary. This procedure takes place mainly in the melt (melt blending) in an twin-screw extruder with a modular screw that allows distributive and intensive mixing of the polymers.

Polycarbonate is known to present notch sensitivity and high melt viscosity, thus one way to overcome these problems is through blending with rubber-containing polymers [4]. A traditional example is blending PC with acrylonitrile-butadiene-styrene terpolymer (ABS), which results in a polymeric system with better notch sensitivity resistance, heat distortion, and improved processability [5]. However, melt blending does not exclusively enhance the properties of the blend, it is not uncommon to have a property tradeoff after blending different materials systems, for example, improving impact resistance can have negative effect on the tensile strength.

Wong observed the effect of ABS addition on the tensile and Izod impact properties of PC/ABS blends, using two types of ABS with different melt flow index (MFI value) [6]. An almost linear decrease of the elastic modulus and yield stress for the ABS with lowest MFI was detected, while for the other ABS, a decrease of the elastic modulus was noticed up to 50/50 (w/w). For the latter, upon increasing the ABS content, the elastic modulus of the blends started to approach the value of neat ABS. Regarding the Izod impact behavior, the authors tested unnotched and notched specimens and observed a decrease in toughness with increasing content of both types of ABS.

Lombardo *et al* also studied the incorporation of different types of ABS in a PC matrix. The ABS's used came from different preparation procedures, with different rubber content and rubber morphology (one bulk ABS made with 16 wt. % of rubber and rubber particle between 0.5-1 μm, and another emulsion made with 50% rubber content and a particle of ca. 0.12 μm) [5]. The authors prepared several blends varying the amount of PC from 0 to 100 wt.% in a multitude of steps but comparable at 90/10, 70/30, 50/50, 30/70 and 10/90 (w/w). For impact strength assessment, they made specimens with notches conforming to ASTM D256 (standard notch) and with sharp notches prepared by pressing a new razor blade against the center of the standard conforming notch. A reduction in impact strength for the standard notch specimen was noticed with increasing ABS content. However, for the specimens with a sharp notch they reported a substantial increase on the impact strength for both systems investigated.

Balakrishnan and Neelakantan investigated blends of PC/ABS with unmodified and modified ABS with maleic anhydride (MA) [7]. Under quasi-static tensile tests, a depreciation of all tensile parameters was reported (tensile strength, modulus and strain at break) for PC/ABS blends with increasing content of ABS. The addition of ABS-*g*-MA causes a general reduction of yield stress and a small positive influence in elastic modulus. The authors noticed a very pronounced increase in the impact strength of Izod notched specimens (almost 7-fold increase) when testing PC/ABS-*g*-MA (75/25, w/w) blend and a noticeable reduction in this parameter for PC/ABS system when compared to the neat PC. This behavior was associated to the poor interfacial interaction between PC and ABS, which was improved by the reaction of the MA groups and the hydroxyl terminals of PC during melt blending. Zhang *et al.* also demonstrated that the Izod impact properties of PC/ABS where improved through the addition of ABS-*g*-MA as compatibilizer [8].

The strain behavior of PC/ABS blends from low to high strain rate was studied by Yin and Wang with quasi-static tensile tests and split Hopkins tensile bars [9]. At a quasi-static level, a decrease in yield stress with increasing ABS content was reported, with a small positive effect on the tensile modulus up to a blend ratio of 60/40 (w/w). At quasi-static conditions, all blends presented a value of strain at break lower than PC. Other elastomeric polymers have also been added to PC in the work performed by Bagotia *et al.*, ethylene-methyl acrylate copolymer (EMA) [10]. The authors found a significant increase, up to 300%, in the Izod strength with only 5 wt.% of EMA. For a higher EMA content the blends did not show any substantial improvements, a decrease in tensile strength and modulus was detected, whilst the elongation at break increased.

Sivaraman *et al.* studied the influence of a thermoplastic copolyether ester elastomer (COPE) on the tensile and impact properties of PC [11], they noticed that elongation at break and Izod impact strength increase for an amount of 10 wt.% of COPE. The elastic modulus was negatively affected only by 6 wt.%, the yield stress slightly decreased, the breaking stress and elongation at break increased by 5 and 50%, respectively.

Garhwal and Maiti investigated the effect of blending PC with SEBS on the mechanical properties of blends through tensile and Izod impact tests [12]. While the incorporation of SEBS lead to a depreciation in the tensile strength, modulus, and elongation at break, the Izod impact strength of PC was improved. For a SEBS volume fraction (ϕ_d) of 0.06, a marginal decrease of the impact strength was obtained, however, for higher ϕ_d the impact strength increased. At a ϕ_d higher than 0.12 the sample did not break during the tests. More recently, the same authors published a study where the same properties were observed as a function of ϕ_d for a PC/SEBS-*g*-MA system [13]. A decrease in modulus and tensile strength as the SEBS-*g*-MA content increased was reported, alongside with an increase in the strain at break. For the latter parameter, a sharp increase was detected up to a ϕ_d of 0.12. For the Izod impact strength, a minimal increase was seen up to a $\phi_d$of 0.12. At higher contents of SEBS-*g*-MA, the blends did not break during the impact tests. Toughening through addition of SEBS-*g*-MA has also been studied for different polymer systems, Huang *et al.* used SEBS-*g*-MA to toughen amorphous polyamide [14]. Their results shown a decrease of modulus and yield stress with increasing content of the maleated SEBS whilst an unclear trend was perceived for the strain at break, but for the latter parameter, large standard deviation was detected. Higher amounts of SEBS-*g*-MA, up to 10 wt.%, produced a considerable toughening effect. Horiuchi *et al.* blended SEBS-*g*-MA with PC at different ratios where tensile properties as well as notched Izod impact strength diminished as rubber phase content increased [15].

The present work aims to perform a systematic study on the effect of blending PC with elastomeric polymers, namely ABS, ABS-*g*-MA, COPE and SEBS-*g*-MA prepared and tested under the same conditions. The effect of blending on morphology and glass transition was evaluated by scanning electron microscopy and differential scanning calorimetry. Mechanical characterization was evaluated through quasi-static and high-speed tensile tests, Charpy impact and dynamic mechanical tests and the fracture behavior by optical microscopy

4.2 Experimental

4.2.1 Material

Acrylonitrile Butadiene Styrene (ABS) Terluran GP-22 was purchased from BASF, polycarbonate (PC) Lexan 103R was obtained from Sabic co.. Styrene-Ethylene-Butylene-Styrene thermoplastic elastomer grafted with maleic anhydride (SEBS-*g*-MA) Taipol 7126 was kindly supplied by TER® AS Chemicals, and thermoplastic copolyether ester elastomer (COPE) HYTREL 4069 was kindly supplied by DuPont. Maleic anhydride (MA) with a purity of 99% was acquired from Acros and the initiator dicumyl peroxide with a purity of 98% (DCP) from Alfa Aesar.

4.2.2 Sample Preparation

4.2.2.1 Grafting MA onto ABS

ABS was grafting with 2.5 and 5 wt.% of MA using a DCP/MA ratio of 0.2 and named as ABS-*g*-MA1 and ABS-*g*-MA2 along the remainder of the manuscript. MA grafting reaction onto ABS was performed in a twin-screw extruder (Leistritz, Germany) using an average barrel melt temperature of 190 °C, a screw speed of 100 rpm and a throughput of 3 kg/h.

4.2.2.2 PC Compounding

Prior to processing, the elastomeric materials and PC were dried overnight in a vacuum oven at 80 and 105 °C, respectively. Melt blending took place in a twin-screw extruder (Leistritz, Germany) for a better level of mixing and dispersion, at an average melt temperature of 230 °C, 100 rpm, and a throughput of 3 kg/h. The residence time of the material inside the extrusion chamber was assessed by introducing pellets containing a blue pigment. From introduction of the pellets in the feeding zone until visual observation of an intense color change at the die took around 3 min, thus this value was assumed as the residence time. After processing, the filament was ground in a knife mill for subsequent processing. Different blend compositions of PC with unmodified and modified ABS, SEBS-*g*-MA and COPE were prepared as described in Table 4.1.

Table 4.1: Blend compositions.

Composition [wt.%/wt.%]	**PC**	**ABS**	**ABS-*g*-MA1**	**ABS-*g*-MA2**	**SEBS-*g*-MA**	**COPE**
PC/ABS		5 / 10	-	-	-	-
PC/ABS-*g*MA1	95 / 90	-	5 / 10	-	-	-
PC/ABS-*g*MA2		-	-	5 / 10	-	-
PC/SEBS-*g*-MA	99	-	-	-	1	-
PC/COPE	90	-	-	-	-	10

4.2.2.3 Injection Molding

For subsequent mechanical characterization, miniaturized tensile specimens and impact bars were prepared by injection molding using a Boy 22A injection molding machine (Dr. BOY, United States). The specimens were produced with a flow rate of 5 cm^3/s and an average barrel and mold temperature of 280 and 80 °C, respectively. Holding pressure was set as 950 bar [specific pressure] for 6 s and the cooling time set to 8 s. Impact bars were also manufactured by injection molding using an Engel 45T. The bars were molded with a melt temperature of 290 °C, an injection velocity of 60 mm/s, a holding pressure of 120 bar [hydraulic pressure] for 11 s followed by 15 s of cooling time. After processing, all the specimens were stored and kept under laboratory (21 °C, 50 % RH) conditions for at least 48h prior to mechanical testing.

4.2.3 Characterization

4.2.3.1 Structural analysis and grafting degree

Grafted ABS samples were dissolved in acetone to remove the unreacted MA, precipitated, and washed several times in methanol. Finally, the recovered material was dried at 180 °C for 1h under constant nitrogen flow. The chemical structure and the grafting degree (GD) were analyzed by Fourier transform infrared (FT-IR) spectroscopy (Jasco FT-IR 4100) in transmission mode from a range of 400 – 4500 cm^{-1}. GD (wt.% MA) was quantified by correlating the absorption peaks of the vibrations at 1780 and 2237 cm^{-1} of carbonyl (-C = O) from MA and ABS nitrile groups (-C≡N), respectively. A linear calibration curve (m = 1.35) was built with different ABS and MA compositions to estimate the GD of the purified samples, following Equation (4.1) [16]:

$$GD\ (wt.\%MA) = m \times \frac{abs.CO_{1780}}{abs.CN_{2237}} \tag{4.1}$$

4.2.3.2 Mechanical characterization

4.2.3.2.1 Quasi-static tensile tests

The quasi-static tensile tests were performed on a universal tensile testing machine Instron 5969 (Instron, EUA) with a load cell of 5 kN, at room temperature and 60% humidity. The stress (σ) and strain (ε) were evaluated by using the engineering stress definition in ISO 527 [17].The tensile properties evaluated were the yield stress (σ_y), elastic modulus (E), strain at break (ε_r) and modulus of toughness (U). The yield stress was defined as the stress at which an increase in strain occurs without an increase in engineering stress. The modulus was determined from the initial linear proportion in the engineering stress- strain (σ – ε) curve. The strain at break was defined as the strain position where the stress decreased to 60% of the maximum stress. The modulus of toughness was defined as the integral of the σ – ε curve up to the strain at break position. The elastic modulus was evaluated with a crosshead velocity of 1 mm/min. Afterwards, the crosshead speed was changed to 50 mm/min to assess the remaining parameters. At least 5 specimens of each blend were analyzed, and an average value calculated. The geometry of the used specimen is illustrated in Figure 4.1 (right).

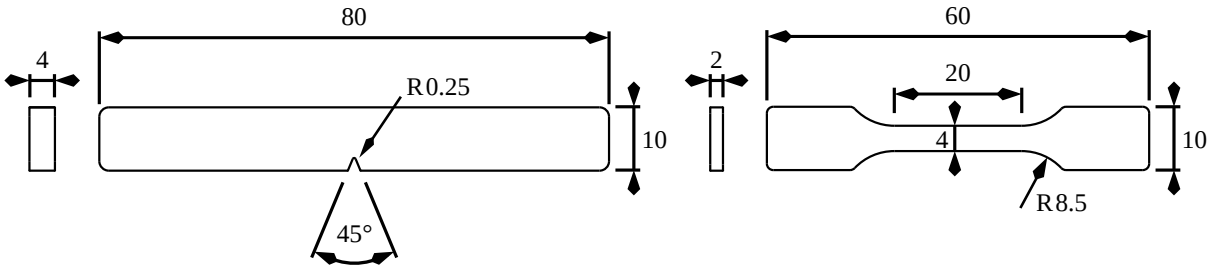

Figure 4.1: On the left: Geometry of the impact. On the right: tensile specimen geometry, in mm.

4.2.3.2.2 High-speed tensile tests

For high-speed tensile tests, a Zwick-Roell Amsler HTM3712 (Zwick-Roell, Germany) tensile machine was used with a load cell of 20 kN. The tests were performed with the same specimen geometry used in the quasi-static tensile tests (Figure 4.1-right) employing a crosshead velocity of 1 m/s. The same tensile parameters and their respective definition were used in the high-speed tensile evaluation.

4.2.3.2.3 Impact tests

Charpy impact tests were performed to evaluate the impact strength (a_{CN}) on unnotched and 2 mm v-notch (type 1A) specimens using an impact test CEAST system and rectangular shape specimens (80 x 10 x 4 mm). The tests were performed according to the procedure defined in ISO 179-1 [18]. The geometry of the specimen is depicted in Figure 4.1-left.

4.2.3.3 Thermo-mechanical characterization

The storage modulus and dissipation factor of the blends were assessed by dynamic mechanical analysis (DMA) using a DMA TRITON. For this test, the gauge length of the tensile specimens was used as a specimen. The distance between grips was 7.5 mm. A load of 1 N was applied at a frequency of 1 Hz in the temperature range of 40 to 180 °C using a heating rate of 2 °C/min.

4.2.3.4 Thermal characterization

The thermal behavior was analyzed using a DSC Netzsch 200 Maya (Netzsch, Germany). The tests were performed under nitrogen atmosphere with a heating rate of 10 °C/min from 30 to 170 °C. Two heating cycles were performed. The first was used to erase the thermal history of the material and the second was used to evaluate the effect of material blending.

4.2.3.5 Fracture surface and Morphological characterization

The fracture surface of the tested specimens was studied using an optical microscope DMS 1000 (Leica, Germany) coupled with a light polarizer. To visually evaluate the specimen stress distribution after injection molding, two light polarizers sheets with perpendicular polarization angle were applied in a light chamber. The morphology of the blends was analyzed by Scanning Electron Microscope (SEM) using a FEI Quanta 400 (FEI, The Netherlands). Tensile samples were previously fractured in liquid nitrogen and coated with a thin film of gold-palladium.

4.3 Results and Discussion

4.3.1 Grafting degree evaluation and blend structural analysis

Figure 4.2 shows the normalized absorbance IR spectra of initial and purified ABS grafted with maleic anhydride. Comparing the spectrum of ABS with the purified samples, it is possible to detect the

appearance of three new absorbance peaks related to the successfully grafting of MA onto ABS, at 1860 and 1781 cm^{-1} of the C=O asymmetric and symmetric stretching from the cyclic anhydride group, respectively, and 1215 cm^{-1} of C-O-C vibrations [16, 19]. Concerning the polybutadiene (PB) backbone chemical structure, the peak located at 1638 cm^{-1} is assigned to the stretching vibration mode of C=C and the peak at 966 cm^{-1} to the deformation of vinylic hydrogen [20, 21]. Both peak intensities decrease with increasing GD, confirming that MA was grafted onto the PB backbone. Since it is reported that grafting of MA onto ABS can occur either into the double C=C bond or by the loss of the vinylic hydrogen of the PB fraction, polyacrylonitrile C≡N bond (2237 cm^{-1}) was used to estimate the grafting degree [22]. The calculated grafting degree of modified ABS was 1.5 and 3.1 % for ABS-*g*MA1 and ABS-*g*MA2, respectively.

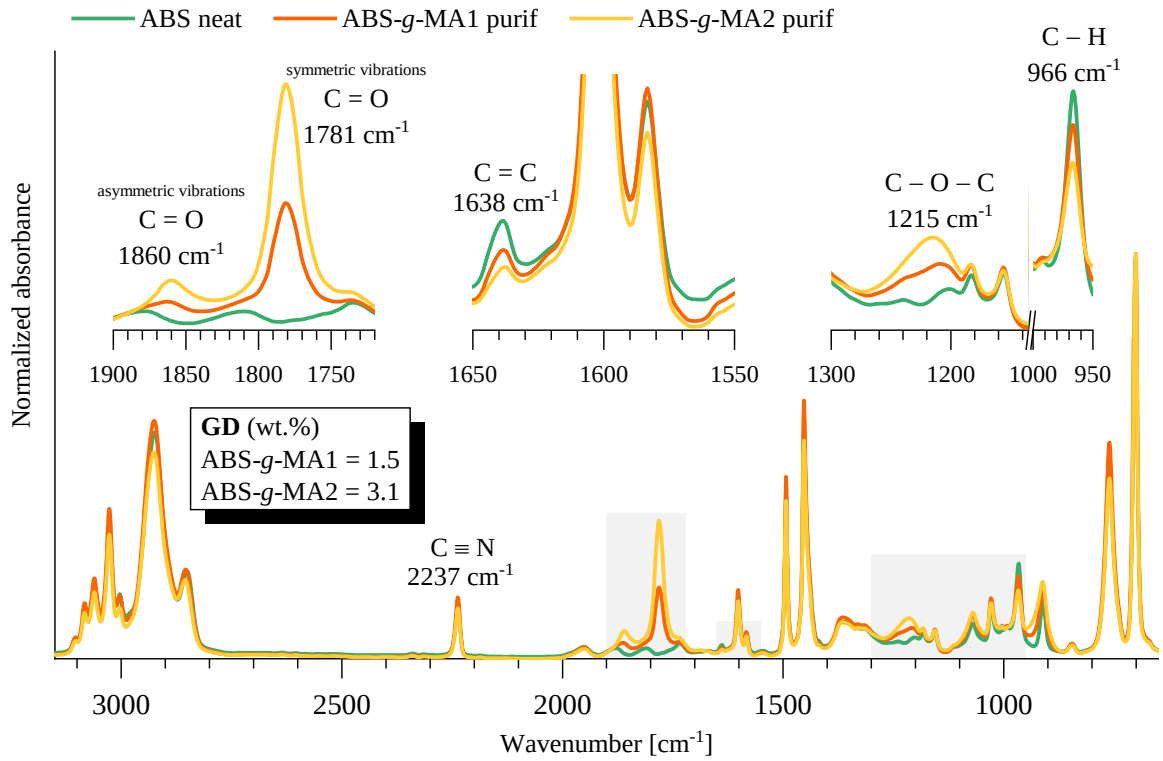

Figure 4.2: IR spectra of ABS ungrafted and grafted with maleic anhydride.

From the IR spectra of the prepared blends (Figure 4.3), it can be perceptible a decrease of C=O peak associated to the PC carbonyl groups with the incorporation of 10 wt.% ABS and ABS-*g*MA, and a shift in the C-H at 761 and 700 cm^{-1}. A slight increase in the C-H bands in the range of 3000 – 2800 cm^{-1} and a minor shift at 700 cm^{-1} is the result of the incorporation of 1 wt.% SEBS-*g*MA. Although the chemical structure of COPE is not known, it is possible to detect the ester (1717 cm^{-1}) and ether (1275 cm^{-1}) characteristic vibration modes. Blending with PC promotes a slight deviation of the COPE ester band to

1720 cm^{-1}, an absence of the ether peak of COPE and also a shift in the C-H vibration around 3000 – 2800 cm^{-1} and 1500 – 1300 cm^{-1}, which are due to the occurrence of a transesterification reaction [23]. This analysis demonstrates that elastomers were successfully incorporated into the PC matrix.

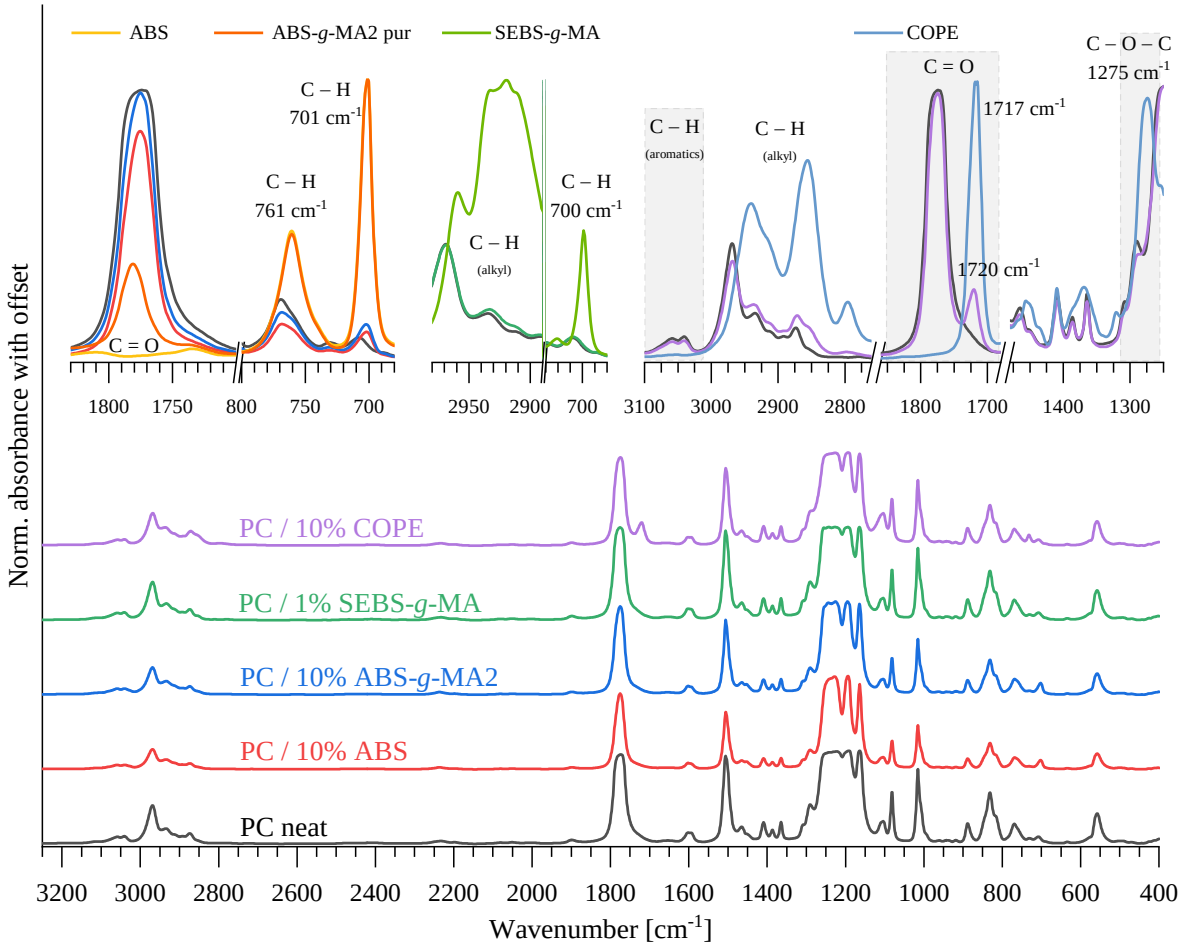

Figure 4.3: IR spectra of PC blended with 10wt.% ABS, ABS-g-MA2, 1wt.% SEBS–g–MA, and COPE, and their respective base materials.

4.3.2 Blends Morphology

It is known that polymer morphology is complex and dependent of several conditions, such as compatibility between materials, polymer rheology and processing parameters used during preparation [11, 24].

While the micrographs of the transversal section of PC (a), PC/10%ABS (b), PC/10%ABS-g-MA1 (c) and PC/10% ABS-g-MA2 (d) are presented in Figure 4.4, Figure 4.5 depicted PC/SEBS-*g*MA (a-c), and PC/COPE (d) blends. PC presents a relatively smooth, clean, and featureless surface, where no relevant plastic deformation is visible, indicating the presence of a very brittle fracture. The addition of elastomeric

materials results on a great change in morphology, ABS phase is dispersed in the PC matrix as droplets, comparing non and modified ABS it can be noticed that an increase in grafting degree improves slightly the compatibility between both phases. While PC/ABS blend exhibits higher interfacial tension between the two phases, PC/ABS-*g*MA micrograph shows a connection between ABS-*g*MA droplets and PC matrix, this might be due to chemical bond between MA and the -OH end groups of PC [24]. Since SEBS-*g*MA was added in a very low amount (1 wt.%), it was not possible to detected two phases by SEM. It is possible to observe the influence of orientation during injection on the morphology (Figure 4.5-a), where a more lamellar like structure is observed for higher shear rates near the walls (highly oriented polymer molecules), contrary to the center of the specimen. The differences noticed between PC and PC/ SEBS-*g*MA micrographs can be attributed to the cavitation phenomenon. In a recent study it was shown that PC/SEBS-*g*MA systems would mechanically fail through cavitation phenomena with the appearance of fibrils during deformation [13]. Figure 4.5-b shows visible fibrils that occur mainly under higher degree of molecular orientation, while rubber cavitation phenomena (formation of voids) is more predominant for lower degree of molecular orientation, Figure 4.5-c. The addition of 10 wt.% COPE results in a very good dispersion on the PC matrix, since it is not possible to distinguish two phases in the micrographs, corroborating IR analysis in Figure 4.3 that transesterification reaction took place. Contrary to Sivaraman *et al.* results where PC / COPE systems blended in a single screw extruder did not promoted compatibilization, which can be due to the processing conditions, such as shear rate, temperature and mixing intensity, these are determinant factors for reactive blending [11]. Crack growth is delayed due to the formation of nanofibrills due to the stretching of the rubber phase (crazing). PC/ABS blends show a PC phase with dispersed rubber droplets, while SEBS-*g*MA and COPE addition resulted in a continuous phase, where cavitation and crazing phenomena is more pronounced. Therefore, it should be expected a better fracture resistance at negative temperature for PC systems reinforced with COPE.

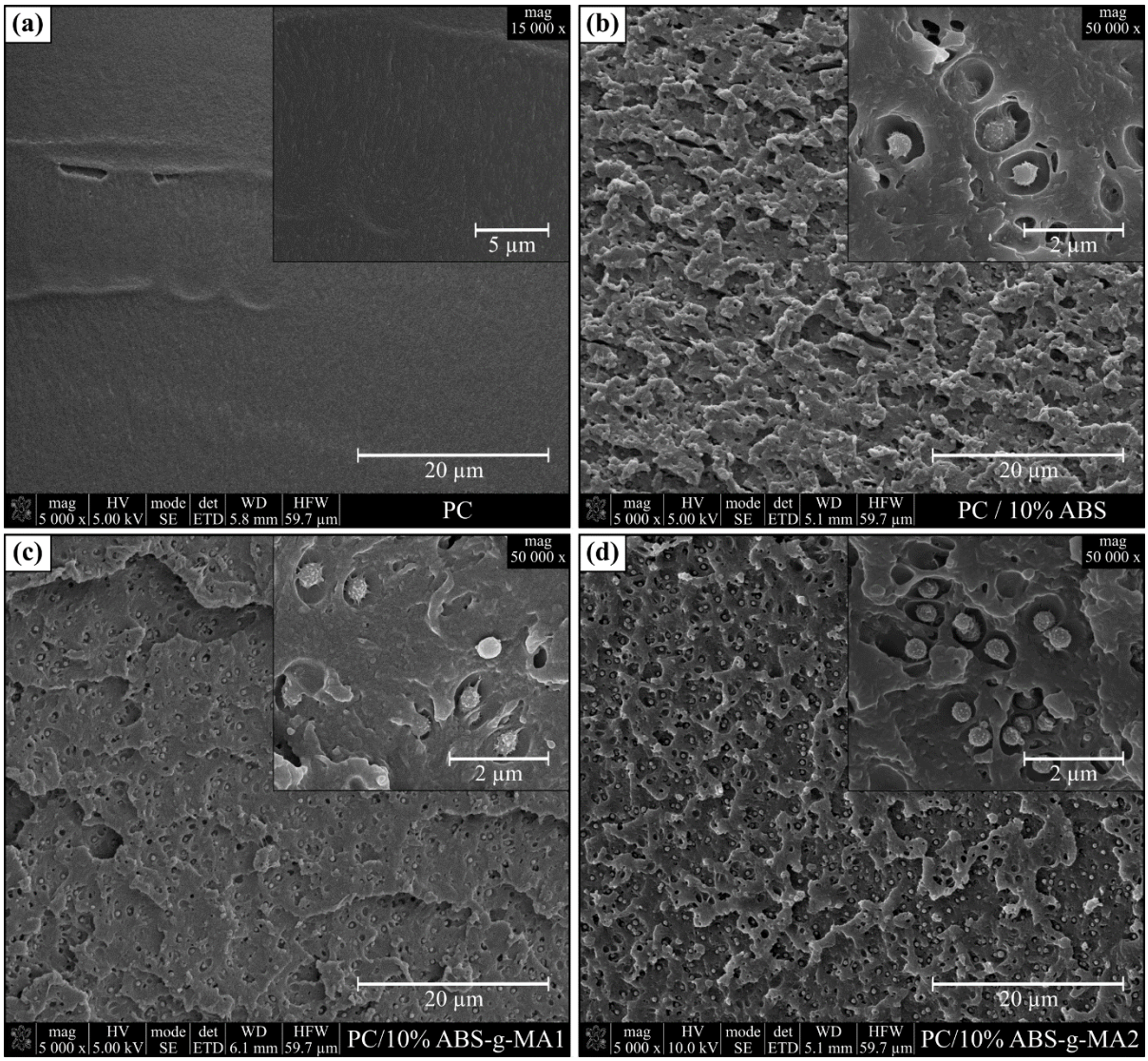

Figure 4.4: SEM micrographs of (a) PC, (b) PC/10%ABS, (c) PC/10%ABS-g-MA1 and (d) PC/10% ABS-g-MA2 blends

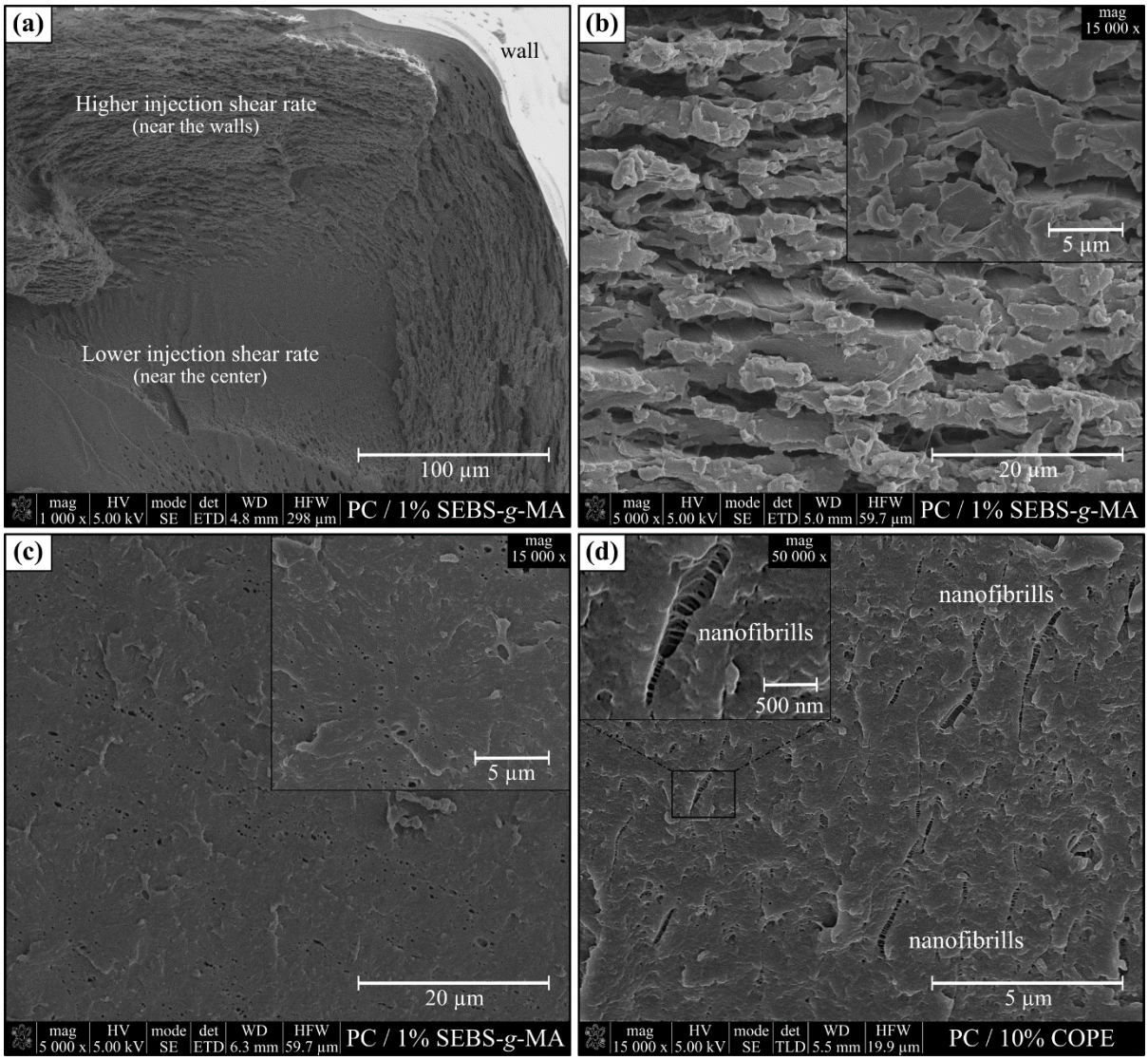

Figure 4.5: SEM micrographs of PC/SEBS-g-MA and PC/COPE blends.

4.3.3 Thermal characterization results

The values of the analyzed glass transition reported in Table 4.2 were calculated using the midpoint technique, in accordance with ASTM D3418-15 standard [25].

Neat ABS and PC present a glass transition temperature at 106 and 145 °C, respectively. After modification of ABS with MA, this value appears to decrease. However, no significant differences can be noticed between the two grafting degrees. Similar trends of T_g have been reported in literature where the authors attributed this to the short flank chain in anhydride maleic in the ABS-*g*-MA, which increase the distance among the polymer chains and increased the free volume [8]. Blends thermograms showed the existence of two T_g's referent to each blend component (T_{g1} for the ABS and T_{g2} for PC) for the PC/ABS and PC/ABS-*g*-MA blends. In these blends, T_{g1} has a value higher than that of the neat ABS and T_{g2} a

value slightly lower than T_g of PC, suggesting a small compatibility between the two polymers (taking into account the error associated with measurement). From the previous reference, the authors indicated that the smaller the different between the T_g's, the better the compatibility between the blend components [8]. The T_g of PC/SEBS-*g*-MA has a marginally higher value than PC, indicating that this small amount of polymer constrains the molecular mobility of PC chains. The addition of COPE into the PC matrix decreases substantially the value of T_g and is in accordance with the SEM results (Figure 4.5-d) where a single phase morphology was observed, showing excellent compatibility between both polymers.

Table 4.2: Thermal properties of initial polymers and blends, using DSC and DMA.

Sample	DSC						DMA
	T_{g1} [ºC]			T_{g2} [ºC]			T_g
	T_{onset}	$T_{midpoint}$	T_{endset}	T_{onset}	$T_{midpoint}$	T_{endset}	[ºC]
ABS	103.8	106.3	110.0	-	-	-	101.6
ABS-*g*-MA1	100.1	103.7	107.6	-	-	-	98.5
ABS-*g*-MA2	100.5	103.9	107.8	-	-	-	97.8
PC	-	-	-	142.8	145.2	148.6	144.1
PC / 10% ABS	108.8	111.8	115.1	141.5	144.5	147.5	142.7
PC / 10% ABS-*g*-MA1	108.8	110.5	112.8	141.6	144.4	147.7	142.2
PC / 10% ABS-*g*-MA2	108.7	112.0	115.0	141.0	144.0	147.6	142.1
PC / 1% SEBS-*g*-MA	-	-	-	143.9	147.1	149.8	146.0
PC / 10% COPE	-	-	-	131.5	138.9	145.1	118.9

4.3.4 Thermo-mechanical results

The thermo-mechanical characterization of the polymers and polymers blends is presented in Figure 4.6, and the DMA T_g values in Table 4.2.

The effect of grafting MA onto ABS can be noticed in Figure 4.6-a, where ABS storage modulus (E') is relatively constant up to 90 °C. After, a sharp drop is observed with increasing temperature, the $tan\,\delta$ peak appears at a temperature around 114 °C, while in ABS-*g*-MA samples the peak is shifted to a lower temperature (111 °C). The T_g values obtained through DMA are in agreement with the DSC data, the presence of grafted MA might increase the distance between the polymers chains resulting in a lower T_g. The difference between DMA and DSC values can be due to the different equipment and testing conditions.

The temperature dependence of the E' of PC depicted in Figure 4.6-b presents a small decrease up to a temperature of 120 °C, after which an inflection can be noticed followed by a non-linear decrease of the modulus with increasing temperature up to 180 °C. The $tan\ \delta$ peak associated to a broad α-relaxation can be observed starting at 120 °C and ending at 165 °C with maxima at ca. 154 °C. PC blends with unmodified and modified ABS, a small decrease in storage modulus is observed around 110 °C due to the presence of the ABS phase, having a noticeable reduction of E' with increasing temperature before reaching the α-transition of PC. A small shift in the maxima of the α-transition to smaller temperatures is perceived when adding ABS in 5 and 10 wt.% with negligible difference in damping intensity. Similar behavior is noticed for E' for blends with modified ABS, but it is clear a small shift of $tan\ \delta$ peak to lower values (Figure 4.6-c), which confirms the existence of compatibility between both polymers .

The effect of SEBS-*g*-MA on the dynamic mechanical properties of PC can be found in Figure 4.6-d, and both the storage modulus and $tan\ \delta$ have a remarkably similar behavior, with a small shift to higher temperatures and an increase in the magnitude of the $tan\ \delta$ peak. The same increase in T_g was observed in DSC and DMA, suggesting that the small rubber particles of SEBS-*g*-MA constricts the molecular movement of PC chains.

The addition of 10 wt.% COPE produces a substantial difference in the elastic modulus. The value of E' starts to decrease at 60 °C, after which the inflection can be detected with a non-linear decremental behavior up to 170 °C. The damping factor of the blend with COPE can be seen to start at ca. 80 °C and to finish at ca 160 °C with a maximum at 148 °C. The $tan\ \delta$ peak has a lower damping intensity with a much broader peak, in agreement with results discussed above. DMA sensitivity is greater than DSC for thermal transition detection, since this type of transitions are more noticeable in the mechanical properties rather than in the thermal capacity, which explains the differences between PC/COPE T_g values determined with DMA (118.9 °C) and DSC (138.9 °C) [26].

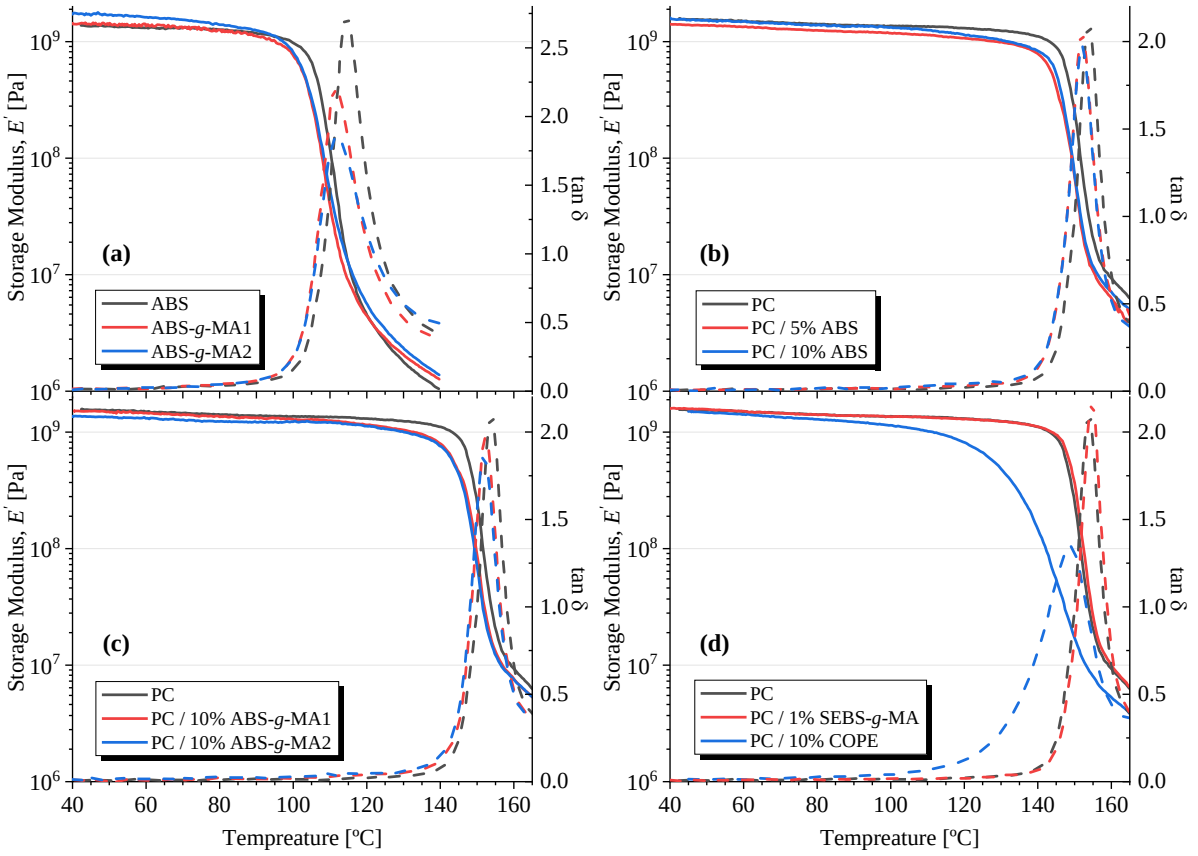

Figure 4.6: Dynamic Mechanical Analysis of non and modified ABS and PC compounds, with the storage modulus (full line) and $tan\ \delta$ (dash line).

4.3.5 Mechanical characterization results

4.3.5.1 Quasi-static tensile behavior of PC and PC blends

The 1 and 50 mm/min of speed test corresponds to a strain-rate of approximately 5×10^{-4} and 2.5×10^{-2} s^{-1}, respectively. The results will be presented and discussed starting with the neat polymers (PC and ABS), followed by the blends of PC/ABS, PC/ABS-*g*MA, PC/ SEBS-*g*MA, and finally PC/ COPE. Figure 4.7 depicts the quasi-static tensile curves of the tested specimens (each curve is the average of at least 5 measurements), and Figure 4.8 the calculated average values of the mechanical properties, namely, toughness ($\overline{U}$), elastic modulus ($\overline{E}$), yield stress ($\overline{\sigma_y}$) and strain at break ($\overline{\varepsilon_r}$).

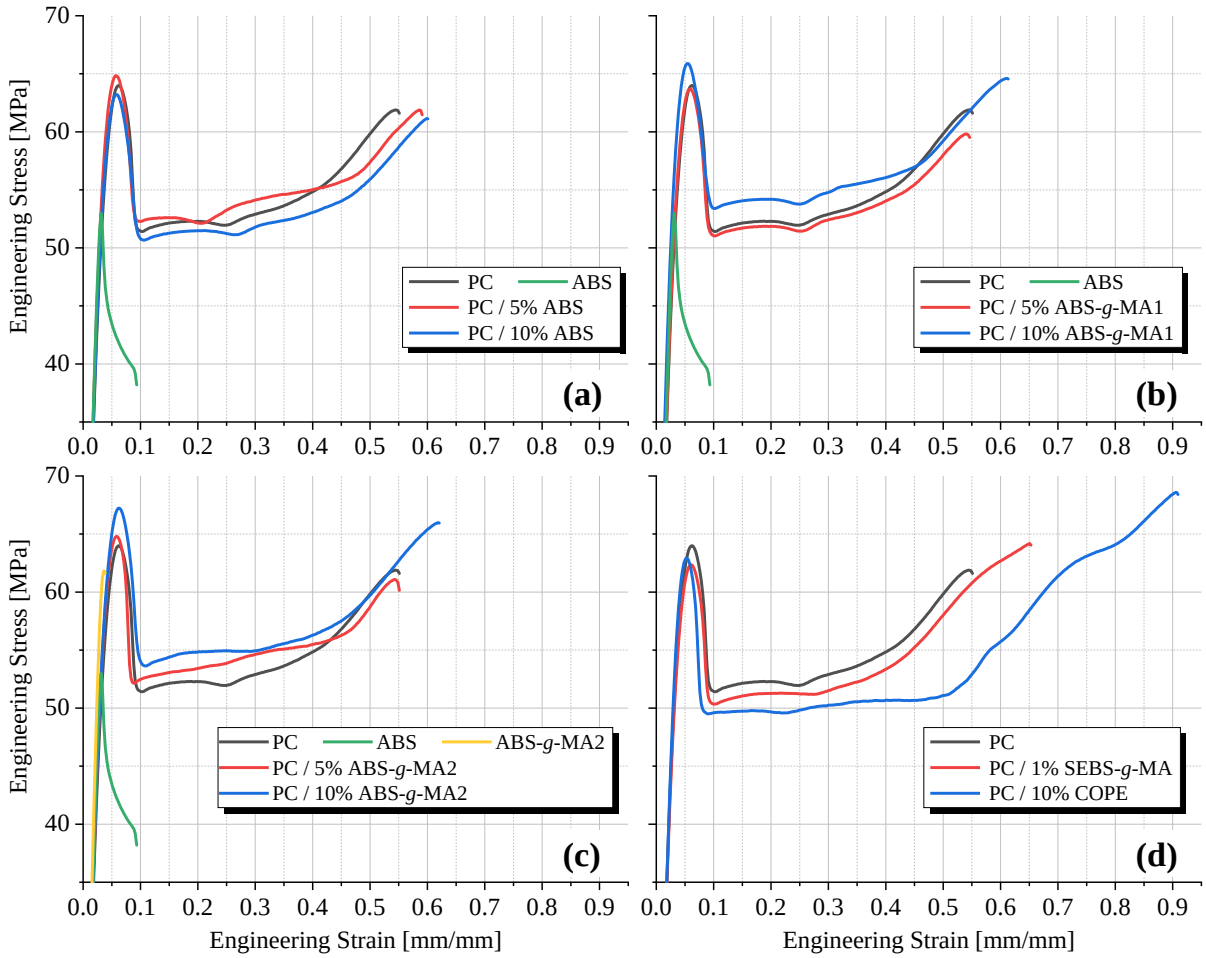

Figure 4.7: Quasi-static tensile curves of PC/ABS (a), PC/ABS-g-MA1 (b), PC/ABS-g-MA2 (c), PC/SEBS-g-MA and PC/COPE (d) blends.

The PC used in this work presents higher yield stress and significantly higher strain at break than ABS (Figure 4.7 a and b), but ABS has higher $\bar{E}$ than PC (Figure 4.8). Analysis of the engineering tensile curve of PC shows a strain softening following the yield stress and subsequent strain hardening until fracture occurs (Figure 4.7 b). ABS exhibits strain softening following the yield stress, but no strain hardening is seen until fracture (Figure 4.7 a). Since PB is responsible for the flexibility of ABS, the insertion of MA groups into PB backbone has a negative impact on this property, turning it into a more fragile material by increasing the modulus of elasticity with no plastic deformation behavior (yellow line in Figure 4.7-c).

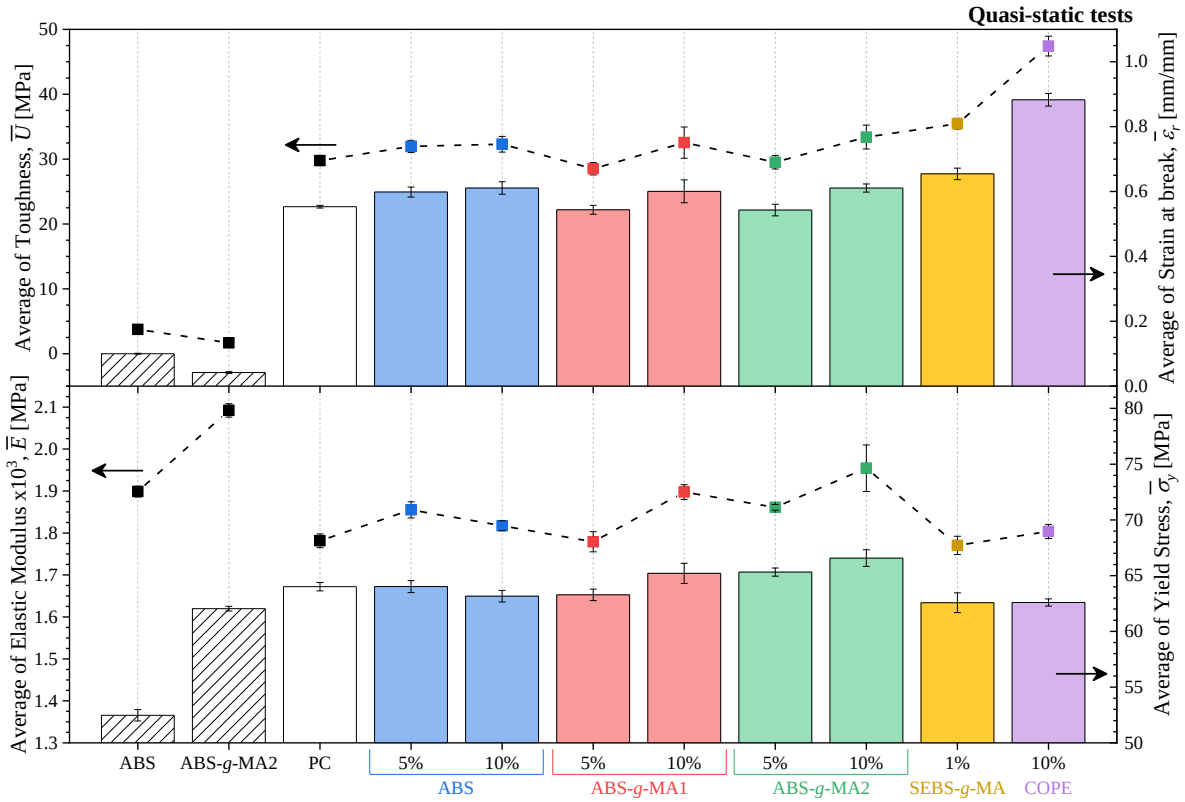

Figure 4.8: Average of yield stress ($\overline{\sigma_y}$), modulus ($\overline{E}$), strain at break ($\overline{\varepsilon_r}$), and toughness ($\overline{U}$) of quasi-static tests on PC, ABS, ABS-g-MA2, and PC blends.

Blending 5 and 10 wt.% of ABS with PC a negligible difference in $\overline{\sigma_y}$ can be noticed when compared to neat PC, the modulus of the blends have a value comprehended between those of the neat materials (Figure 4.8). The strain at break increases in average 9 % and the $\overline{\sigma_y}$ and $\overline{E}$ are in agreement with results reported in the literature, where the addition of ABS to PC matrix reduced the modulus of elasticity of the blend [5, 6, 9]. For the variation in $\overline{\varepsilon_r}$, in Lombardo *et al.* the authors depicted a conflicting trend up to 40 wt.% ABS, where the strain at break variation was dependent on the type of ABS used [5]. Additionally, Yin *et al.* reported a decrease in $\overline{\varepsilon_r}$ with increasing addition of ABS in quasi-static tests [9]. This variation in behavior can also be due to the influence of ductile to brittle transition of PC, situated for specimens with thickness between 3.18-6.35 mm and dependent upon the PC type, molecular weight and processing conditions [11].

Blends of PC with 5 wt.% of modified ABS with different grafting degree values does not seem to have a significant effect on the measured tensile properties. These blends present a yield stress and modulus between the performance of the neat constituents, and a negligible reduction in the strain at break (Figure 4.8). A different behavior was noticed in blends containing 10 wt.% ABS, the increase of grafting MA increased slightly the yield stress and modulus and lowered the strain at break. From the tensile results

it is also apparent that the increase of grafting MA induces more variability in the mechanical properties results. Also, it is visible that the introduction of MA groups onto ABS has a positive effect for higher amounts of ABS. Results from literature show a decrease in tensile strength and strain at break with increasing content of ABS-*g*-MA, which are in agreement with the obtained results [7].

When a small amount of SEBS-*g*-MA is blended with PC a small decrease in the yield stress and modulus can be noticed, whilst a significant increase occurs in the strain at break (Figure 4.8). Both $\sigma-\varepsilon$ curves have a similar behavior, where a strain softening of roughly the same order of magnitude can be seen for both neat material and blend followed by a strain hardening behavior up to fracture (Figure 4.7-d). The stress values obtained in the strain hardening regime for the neat PC curve are always higher up to fracture of specimen, however, the PC/SEBS-*g*-MA blend presents a higher tensile strength at fracture. This additional elongation allows the material to absorb more strain energy per unit volume before fracture. Similar results are also found in literature, where increasing content of SEBS-*g*-MA in PC blends were associated to decrease of tensile strength and tensile modulus [13]. The authors of the previous reference reported that the strain at break greatly increase up to a volume fraction of 0.12. After this value, a negative trend was observed, although at the highest volume fraction tested (0.39) the strain at break values were still considerably higher than that of the neat PC. Comparable results were related by Horiuchi *et al.*, a decrease in yield stress and elastic modulus, and a sharp decrease for the strain at break with increasing content of SEBS-*g*-MA [15]. The results shown in the present work demonstrate that even with a small amount of SEBS-*g*-MA the deformation capability in tensile tests of PC can be improved (around 18 %) with a small trade-off of in yield stress and elastic modulus.

PC/COPE blend presents a mechanical behavior alike to PC/SEBS-*g*-MA, where a decrease in yield stress and minimal difference in the tensile modulus can be seen (Figure 4.8). However, the deformation behavior is clearly different, a significant improvement (% 60 increase) in the strain at break is achieved when adding 10 wt.% of COPE. Similar to what was perceived in the blend containing SEBS-*g*-MA, the stress value after yield is always higher in the neat material up to fracture, however, due to the increase in elongation and strain hardening, the stress at break of the blend is higher (Figure 4.7-d). Moreover, a funky behavior is observed in the PC/COPE blend after the strain value where the neat specimen fractures. The increase appears to be highly nonlinear with a wavy behavior. These results corroborate the observations made in for quasi-static tensile tests in the literature [11]. The mechanical properties can also be explained by the morphology as these two blends only showed one phase and the presence of crazing phenomena after fracture, which are associated to an improvement in toughening.

4.3.5.2 High speed tensile behavior of PC and PC blends

The 1 m/s speed corresponds to a strain-rate of approximately 30 s^{-1}. Analogously, to the description made in the quasi-static section, here the discussion will follow the same trend, neat polymers and then the blends.

Since the high-speed tensile curves of the tested specimens presented a similar trend as the quasi-static, only the calculated average values of the mechanical properties are depicted in Figure 4.9.

The results of the neat polymers have the same trend reported in the quasi-static tests, ABS presents a lower $\overline{\sigma_y}$, a slightly higher $\bar{E}$ and a substantial reduction in $\overline{\varepsilon_r}$ when compared to the neat PC. The PC / ABS blends show a slight increase in the tensile strength whilst the modulus of the blends presents a behavior in between the limits of the neat components. The blend with 5 wt.% ABS presented a reduction of stress at break whilst an improvement is reported for the blend with 10 wt.%. In fact, the latter shows an improved behavior over the neat PC with higher stress values along the σ-ε curve. At this strain rate the use of PC with 10 wt.% ABS indicates a higher toughness than the neat PC, thus providing a synergetic effect with the base polymer.

The results of the blends with 5 and 10 wt.% of ABS-*g*-MA2 demonstrate that the blends have a slight increase in yield stress, a modulus value comprehended between the values of the neat constituents and a similar trend to blends with unmodified ABS blend. The blends containing 10 wt.% of modified ABS presents higher stress values than neat PC over the whole σ-ε curve, which shows higher toughness at this strain-rate.

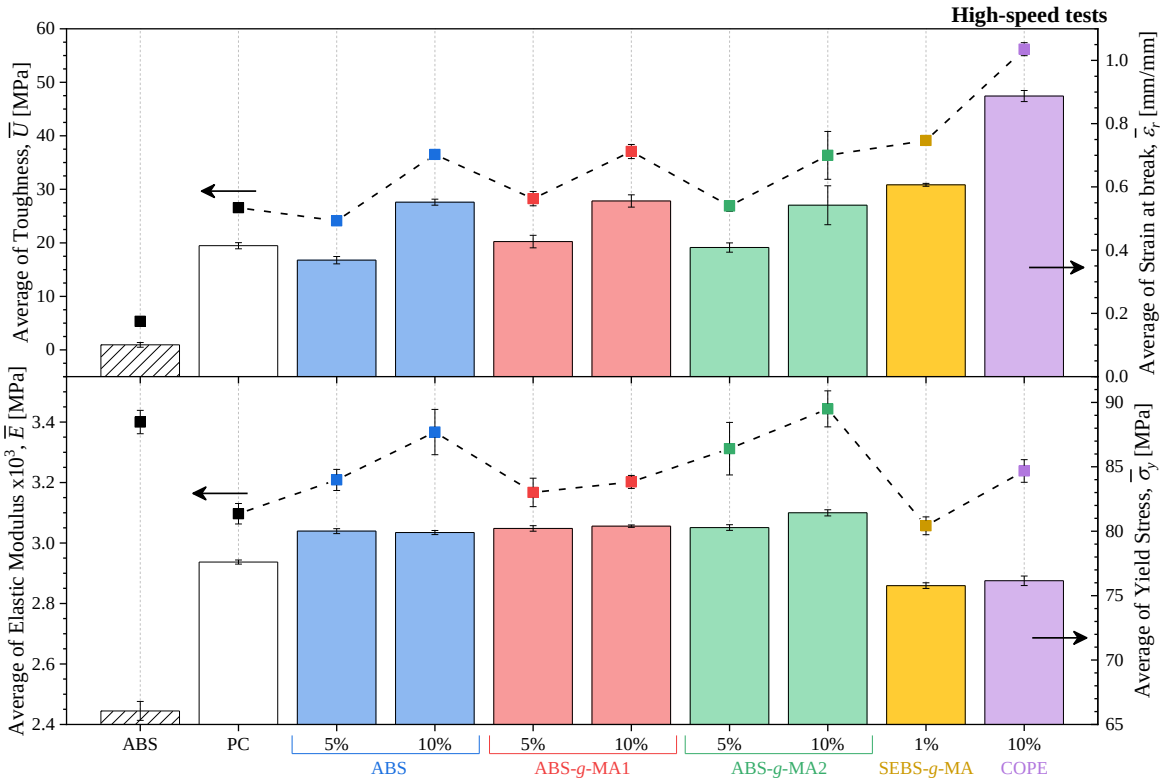

Figure 4.9: Average of yield stress ($\overline{\sigma_y}$), modulus ($\overline{E}$), strain at break ($\overline{\varepsilon_r}$), and toughness ($\overline{U}$) of high-speed tests on PC, ABS and PC blends.

Blending 1 wt.% of SEBS-*g*MA with PC decreases the yield stress and modulus and increases significantly the elongation at break. The addition of a small amount of SEBS-*g*MA appears to increase the toughness of PC, this could be explained by the cavitation phenomena observed in SEM as a toughening mechanism. Both PC and PC / SEBS-*g*MA present strain hardening, where the stress level in the neat material is always higher up to the fracture of the specimen.

The PC / COPE indicates a slight decrease in the yield stress and modulus, whereas a pronounced increase in the elongation at break. As described above, the effect of using 10 wt.% of COPE is similar to SEBS-*g*MA, where both materials present a strain softening after yield followed by a strain hardening, where the stress level is always higher in the neat polymer up to fracture. However, the ultimate tensile strength at fracture is higher in the blend. Additionally, due to the pronounced increase in the strain at break, the toughness of the material increases substantially, possibly due to presence of fibrils that originates during crazing, as observed in SEM.

4.3.5.3 Optical Microscopy of tensile specimens

It is well known that the thermomechanical environment developed during injection molding can induced residual stresses. Different flow channel geometries in the part (thickness, convergent and divergent channels) can generate a gradient of shear stress that orientates polymer molecules in an anisotropic fashion (flow-induced stresses). This orientation is frozen in the part due to the rapid cooling system of the mold, resulting in a non-equilibrium state of the material. Also, different cooling rate distribution can contribute to residual stress phenomena because shrinkage of the part is not uniform (thermal-induced stresses) [27]. All these phenomena can be responsible for anisotropy in material properties, part warpage and premature failure. Therefore, to better understand the tensile results, samples were analyzed by optical microscopy using two crossed polarized sheets in a light chamber, to observe the way light interacts with a transparent polymer and infer about their state of induced residual stress [28].

Figure 4.10 and Figure 4.14 presents pictures of the stress distribution along the injected specimens used for impact (bar) and tensile (dumbbell) tests. While bar specimen presents a fair and equal distributed residual stress through all geometry, the dumbbell specimen clearly has anisotropy in its structure. This stress distribution was detected during the tensile tests where the preferred fracture site in quasi-static conditions was located on the opposite side of the gate where a high state of stress concentration seems to exist.

4.3.5.3.1 Quasi-static behavior

PC blends tested under quasi-static tests (Figure 4.10) clearly show the effect of stress distribution discussed above, where the injection process created a localized high stress concentration zone of the specimen. All samples, except for PC/COPE, have their rupture point in this zone. During processing, all the blends presented a reduction in the injection pressure required to fill the cavity in comparison to the neat PC, being more pronounced for the blend containing COPE. This decrease is related to an increase in fluidity of the melt that prevented the formation of critical zones due to residual stress. It can also be seen the formation of micro-crack along the specimen gauge length. Since PC/COPE blend had the higher deformation, it presents a higher number of these cracks. A more detailed view of the micro-cracks can be seen in Figure 4.11. This shows a similar crack pattern for PC/ABS and PC/SEBS-*g*-MA specimens, where it is possible to detect the presence of wide cracks due to the higher deformation. The blend of PC/COPE crack pattern is very different since it was the one which presented the highest deformation, resulting in the formation of a higher number of micro-cracks dispersed along the gauge specimen length,

and also a visible reduction on the cross section. This behavior is consistent with SEM observation, where fibrils delayed the crack propagation of cryogenic fractured samples.

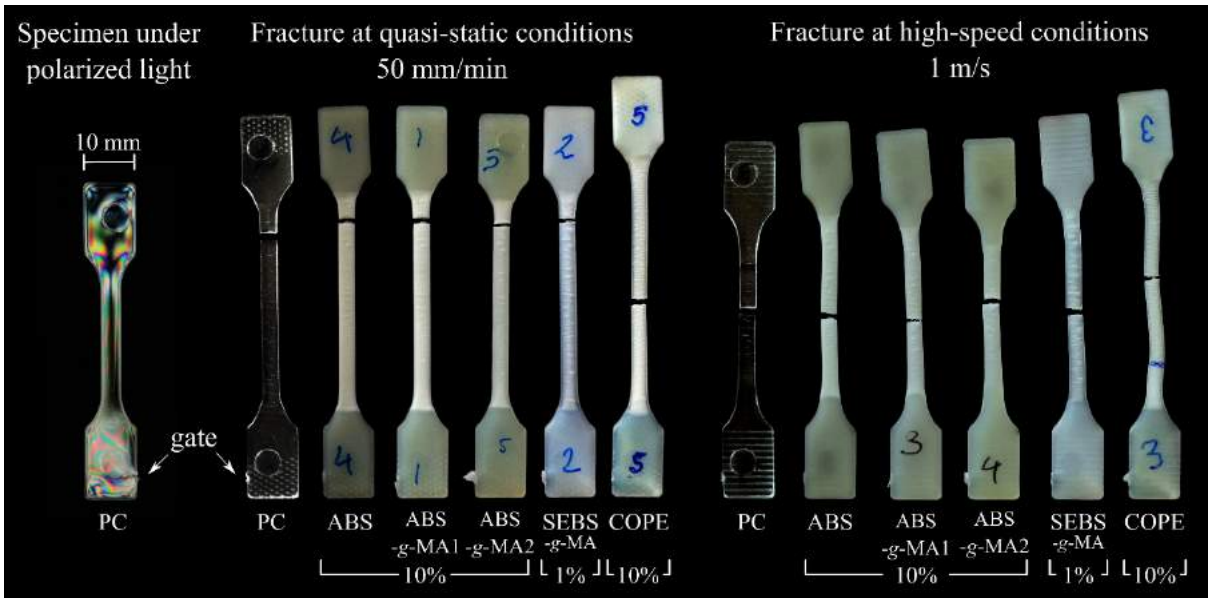

Figure 4.10: PC Tensile dumbbell specimen under two perpendicular polarized sheets on optical microscopy, and tested tensile specimen under quasi-static velocity.

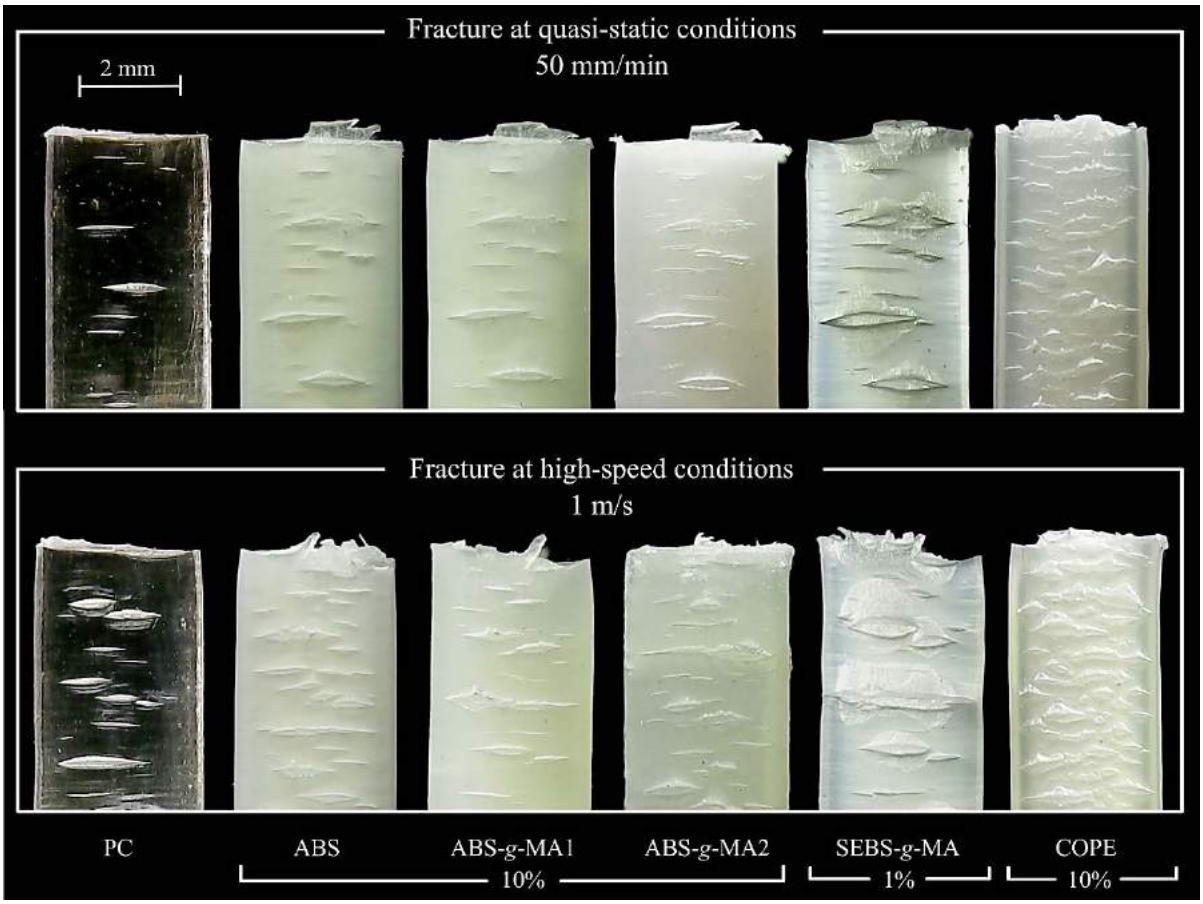

Figure 4.11: Zone of fracture view from tensile specimens at quasi-static conditions.

The fracture pattern of the cross section of the specimens is depicted in Figure 4.12, it is visible the embrittlement phenomena expected when using modified ABS. While PC/ABS-g-MA2 presents a brittle fracture, neat ABS has some ductile behavior, which are in agreement with quasi-static results. Also, it seems that a higher degree of grafting and higher content of ABS-g-MA2 can induce some ductile behavior, since for PC/ABS blend only a clear fracture is visible, while for PC/ABS-*g*MA large shear bands with stress whitening behavior is obtained, increasing the extend of these fracture mode for higher grafting degrees. This fracture mode is also visible for PC/SEBS-*g*MA and PC/COPE blends with thickness reduction, which are explained by the SEM results and the higher strain deformation of these blends under quasi-static conditions. For all samples, the crack origin seems to occur at the wall (point of local inhomogeneity) and propagates through crazing over the thickness [1].

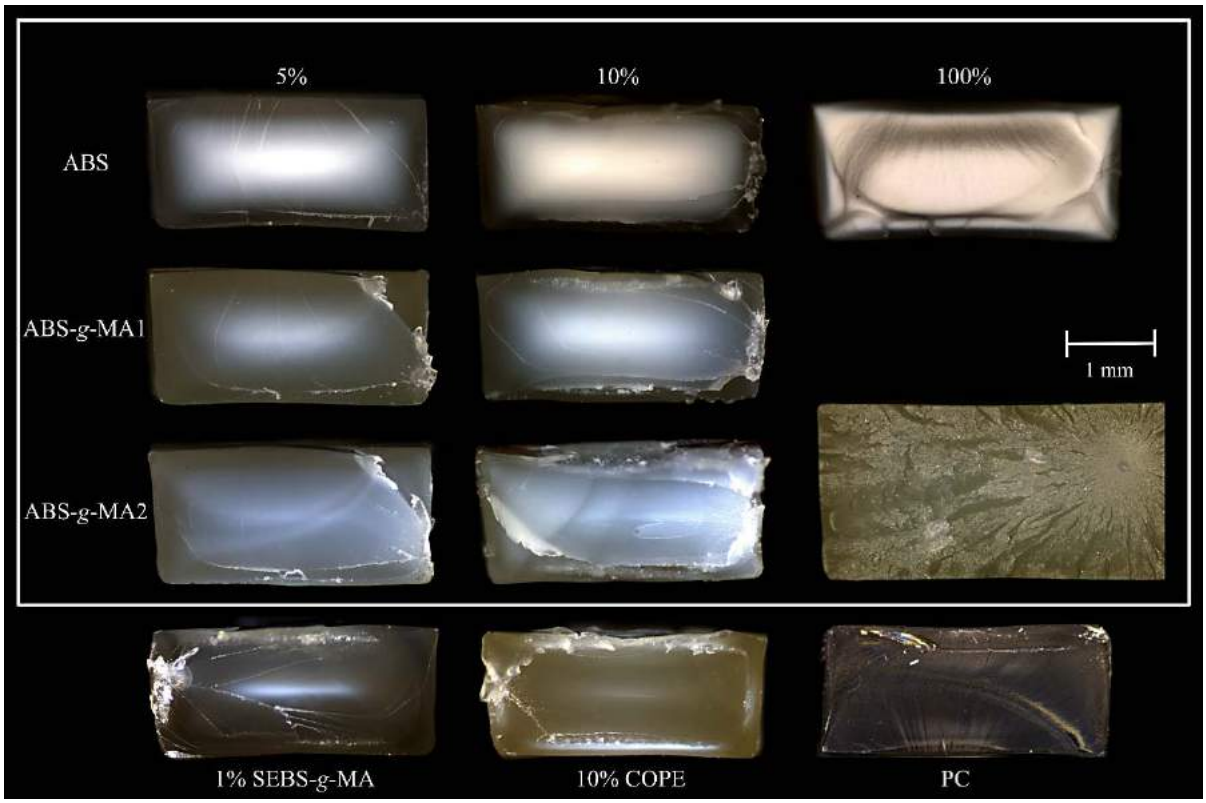

Figure 4.12: Cross-section view of the fracture tensile specimens at quasi-static conditions.

4.3.5.3.2 High-speed tensile behavior

PC blends tested under of high-speed, Figure 4.10, demonstrate that at higher strain rates the material sensitivity to residual stresses changes, and the material behaves as more homogeneous. All high-speed specimens fractured at the middle of the sample.

Comparing with quasi-static specimens, PC/COPE presents a different deformation behavior with severe warpage. Figure 4.11 demonstrate that micro-crack pattern is now material dependent, with different crack disposition along the specimen.

For PC/SEBS-*g*MA micro-cracks are surrounded by a visible region related to plastic deformation of the material. Analyzing the fracture pattern of the samples, the crack initiation occurs preferentially at the wall.

PC blends with 5 wt.% unmodified and modified ABS present a similar fracture surface, with a relative clear surface and large shear bands. Increasing the load content up to 10 wt.% the material ripples after fracture at the wall, which could be a result of the elastic recuperation after the rapid deformation imposed. The same behavior is visible for PC/SEBS-*g*MA and PC/COPE samples, but at a less extent. These observations are coherent with the high-speed test results, where these samples presented higher toughening compared to neat PC, resulting in larger strain at break and, consequently, a reduction of the cross section as a result of the plastic deformation.

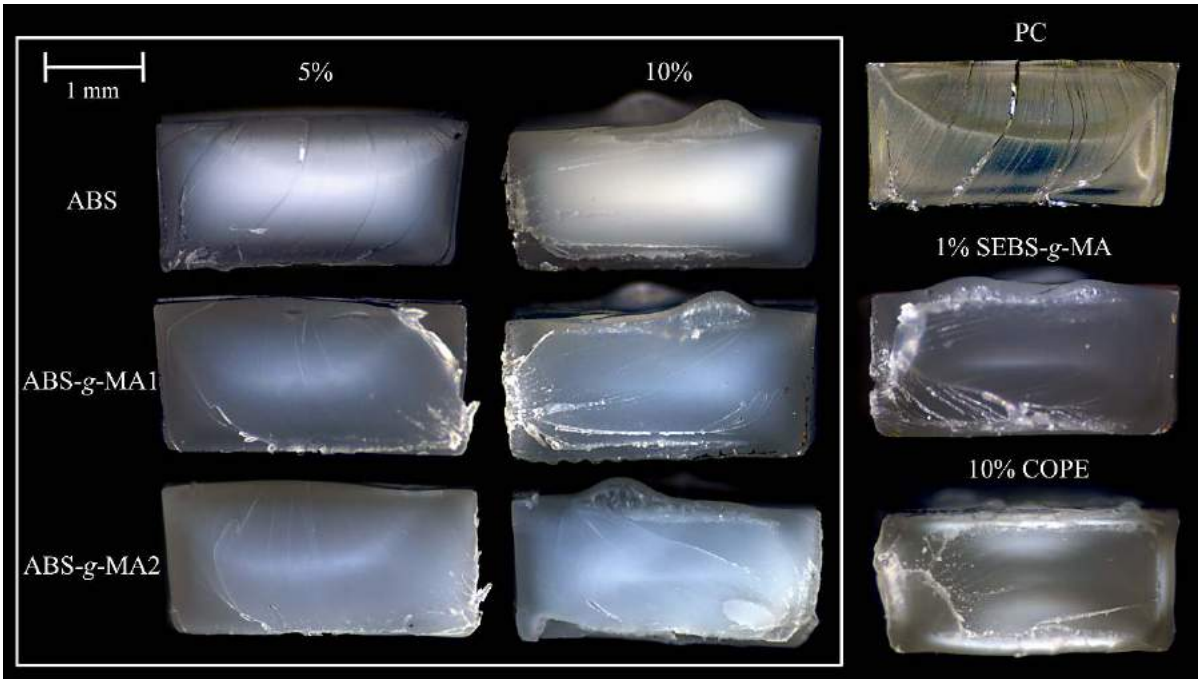

Figure 4.13: Cross-section view of the fracture tensile specimens at high-speed test conditions.

4.3.5.4 Impact tests and Optical Microscopy

Taking into account the results from tensile tests, samples with potential to toughen PC were PC/SEBS-*g*MA and PC/COPE, and were selected for impact strength analysis. Also, PC/5%ABS-*g*MA1,

PC/5%ABS-*g*MA2 and PC/10%ABS-*g*MA2 were used to evaluate if different grafting degree has effect on impact behavior. As it is presented in Table 4.3, the results from the impact tests none of the elastomers had a value higher that neat PC. This can probably be explained by the number of processing times of PC and the blends since PC neat was only injected for testing. Therefore, the value of PC with same processing cycles could be lower and the elastomers would have a positive effect. Comparing the same amount, 10 wt.%, COPE has a less influence on the impact strength than ABS-*g*MA2 for v-notch samples. Comparison of the unnotched samples with PC will not be made since the tests have a high standard deviation. However, within the unnotched tested blends, it possible to noticed two different behavior, PC/10wt.% ABS-*g*MA2 presents the lowest value of impact strength, PC/10wt.% COPE the highest. This result was expected from SEM and tensile analysis that showed a promising toughening mechanism through fibrils.

Table 4.3: Impact strength of notched and unnotched specimens.

	Impact strength [kJ/m^2]	
Specimen	**v-Notch**	**No notch**
PC	93.9 ± 3.5	272.3 ± 25.8
PC/5% ABS-g-MA1	21.4 ± 2.1	265.2 ± 7.7
PC/5% ABS-g-MA2	15.5 ± 1.7	268.2 ± 6.8
PC/10% ABS-g-MA2	17.2 ± 1.4	277.3 ± 3.4
PC/1% SEBS-*g*MA	77.8 ± 1.6	259.3 ± 1.8
PC/10% COPE	89.1 ± 1.4	253.8 ± 6.1

The fracture analysis at the impact shows that PC neat exhibits a fully ductile failure behavior, proved by the reduction in specimen thickness due to plastic deformation (dash line in Figure 4.14). While the addition of ABS-*g*MA mainly confers a brittle behavior to PC (no thickness reduction phenomenon was observed), SEBS-*g*MA and COPE maintain a ductile fracture. While systems containing ABS-*g*MA the crack initiates with a local stress whitening area, for the others it occurs around all the deformed area through the perpendicular plane of the crack propagation. Observing the crack fronts of PC/ABS-*g*MA on a different view angle, Figure 4.15, it possible to detect a crack propagation consistent with a brittle behavior, changing direction when it is about to reach the opposite side of the specimen. This behavior was also reported by Aranda-Ruiz *et al.* for polycarbonate associating this brittle fracture to a fracture in mode I [29]. Before the wave propagation zone, the surface is smooth and clear, switching into a more irregular morphology at the end of the crack propagation. Also, when the fracture was completed no hinge was observed, while for PC neat, PC/SEBS-*g*MA and PC/COPE the fracture was not complete. Probably

these results are related with samples thickness (around 4 mm), since the PC plane stress (ductile) to plane strain (brittle) transition lies between 3.18 – 6.35 mm of thickness [11].

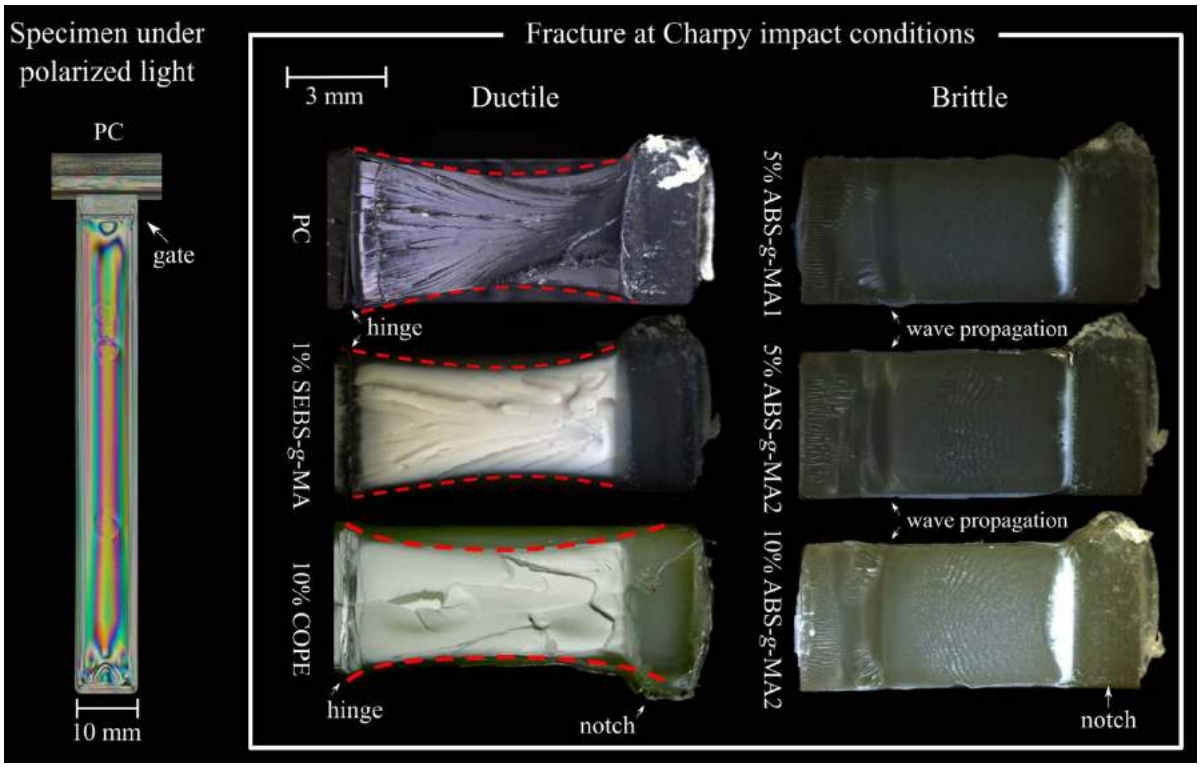

Figure 4.14: Specimen fracture morphology under impact for ductile (PC neat, 1%SEBS-g-MA, 10%COPE) and brittle (ABS-g-MA) samples.

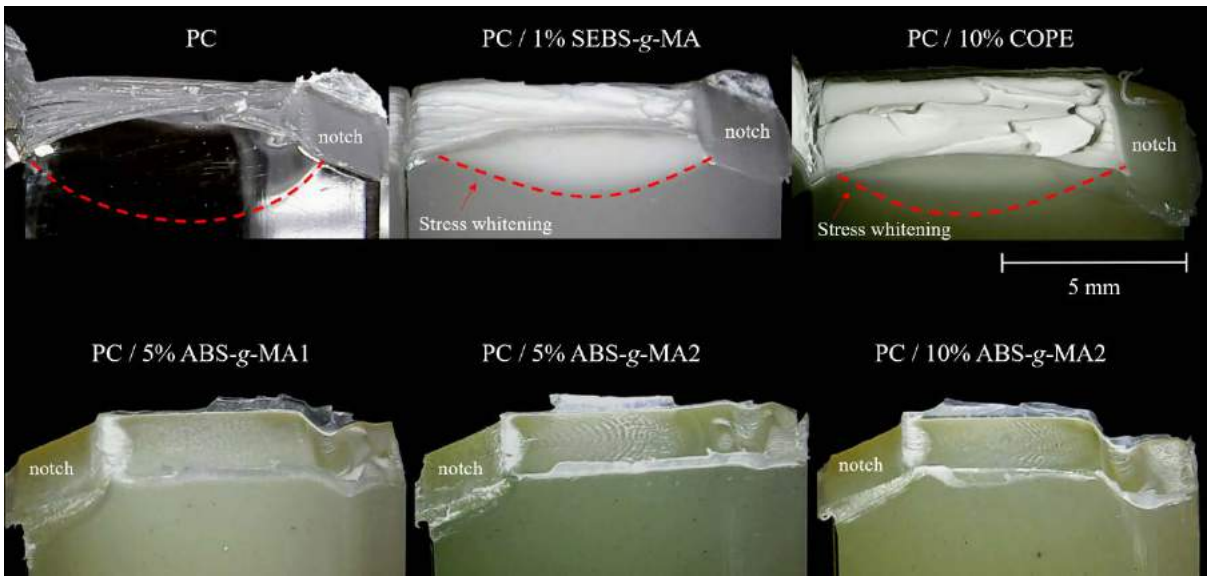

Figure 4.15: Specimen fracture side view under impact for ductile (PC neat, 1%SEBS-g-MA, 10%COPE) and brittle (ABS-g-MA1 and ABS-g-MA2) samples.

4.3.6 General Discussion

Table 4.4 depicts the variation of the mechanical properties compared to neat PC, for DMA, quasi-static, high-speed and impact tests.

Thermo-mechanical behavior of PC does not change with the incorporation of modified and unmodified ABS and SEBS-*g*-MA, but with 10 wt.% COPE it is possible to decrease T_g up to 17% of the neat PC value, increasing the deformation with temperature.

The variation in properties is more sensitive for medium shear rates (high-speed test), since the blend values deviate more compared to the neat PC. For neat PC, medium shear rate increases the material elastic response (σ_y from 64 to 78 MPa, and E from 1.8 to 3.1 GPa) at the expense of toughening (ε_r from 55 to 41% and U from 30 to 27 MPa). Small amounts (5 wt.%) of ABS and ABS-*g*-MA did not impact substantially the tensile properties, but for a higher content (10%) there was a substantial increase in toughening, up to 40%. This improvement tendency was coherent in all mechanical indexes for PC/10%ABS-*g*-MA1 and PC/10%ABS-*g*-MA2 and also increased the elastic modulus and toughening at the same time, and therefore no properties trade-off was observed. PC / 1 wt.% SEBS-*g*-MA blend had a substantial effect on toughening increasing the neat PC value to almost 20% and 50% for quasi-static and high-speed tests, respectively, with a negligible impact on resilience. PC with 10 wt.% COPE enhanced substantially the strain at break up to 60% and 110% for quasi-static and high-speed tests, respectively, with a small increase in the modulus of elasticity (5%) for the latter.

Regarding impact tests, COPE and SEBS-*g*-MA showed the most potential to be used as a toughening agent in polycarbonate systems for tension and impact solicitations.

Table 4.4: Variation in PC properties at quasi-static, high-speed and impact tests.

		PC /		PC /		PC /		PC /	PC /
	PC	**ABS**		**ABS-*g*-MA1**		**ABS-*g*-MA2**		**SEBS-*g*-MA**	**COPE**
Wt.%	100	5	10	5	10	5	10	1	10
DMA									
T_g [°C]	144	-	1% ▼	-	1% ▼	-	1% ▼	1% ▲	17% ▼
Quasi-static									
σ_y [MPa]	64	0% —	1% ▼	1% ▼	2% ▲	2% ▲	4% ▲	2% ▼	2% ▼
E [GPa]	1.8	4% ▲	2% ▲	0% —	7% ▲	4% ▲	10% ▲	1% ▼	1% ▲
ε_r [%]	55	8% ▲	10% ▲	2% ▼	9% ▲	2% ▼	10% ▲	18% ▲	60% ▲
U [MPa]	30	7% ▲	9% ▲	4% ▼	9% ▲	1% ▼	12% ▲	19% ▲	59% ▲
High-speed									
σ_y [MPa]	78	3% ▲	3% ▲	3% ▲	4% ▲	3% ▲	5% ▲	2% ▼	2% ▼
E [GPa]	3.1	4% ▲	9% ▲	2% ▲	3% ▲	7% ▲	11% ▲	1% ▼	5% ▲
ε_r [%]	41	11% ▼	33% ▲	3% ▲	34% ▲	1% ▼	31% ▲	47% ▲	114% ▲
U [MPa]	27	9% ▼	37% ▲	6% ▲	40% ▲	1% ▲	37% ▲	47% ▲	111% ▲
Impact [kJ/m²]									
v-notch	93.9	-	-	77% ▼	-	84% ▼	82% ▼	17% ▼	5% ▼
No notch	272	-	-	3% ▼	-	2% ▼	2% ▲	5% ▼	7% ▼

4.4 Conclusions

Blends of PC and ABS, ABS-*g*-MA, SEBS-*g*-MA and COPE were prepared and characterized in a systematic way. SEM analysis showed a better compatibility after grafting ABS with MA, COPE seems to have full compatibility with PC matrix since no dispersed phase was observed, and since the amount of SEBS-*g*-MA was too low it was not visually detected. COPE compatibilization was also supported by FT-IR and shifting of PC's T_g to lower values. The influence of shear rate in the tensile specimens was observed for SEBS-*g*-MA system, with a clear fracture at the center and a lamellar like structure near the walls.

For small strain rates, only the PC/COPE system was not influenced by the induced stress distribution of injection molding. This dependency was lost for all specimens at medium strain rates. The addition of 1wt.%SEBS-*g*-MA to PC increased substantially the elongation at break with a slight trade-off in yield stress and modulus. A similar, but more pronounced effect was observed in the blend with 10 wt.% COPE. Toughening was achieved in tensile conditions for PC with 1% SEBS-*g*-MA, 10% of unmodified and modified ABS, and 10% COPE. The latter showed an improvement up to 60% and 110% in quasi-static and high-speed tensile conditions, respectively. Through SEM and OM analysis, it was possible to identify the main toughening mechanisms. For SEBS-*g*-MA and COPE the main toughening mechanism was

cavitation and crazing delayed with fibrils, respectively, and for unmodified and modified ABS systems stress whitening was detected. Regarding the impact analysis, the blend with SEBS-*g*-MA and COPE show more potential to toughen PC. The ductile behavior of PC was kept with the incorporation of SEBS-*g*-MA and COPE elastomers, while for ABS and ABS-*g*-MA the ductile to brittle transition of PC was shifted to lower values of thickness. In the analysis performed a specimen of 4 mm thickness is not enough to test this PC in a brittle mode.

According to the results of this work, blending PC with different elastomeric polymers allows the tailoring of PC properties. Modified ABS with MA can increase the elastic modulus in tensile solicitations, while better toughening is achieved with SEBS-*g*-MA and COPE. Regarding thermomechanical properties, COPE has a substantial impact in decreasing T_g value and damping factor. Also, it was the only one that was not affected by the induced stresses originated from injection molding during mechanical characterization.

4.5 Acknowledgements

The authors would like to thank and acknowledge the financial support by Portugal 2020, and Fundo Social Europeu (FSE) through Programa Operacional Regional do NORTE (NORTE-08-5369–FSE-000034), developed under the program "IMPULSE - Polímeros e Compósitos: Drivers da inovação tecnológica e da competitividade industrial". The authors also acknowledge the Portuguese Foundation of Science and Technology (TSSiPRO - TECHNOLOGIES FOR SUSTAINABLE AND SMART INNOVATIVE PRODUCTS - NORTE-01-0145-FEDER-000015) and UID/CTM/50025/2013 for the financial support.

4.6 References

[1] U. A. Dar, Y. J. Xu, S. M. Zakir, and M.-U. Saeed, "The effect of injection molding process parameters on mechanical and fracture behavior of polycarbonate polymer," *J. Appl. Polym. Sci.*, vol. 134, no. 7, p. 29, 2017, doi: 10.1002/app.44474.

[2] C. R. Siviour, "High strain rate characterization of polymers," *AIP Conference Proceedings*, vol. 1793, no. 1, p. 60029, 2017, doi: 10.1063/1.4971585.

[3] C. R. Siviour and J. L. Jordan, "High Strain Rate Mechanics of Polymers: A Review," *Journal of Dynamic Behavior of Materials*, vol. 2, no. 1, pp. 15–32, 2016, doi: 10.1007/s40870-016-0052-8.

[4] K. Cho, J. Yang, B. Il, K. Chan, and E. Park, "Notch sensitivity of polycarbonate and toughened polycarbonate," *J. Appl. Polym. Sci.*, vol. 89, no. 11, pp. 3115–3121, 2003, doi: 10.1002/app.12502.

[5] B. S. Lombardo, H. Keskkula, and D. R. Paul, "Influence of ABS type on morphology and mechanical properties of PC/ABS blends," *J. Appl. Polym. Sci.*, vol. 54, no. 11, pp. 1697–1720, 1994, doi: 10.1002/app.1994.070541113.

[6] A. C.-Y. Wong, "Polycarbonate Effects on Selected Mechanical Properties of Polycarbonate/Acrylonitrile-Butadiene-Styrene (PC/ABS) Binary Blending Systems," *Polymer-Plastics Technology and Engineering*, vol. 42, no. 2, pp. 171–180, 2003, doi: 10.1081/PPT-120017920.

[7] S. Balakrishnan and N. R. Neelakantan, "Mechanical properties of blends of polycarbonate with unmodified and maleic anhydride grafted ABS," *Polymer International*, vol. 45, no. 4, 1998.

[8] X. Zhang, Y. Chen, Y. Zhang, Z. Peng, Y. Zhang, and W. Zhou, "Effects of ABS-g-MAH on mechanical properties and compatibility of ABS/PC alloy," *Journal of Applied Polymer Science*, vol. 81, no. 4, pp. 831–836, 2001, doi: 10.1002/app.1502.

[9] Z. Yin and T. Wang, "Investigation of tensile deformation behavior of PC, ABS, and PC/ABS blends from low to high strain rates," *Applied Mathematics and Mechanics*, vol. 33, no. 4, pp. 455–464, 2012, doi: 10.1007/s10483-012-1563-x.

[10] N. Bagotia, B. P. Singh, V. Choudhary, and D. K. Sharma, "Excellent impact strength of ethylene-methyl acrylate copolymer toughened polycarbonate," *RSC Adv.*, vol. 5, no. 106, pp. 87589–87597, 2015, doi: 10.1039/C5RA18024D.

[11] P. Sivaraman *et al.,* "Thermoplastic copolyether ester elastomer toughened polycarbonate blends: 1. Mechanical properties and morphology of the blends," *Polymer Testing*, vol. 23, no. 5, pp. 527–532, 2004, doi: 10.1016/j.polymertesting.2003.12.001.

[12] A. Garhwal and S. N. Maiti, "Influence of styrene–ethylene–butylene–styrene (SEBS) copolymer on the short-term static mechanical and fracture performance of polycarbonate (PC)/SEBS blends," *Polym. Bull.*, vol. 73, no. 6, pp. 1719–1740, 2016, doi: 10.1007/s00289-015-1573-3.

[13] A. Garhwal and S. N. Maiti, "Fabrication of Super Tough Polycarbonate/Styrene-Etylene-Butylene-Styrene Grafted Maleic Anhydride (SEBS-g-MA) Blends: Morphological, Short Term Static Mechanical and Fracture Performance Interpretation," *Polymer-Plastics Technology and Materials*, vol. 58, no. 2, pp. 113–125, 2019, doi: 10.1080/03602559.2018.1466167.

[14] J. J. Huang, H. Keskkula, and D. R. Paul, "Rubber toughening of an amorphous polyamide by functionalized SEBS copolymers: morphology and Izod impact behavior," *Polymer*, vol. 45, no. 12, pp. 4203–4215, 2004, doi: 10.1016/j.polymer.2004.04.002.

[15] S. Horiuchi, N. Matchariyakul, K. Yase, T. Kitano, H. K. Choi, and Y. M. Lee, "Compatibilizing effect of maleic anhydride functionalized SEBS triblock elastomer through a reaction induced phase formation in the blends of polyamide6 and polycarbonate: 2. Mechanical properties," *Polymer*, vol. 38, no. 1, pp. 59–78, 1997, doi: 10.1016/S0032-3861(96)00465-X.

[16] R. Qi, Z. Chen, and C. Zhou, "Solvothermal preparation of maleic anhydride grafted onto acrylonitrile–butadiene–styrene terpolymer (ABS)," *Polymer*, vol. 46, no. 12, pp. 4098–4104, 2005, doi: 10.1016/j.polymer.2005.02.116.

[17] *Plastics — Determination of tensile properties — Part 1: General principles*, ISO 527-1:1996, 1996.

[18] *Plastics — Determination of Charpy impact properties — Part 1: Non-instrumented impact test*, ISO 179-1:2010, 2010.

[19] R. Qi, Q. Yu, Y. Shen, Q. Liu, and C. Zhou, "Grafting copolymerization of maleic anhydride onto styrene-butadiene-styrene block copolymer through solvothermal process," *J. Appl. Polym. Sci.*, vol. 102, no. 6, pp. 5274–5279, 2006, doi: 10.1002/app.24780.

[20] R. Scaffaro *et al.,* "On the modification of the nitrile groups of acrylonitrile/butadiene/styrene into oxazoline in the melt," *J. Polym. Sci. A Polym. Chem.*, vol. 38, no. 10, pp. 1795–1802, 2000, doi: 10.1002/(SICI)1099-0518(20000515)38:10<1795::AID-POLA640>3.0.CO;2-6.

[21] C. Desrousseaux *et al.,* "Fabrication of Acrylonitrile-Butadiene-Styrene Nanostructures with Anodic Alumina Oxide Templates, Characterization and Biofilm Development Test for Staphylococcus epidermidis," *PLOS ONE*, vol. 10, no. 8, e0135632, 2015, doi: 10.1371/journal.pone.0135632.

[22] B. M. Rao, P. R. Rao, and B. Sreenivasulu, "Grafting of Maleic Anhydride onto Acrylonitrile-Butadiene-Styrene Terpolymer: Synthesis and Characterization," *Polymer-Plastics Technology and Engineering*, vol. 38, no. 5, pp. 967–977, 1999, doi: 10.1080/03602559909351625.

[23] P. Sivaraman *et al.,* "Thermoplastic copolyether ester elastomer toughened polycarbonate blends: 2. Thermal and rheological studies," *Polymer Testing*, vol. 23, no. 6, pp. 645–649, 2004, doi: 10.1016/j.polymertesting.2004.01.012.

[24] S. Balakrishnan, N. Neelakantan, D. Saheb, and J. P. Jog, "Rheological and morphological behaviour of blends of polycarbonate with unmodified and maleic anhydride grafted ABS," *Polymer*, vol. 39, no. 23, pp. 5765–5771, 1998, doi: 10.1016/S0032-3861(98)00088-3.

[25] *Standard Test Method for Transition Temperatures and Enthalpies of Fusion and Crystallization of Polymers by Differential Scanning Calorimetry*, ASTM D3418 - 15, 2015.

[26] M. G. Abiad, O. H. Campanella, and M. T. Carvajal, "Assessment of Thermal Transitions by Dynamic Mechanical Analysis (DMA) Using a Novel Disposable Powder Holder," *Pharmaceutics*, vol. 2, no. 2, pp. 78–90, 2010, doi: 10.3390/pharmaceutics2020078.

[27] M. Chen, D. Yao, and B. Kim, "Eliminating Flow Induced Birefringence And Minimizing Thermally Induced Residual Stresses In Injection Molded Parts*," *Polymer-Plastics Technology and Engineering*, vol. 40, no. 4, pp. 491–503, 2001, doi: 10.1081/PPT-100002072.

[28] R. J. Klein, N. S. Billade, S. D. Lince, and M. T. Bryant, "Combined Birefringence-Tensile Testing of Medical Plastics and Comparison to Finite Element Analysis," *SPE ANTEC®*, 2017.

[29] J. Aranda-Ruiz, K. Ravi-Chandar, and J. A. Loya, "On the double transition in the failure mode of polycarbonate," *Mechanics of Materials*, vol. 140, p. 103242, 2020, doi: 10.1016/j.mechmat.2019.103242.

CHAPTER 5

5 ASSESS THE COMPRESSIVE AND IMPACT BEHAVIOR OF POLYMERIC SAFETY TOE CAPS THROUGH COMPUTATIONAL MODELLING

In this chapter, an open source computational library, OpenFOAM®, was used to simulate two laboratory standard tests required for safety toe caps. A fluid-solid interaction solver, *solids4Foam*, was used to simulate both compressive (15 kN) and an impact (200 J) tests. To model the polymeric material behavior a neoHookean material law with plastic criteria was employed. A commercially available plastic toe cap was experimentally characterized, and the data collected was used for assessment purposes. On the numerical side, a mesh convergence analysis was performed in order to assure mesh size independency results. Very good correlations, between experimental and simulated values, were obtained for both tests, with an approximate error of 5.4% and 6.8% for the compression and impact tests simulations, respectively. This work clearly demonstrates that *solids4Foam* toolbox can offer an significant support in future R&D in the footwear industry.

Keywords: toe cap, structural analysis, safety footwear, non-linear behavior, OpenFOAM, solid4Foam

Submitted to the OpenFOAM® Journal

5.1 Introduction

5.1.1 Safety Footwear

Worker safety is of primary concern inside the workplace. According to Eurostat [1], since 2010 the total number of accidents in the workplace exceeds 3 million per year. From these, more than 28% were in the lower extremities of industrial workers, which are the most prone group to this kind of injury. Employers from industrialized countries are required to provide personal protective equipment (PPE), to help mitigating any work-related injuries. PPE for safety footwear is available in three different standardized categories: safety shoes, protective shoes and occupational shoes, Table 5.1 [2–4]. They mainly differ in the protection level provided to the wearer through the use of a toe cap. This structural reinforcement is placed at the front of the shoe and is intended to protect the user toes from falling objects and compressive loads [5]. The required mechanical performance for each type of protective footwear according to the ISO standards is given in Table 5.1.

Traditional safety shoes are made of robust materials, which helps to withstand harsh environments. Although it may increase protection, an over dimensioning can lead to excessive weight. There are studies that correlate the extra weight and inflexible design of safety shoes with an increase of the physical effort (body oxygen consumption is increased) [6, 7]. Fatigue alongside with other factors (uncomfortable and non-aesthetic design, inadequate ventilation) lead workers to reject and/or neglect the usage of this kind of PPE [8, 9]. Therefore, the development of new solutions urges in the market, to make safety footwear more appealing and comfortable.

Historically, steel toe caps started to be manufactured in the early 1920s [10–13], and they are still used today due to their high mechanical properties. Although it is possible to manufacture thin steel toe caps, its high density makes this component one of the main contributors to the total shoe weight, representing up to 35% of the total mass [14], thus contributing to users fatigue and leading to the abandonment of this kind of PPE.

Nowadays, several types of materials can be used to manufacture toe caps. Apart from steel, one can find commercial solutions made of aluminum [15], and non-metallic solutions, such as plastic [16] and plastic based composites [17]. Non-metallic solutions are highly attractive due to their specific mechanical properties, relative ease of manufacturing, freedom of design and, additionally, can enhance the product through being non-magnetic and non-electrical conductors, while providing better thermal insulation than their metallic counterparts [18, 19]. Another advantage of plastic toe caps is the ability to recover part of

its original shape after imposing a high deformation [20, 21]. Despite these advantages, to fulfill the requirements in Table 5.1, the current non-metallic options are bulky, resulting in clear aesthetics problems [22]. To push new toe cap solutions to the market some research has been made in two fronts: material development and design optimization.

For material development, some studies shown an up to 40-56% weight reduction by using fiber reinforced polymer. Lee *et al.* [20] developed an optimized stacking sequence layer of glass fiber polyester composite toe cap, with excellent impact and static compression behavior, which is 40% lighter than their steel solution. Yang *et al.* [18] presented a thermoplastic solution of polypropylene matrix reinforced with sisal fibers, which were modeled and, later, validated with experimental data. The same author also developed a biodegradable solution of flax fibers and polylactic acid polymer for a toe cap, accomplishing a 50 % weigh reduction when compared to their steel counterpart while sustaining the requirements for quasi-static compressive loading according to ISO 12568 [23]. Zukas *et al.* [24] found a 20% improvement in low velocity impact response, by the addition of nanofillers in carbon fiber reinforced toe caps made of methyl methacrylate resin. More recently, an optimized stacking layers of E-fiber glass, carbon and aramid fabric toe cap was suggested by Erden *et al.* [19]. An overshoe protector that comprises this toe cap alongside a cover made of aramid fabric and TPU resin was also presented, resulting in the creation of a 56% lighter solution than steel counterparts, that were approved in an impact test done with 100 J. Several studies are also reported in the field of metallic toe caps, where different grades of steel and geometries were tested, resulting in an up to 50% thickness and weight saving when compared to their initial designs [14, 22, 25–27]. Although non-metallic solutions presents promising results, the manufacturing process is not compatible with the high demand in industry, slowing the overall production rate and increasing the product price.

Design optimization through computational modeling is also reported for metallic [14, 22, 25–29] and non-metallic toe caps [18, 20, 23], resulting in up to 50% weight with thickness reduction compared to traditional solutions. Since the implementation of CAD (computer-aided design) /CAE (computer-aided engineering) tools, optimization of product design has been an ongoing pursuit. Even in the niche market of security footwear, commercial software solutions, such as ANSYS LS-Dyna solver, and ABAQUS, have been used to simulate the impact and compressive behavior required by European standards for toe caps. These approaches have shown good agreements with experimental results providing a better understanding on stress distribution and resultant deformation, pushing innovation on toe cap design. However, the use of commercial software for the analysis of dynamic loadings requires a license that can

be very expensive, and thus, inaccessible to small/medium size companies. Here it worth to note that a report from the European Union [30] stated that in 2012 the footwear industry was heavily populated with small and medium sized companies with 10-15 workers. For these companies to acquire commercial software is usually prohibitive and, consequently, the majority of times R&D is mainly made by trial and error without support of CAE.

In this work, a computational tool based on an open-source computational solver for solid mechanics and fluid-solid interaction (FSI), built within the OpenFOAM® framework, *solids4Foam* [31], was used to simulate the impact and quasi-static compression behavior of a safety footwear polymer toe cap under the conditions defined in EN 12568 [32]. This manuscript is organized in the following way: in subsection 1.2 a brief description of the toolbox used is given. Then, in Section 2, morphological and mechanical tests performed on a commercial toe cap, kindly provided for this work, are reported (subsection 2.1). Subsequently, compression and impact tests performed to the toe cap are described along with the description of the numerical setup within *solids4Foam* to simulate the mechanical tests (subsection 2.2). A mesh convergence study to obtain a mesh size independence results is presented next. In Section 3, the results from the characterization performed to the material is presented along with the mesh convergence study and a comparison between the results obtained with the actual component performance evaluated in laboratory testing and the numerical simulations. Finally, in section 4, conclusions are drawn about the use of the toolbox for this kind of simulations with special focus on the footwear industry.

Table 5.1: Mechanical requirements for each type of protective footwear [2–4].

	Category of footwear		
Toe cap requirements	**Safety** *ISO 20345*	**Protective** *ISO 20346*	**Occupational** *ISO 20347*
Impact energy (J)	200	100	-
Compression load (kN)	15	10	-

5.1.2 Fluid-solid interaction within OpenFOAM®

In the last two decades, OpenFOAM® became a staple for open-source CFD simulations. Its open-source framework based on object-oriented paradigm allowed several contributions from academia and industry to be implemented leading to substantial improvements in performance and reach in continuum mechanics solvers. One of such contributions is the *solids4Foam* toolbox [31]. This is a freely available

solid mechanics and FSI package distributed via the foam extend fork [33]. The open-source character has the advantage of allowing the user to check and adapt the source code to suit its needs. This tool has been used in some works [34–36] and compared with other industrial commercial software, mostly based on the finite element method. The results shown are quite impressive indicating that finite volume method is a suitable alternative to the conventional finite element method, used to solve solid mechanics problems. The toolbox was designed for simulations of solid mechanics and fluid-solid interaction and aims at solving the standard governing equations: conservation of mass, Equation (5.1), conservation of energy, Equation (5.2) , and conservation of linear momentum, Equation (5.3) [31].

$$\frac{D}{Dt}\int_{\Omega} \rho \, d\Omega = 0 \tag{5.1}$$

$$\frac{D}{Dt}\int_{\Omega} \rho c_p T d\Omega = -\oint_{\Gamma} \boldsymbol{n}.\boldsymbol{q} d\Gamma + \int_{\Omega} \sigma : \boldsymbol{\nabla U} \, d\Omega \tag{5.2}$$

$$\frac{D}{Dt}\int_{\Omega} \rho \boldsymbol{U} \, d\Omega = \oint_{\Gamma} \boldsymbol{n}.\boldsymbol{\sigma} \, d\Gamma + \int_{\Omega} \rho \boldsymbol{b} \, d\Omega \tag{5.3}$$

The symbols used in the above equations are: material density ($\boldsymbol{\rho}$), cell volume ($\boldsymbol{\Omega}$), cell surface ($\boldsymbol{\Gamma}$), normal vector to cell surface ($\boldsymbol{n}$), specific heat capacity at constant pressure ($\boldsymbol{c_p}$), temperature ($\boldsymbol{T}$), heat flux ($\boldsymbol{q}$), Cauchy stress tensor ($\boldsymbol{\sigma}$), velocity vector ($\boldsymbol{U}$) and body force per unit mass ($\boldsymbol{b}$). For solid mechanics analysis, Equation (5.3) is the most important and a Lagrangian approach is employed for structural analysis. In the present research it is important to use a solid constitutive law able to describe large deformations or rotations since the compression and the impact events can cause high levels of deformation to the toe cap. At the time, the *solids4Foam* toolbox has available some non-linear elastic constitutive laws, such as: neo-Hookean elastic, St. Venant Kirchhoff elastic, Orthotropic St. Venant Kirchhoff elastic; and a non-linear elastic/plastic constitutive law: neo-Hookean elastic with Mises plastic [31]. Since the post yield material behavior is an important parameter to consider to adequately simulate the real behavior of the toe cap, the neo-Hookean elastic with Mises plastic was chosen. This law describes the Cauchy (true) stress tensor as follows:

$$\boldsymbol{\sigma} = \mu \, dev[\boldsymbol{B}] + \frac{K}{2}\left(\frac{J^2 - 1}{J}\right)\boldsymbol{I} \tag{5.4}$$

where μ is the shear modulus, $dev[\boldsymbol{B}]$ is the left Cauchy-Green deformation tensor, K the bulk modulus, J the Jacobian of the deformation gradient, and I the second order identity tensor.

5.2 Materials and methods

5.2.1 Material characterization

Commercially available thermoplastic toe caps used in safety footwear were kindly provided by a company partner for this work. To assess information regarding the toe cap's material as well as its mechanical properties, common characterization techniques, Fourier Transform InfraRed (FT-IR) spectroscopy, Differential Scanning Calorimetry (DSC) and Scanning Electron Microscopy (SEM) were used to identify the material type, and quasi-static tensile tests performed to obtain the stress-strain behavior of the material.

5.2.1.1 FT-IR

To identify the type of polymeric material, FT-IR analysis was used. For that purpose, a film with ca. 10 μm was prepared using a small amount of sectioned toe cap material placed in between two aluminum plates in a small hydraulic press heated at 200 °C under a pressure of 10 ton for 30 s. The analysis was performed in a Jasco 4100 spectrophotometer (JascoInc., USA) in transmission mode in the wavenumber range of 400-3500 cm^{-1}, with 2 cm^{-1} resolution and an accumulation of 32 spectra.

5.2.1.2 DSC

The thermal behavior of the material was analyzed by DSC, in a Netzsch 200 Maya (Netzsch, Germany), under a nitrogen atmosphere with a heating rate of 10 °C/min from 30 to 200 °C. To eliminate the thermal history of the material two scans were performed. The results shown in this work are referent to the second scan only.

5.2.1.3 SEM

The material morphology was assessed by SEM analysis, using a FEI Quanta 400 (FEI, The Netherlands). The samples were previously fractured in liquid nitrogen and coated with a thin gold-palladium film.

5.2.1.4 Mechanical characterization

To evaluate the toe cap's material mechanical properties, several toe caps were frozen in liquid nitrogen and fractured with a hammer. The material was subsequently grinded to obtain granules of appropriate size for processing. Finally, type 1A specimens according to ISO 527 were prepared by injection molding. Five specimens were used to test the material according to ISO 527 specifications, with a crosshead velocity of 50 mm/min, on an Instron 5969 (Instron, USA) with an optical extensometer. Elastic and post yield properties were obtained from the tests. The elastic modulus was obtained from the slope of the initial linear relationship of the stress *vs* strain curve. For the post-yield behavior, the definition of a "true" stress in ASTM D 638 was considered by assuming a homogeneous deformation of the specimen cross-section, following Equation (5.5) and (5.6).

$$\sigma_{Hom} = \sigma_{Eng} \times (1 + \varepsilon_{Eng}) \tag{5.5}$$

$$\varepsilon_{true} = ln(1 + \varepsilon_{Eng}) \tag{5.6}$$

Where σ_{Eng} is the engineering stress, defined as the ratio between the recorded force (F) and the initial specimen cross-sectional area (A_0). ε_{Eng} is the engineering strain, defined as the ratio between the recorded grip displacement (dl) and the initial distance between the grips (l_0). However, this should be understood as an estimation of the real material behavior because it does not account for necking effects. As such, this curve will be named homogeneous tensile curve and will be taken as a more representative description of the material's stress-strain behavior that will be used to describe the non-linear material behavior as a multi-linear isotropic hardening in the neo-Hookean model.

5.2.2 Simulation Setup

5.2.2.1 Toe Cap Geometry

The geometry used was scanned from one of the toe caps provided by the company partner. A left side, size 10 toe cap, was chosen for the present work. In accordance with ISO 20345 and EN 12568 standards, this toe cap size alone should have a minimum clearance under the toe cap of 22 mm, while assembled in safety footwear the value should be greater than 15 mm. Some general dimensions regarding the toe cap are provided in Table 5.2.

Table 5.2: Minimum clearance value after impact and compression as a function of the size of toe cap alone and assembled inside the safety footwear [2, 32].

	Clearance under the toe cap (mm) alone/ in safety shoes					
size	**≤ 5**	**6**	**7**	**8**	**9**	**≥ 10**
Toe cap alone	19.5	20.0	20.5	21.0	21.5	22.0
size	**≤ 36**	**37-38**	**39-40**	**41-42**	**43-44**	**≥ 45**
Toe cap assembled in shoe	12.5	13.0	13.5	14.0	14.5	15.0

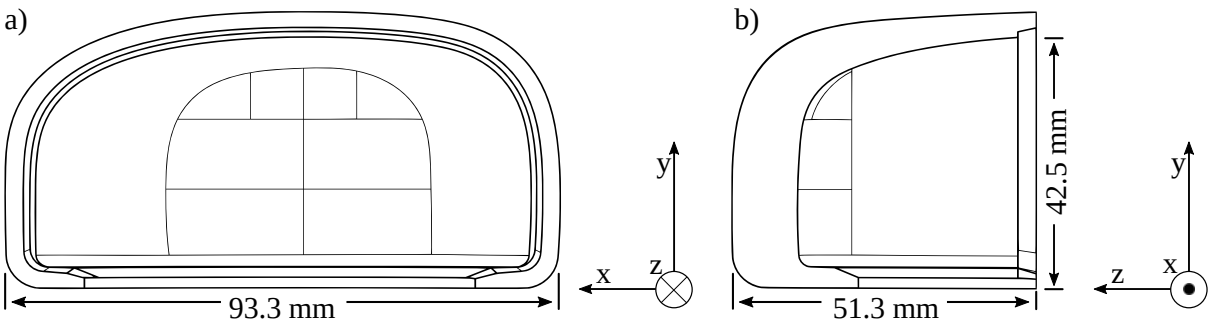

Figure 5.1:Dimensions of the scanned left side, size 10 toe cap, a) back view, b) cross-section view.

For result analysis purposes, the value 42.5 mm of inner high of the toe cap ($\boldsymbol{h_i}$) will be used to estimate the final clearance after each simulation. In practice, the final clearance is the final height of the clay ($\boldsymbol{h_{clay}}$) placed under the toe cap for each experimental test, which is equal to inner high plus the toe cap inner height variation ($\boldsymbol{\Delta h_i}$), Equation (5.7).

$$\boldsymbol{h_{clay} = h_i + \Delta h_i} \tag{5.7}$$

5.2.2.2 Mesh sensitivity analysis

To get grid independent results an interactive mesh convergence study was performed using progressively finer grids, increasing 3-fold the number of cells with each mesh. This study comprised five different meshes with 25 k, 76 k, 228 k, 671 k and 2 M cells. The computational grids were generated with the utility *cfMesh* [37], a library for automatic mesh generation that is compatible with OpenFOAM®, using the cartesian mesh subroutine. To assess the refinement effect, the von Mises Stress (σ_{Eq}) and the cell displacement along the *y*-axis (D_{yy}) were averaged with a weight corresponding to the cell volume for the overall domain, Equation (5.8) and (5.9). Additionally, the variables of interest for the study were also tested, such as striker velocity ($\boldsymbol{U_{y\ striker}}$), plate force ($\boldsymbol{F_{y\ plate}}$) and plate displacement ($\boldsymbol{D_{y\ plate}}$), and

the toe cap clearance variation ($\boldsymbol{\Delta h_i}$), to confirm that grid independent results were obtained. Table 5.3 displays each mesh cell size and total number of cells.

$$\overline{\boldsymbol{\sigma_{Eq}}} = \frac{\sum(V_{cell}\sigma_{Eq})}{\sum V_{cell}} \tag{5.8}$$

$$\overline{\boldsymbol{D_{yy}}} = \frac{\sum W(V_{cell}D_{yy})}{\sum V_{cell}} \tag{5.9}$$

It is well known that non-orthogonality and skewness is an important parameter for simulation stability and reliability in finite volume methods [38, 39] and is very often used as a mesh quality indicator. A value of zero for the first parameter is an indicator of a fully orthogonal mesh grid where all grid lines are parallel to each other. Most geometries do not allow to generate a fully orthogonal mesh, and, therefore, non-orthogonal correction must be implemented in order to assure the simulation stability. Skewness also affects the solutions accuracy and must be as lower as possible so diffusion error during calculation is reduced [40]. It is desired to have the lowest possible value of these parameters due to the discretization method used to solve the diffusive terms, which uses the normal face vector of each face cell to calculate how fluxes travel through cells. For instance, hexahedron cell type and a more refine mesh tends to have lower average non-orthogonality and skewness values, improving the solution accuracy but at the cost of computational effort.

The five toe cap meshes used for mesh sensitivity analysis are illustrated in Figure 5.2 with the mesh quality parameters presented in Table 5.3. In a first analysis, the average cell size decreases the total number of cells in the mesh increases. Although maximum non-orthogonality and skewness did not decrease with mesh refinement, average non-orthogonality and average skewness decreases consistently, and, therefore, an improvement in the quality of the mesh is obtained with small cell sizes. In complex geometries such as toe caps, it is difficult to use just cartesian cells to generate the mesh near curved surfaces. Therefore, those regions are expected to have cells with lower mesh quality. To prevent simulation problems, this effect can be mitigated by refining the overall mesh locally. The first approach was used because better mesh results were obtained instead of using local refinements. In Figure 5.2 a slice of the vertical section is displayed (cross-section view) to show this effect where a better definition of the geometry is obtained for M4 and M5, especially near the edges/corners, while the interior of the toe cap mesh is dominated by quasi-orthogonal cell. Modeling the toe cap with small cells, the percentage

of hexahedron cell type approaches 100%, in comparison with the remain types of cells (Table 5.3). In the next section, a comparison between toe cap mesh, striker and plates is briefly discussed.

Table 5.3: Toe cap meshes properties.

Mesh properties / Cell type (number/%)	**M1**	**M2**	**M3**	**M4**	**M5**
cell average size (mm)	1.7	1.1	0.65	0.449	0.31
Total number of cells	25 216	74 272	227 541	670 640	1 973 199
Max. non-orthogonality	64.16	67.75	61.40	57.11	58.69
Average non-orthogonality	19.28	15.6	3.98	3.15	2.61
Max. skewness	1.12	0.99	1.22	1.86	0.99
Average skewness	0.29	0.22	0.09	0.07	0.05
Hexahedron	24 598 (97.55%)	73 243 (98.61%)	226 626 (99.60%)	669 560 (99.84%)	1 971 480 (99.91%)
Prism	56 (0.22%)	74 (0.10%)	98 (0.04%)	136 (0.02%)	206 (0.01%)
Pyramid	258 (1.02%)	409 (0.55%)	383 (0.17%)	472 (0.07%)	715 (0.04%)
Tetrahedron	304 (1.21%)	546 (0.74%)	434 (0.19%)	472 (0.07%)	798 (0.04%)

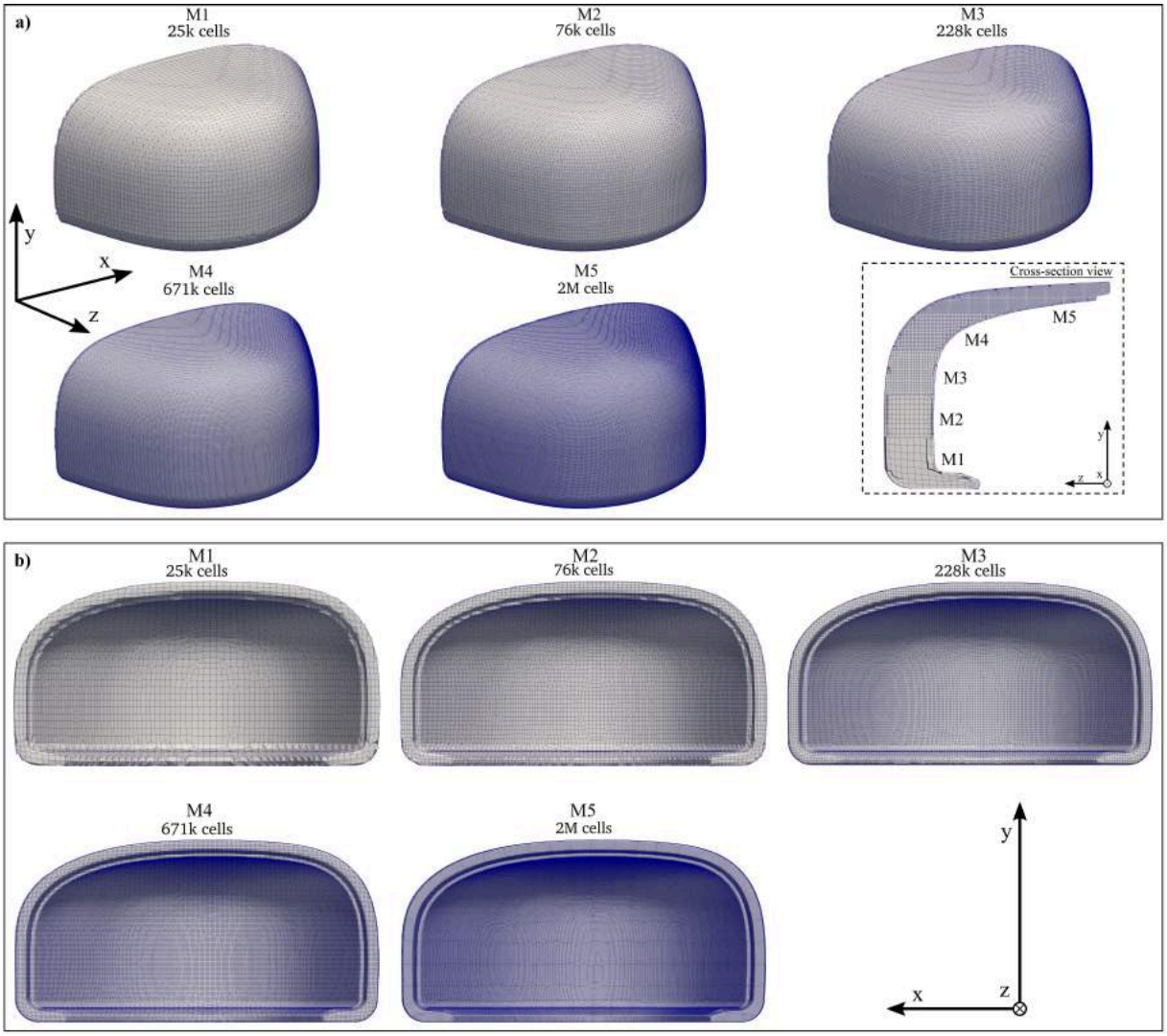

Figure 5.2: Meshes used on the sensitivity analysis: a) isometric view, and b) back view.

5.2.2.3 Quasi-static compression test

The most demanding category of footwear is the safety class, according to ISO 20345 [2] this type of footwear must withstand a compressive load of 15 kN while preserving a minimum standardized clearance value, which is dependent on the toe cap size that was measured with the help of a standardized clay cylinder [L=25 mm, ø = 25 mm]. The test methodology for footwear is defined in ISO 20344 [41], and for toe cap alone in EN 12568 [32]. The case setup and the simulated scenario are depicted in Figure 5.3. To perform this simulation the digitalized commercial polymeric toe cap geometry was modelled and placed between two steel plates, mimicking the experimental setup. The boundary conditions for the components in the simulation were the following:

- the bottom plate was set to have a null displacement in all cartesian directions (Fixed Walls patch in Figure 5.3-right);

- the top plate was set to have a velocity of 5 mm/min along the negative *y*-axis (Mixed walls patch in Figure 5.3-right);
- the toe cap was set as a contact region between the top and bottom plates, using a penalty scale method for the direction normal to the contact and a Coulomb friction law with friction coefficient of 0.3 [42, 43] for the tangent direction (Bottom and Upper contact patches in Figure 5.3-right).

Although with a small test velocity, the simulation was performed considering inertial effects. The discretization schemes for each term in the governing equation and the solver control parameters are presented in Table 5.4. A time step of 0.5 s was chosen and the simulation was allowed to run until the force registered in the top plate (upper contact patch in Figure 5.3 right) reached a value of 15 kN.

Table 5.4: Discretization schemes and solver control parameters.

Discretization schemes	
d2dt2	Euler
Time	Euler
Gradient	Least Squares
Divergence	Gauss Linear
Laplacian	Gauss Linear corrected
laplacian(DD,D)	
laplacian(DDD,DD)	
Surface Normal Gradient	New Skew Corrected 1
snGrad(D)	
nGrad(DD)	
Interpolation	Linear

Solver control parameters	
D and DD	Solver: PCG Preconditioner: FDIC Tolerance: 1 x 10^{-7} Relative Tolerance: 0.1
sigmaHyd	Solver: PCG Preconditioner: FDIC Tolerance: 1 x 10^{-7} Relative Tolerance: 0.1

One of the advantages of using OpenFOAM® is the possibility of parallelizing the calculation. Since there are no limits associated to licenses, parallelization is only constrained by the accessible hardware. For this simulation, the computational domain was divided into 8 physical processors (2.6 GHz and 2 Gb of RAM) using the Metis decomposition method and ran on a computational cluster using 1 node.

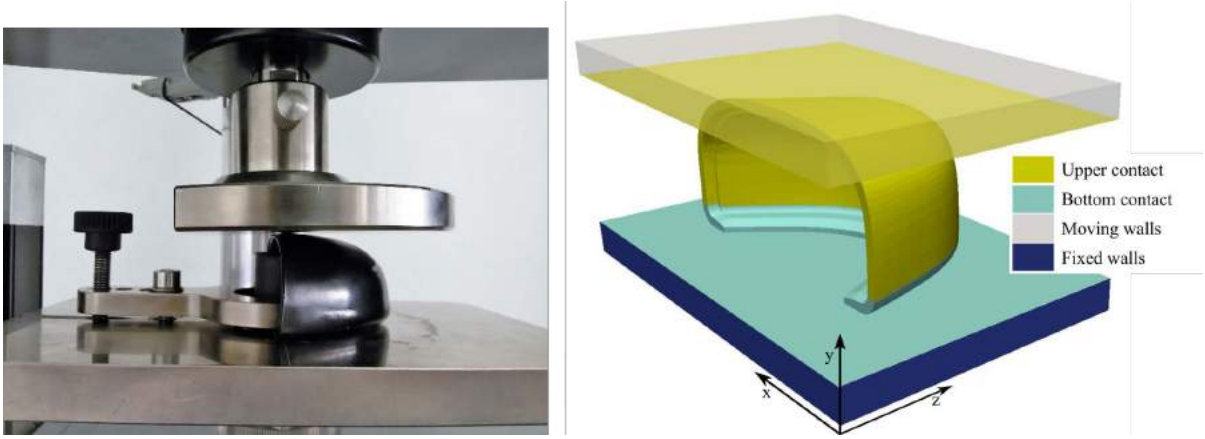

Figure 5.3: Compression test setup for the safety footwear toe cap - experimental configuration (left), computational model with the indication of the boundary patches (right).

5.2.2.4 Impact test

Toe caps used in safety footwear must withstand an impact loading of 200 J, the ISO standard gauges the impact behavior by measuring the height to which a standardized clay cylinder is compressed to. These values must be within a specified clearance range product validation, as shown in Table 5.2. For the geometry used in this work, the toe cap should withstand the impact event with a clearance larger than 22.0 mm. ISO 20344 [41] defines that the impact test must be performed with a 20 kg steel striker positioned at a predetermined height in order to achieve the required impact energy during the free fall. For simulation purposes this condition was met by modeling the impact striker geometry as defined in [41], placing it very close to the toe cap top surface, and adjusting its velocity to assure the required impact energy. After designing the striker and considering the density of steel at ambient temperature (7850 kg/m^3), the final weight was 1.547 kg and the resulting velocity set to 16.081 m/s to assure the impact energy requirement. The case setup and the simulated scenario are depicted in Figure 5.4.

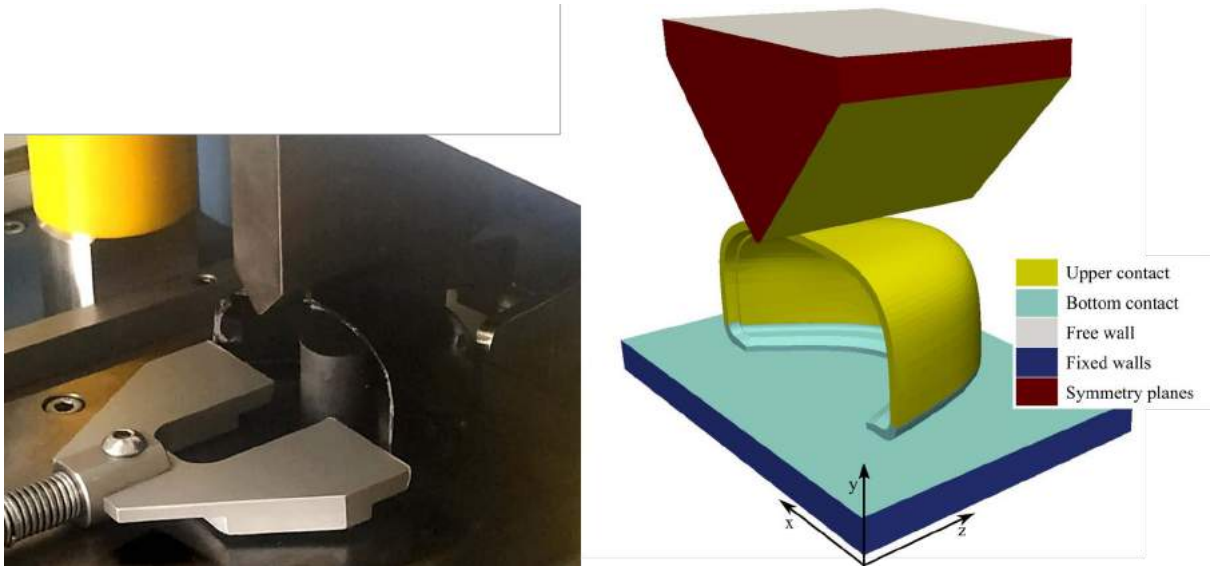

Figure 5.4: Impact test setup for the safety footwear toe cap: experimental configuration (left), computational model with the indication of the boundary patches (right).

In this simulation the inertial effects are of uttermost importance, the numerical schemes and solver controls were the same used on the compression simulation with the addition of a relaxation factor of 0.95 applied to the computational fields, a time step of 8 x10^{-6} s was chosen, and the simulation ran until the striker velocity along the *y*-axis reached value of 0 m/s. The boundary conditions for the components in the simulation were the following:

- the base plate was defined to have a fixed null displacement in all cartesian directions (Fixed walls patch in Figure 2-right);
- To constrain the striker to the *y*-direction, the faces with normal vector pointing into *x*- and *z*-direction were set as symmetry planes (Symmetry planes patches in Figure 2-right);
- The contact regions were simulated with the same method and values used for the compression structural analysis (Upper and Bottom contact patches in Figure 2- right).
- The initial velocity was imposed on the striker by using the OpenFOAM ® utility, *setFields.*

5.3 Results and Discussion

5.3.1 Toe cap material characterization

Figure 5.5 a) presents a FT-IR transmission spectra of the sample from the toe cap and a sample of PC grade INFINO SC-1220UR. The sample from the toe cap shows several intense peaks at 1776 cm^{-1}, 2968 cm^{-1} , 2873 cm^{-1}, and the doublet at 3060 and 3042 cm^{-1},where the first corresponds to the carbonyl stretching, and the others assigned to the aromatic bisphenol structure, these peaks are

characteristic of a polycarbonate (PC) thermoplastic [44]. To confirm, a sample of PC grade INFINO SC-1220UR from LOTTE Advanced Materials available in our laboratory was also analyzed. A sample was prepared under the same conditions as the previous and the FT-IR spectrum presented in Figure 5.5 a). All peaks are at the same position, which allows to assume that the toe cap material was mainly PC.

The DSC test was performed to check the glass transition (T_g) of both materials. Figure 5.5-b) demonstrates that both have a single T_g around 150 °C, which is coincident with known T_g values reported in literature for amorphous PC [45].

The surface morphology presented in Figure 5.5-c) does not show any particles in the polymer matrix, in fact, only one phase can be detected which is characteristic of a neat polymer. Through the previous analysis we can infer that the toe cap material is composed of neat PC without any reinforcements or other polymer added.

Figure 5.5-d) illustrates the engineering (black line) and the calculated homogeneous tensile curve (red line). One can observe that the material presents a strain softening due to yielding and neck formation at a strain encompassed between 0.05-0.175. Following this, a strain hardening effect can be observed due to the orientation of the macromolecules along the load direction until the fracture of the specimen. For the simulation, the material was defined as neoHookean with the nonlinear material behavior defined as starting after the end of the linear relationship between σ-ε on the homogeneous curve. The blue "*X*" symbols, Figure 5.5-d), are the points added to the constitutive model as a multi-linear isotropic hardening used on the computational studies. Conventionally, the yield stress is the transition point between elastic and plastic domain, but it is known that polymeric materials presents some plastic deformation for lower stresses. Therefore, for simulation purposes, yield stress point was chosen to be the value where stress-strain curve loses its initial linearity, around 35 MPa.

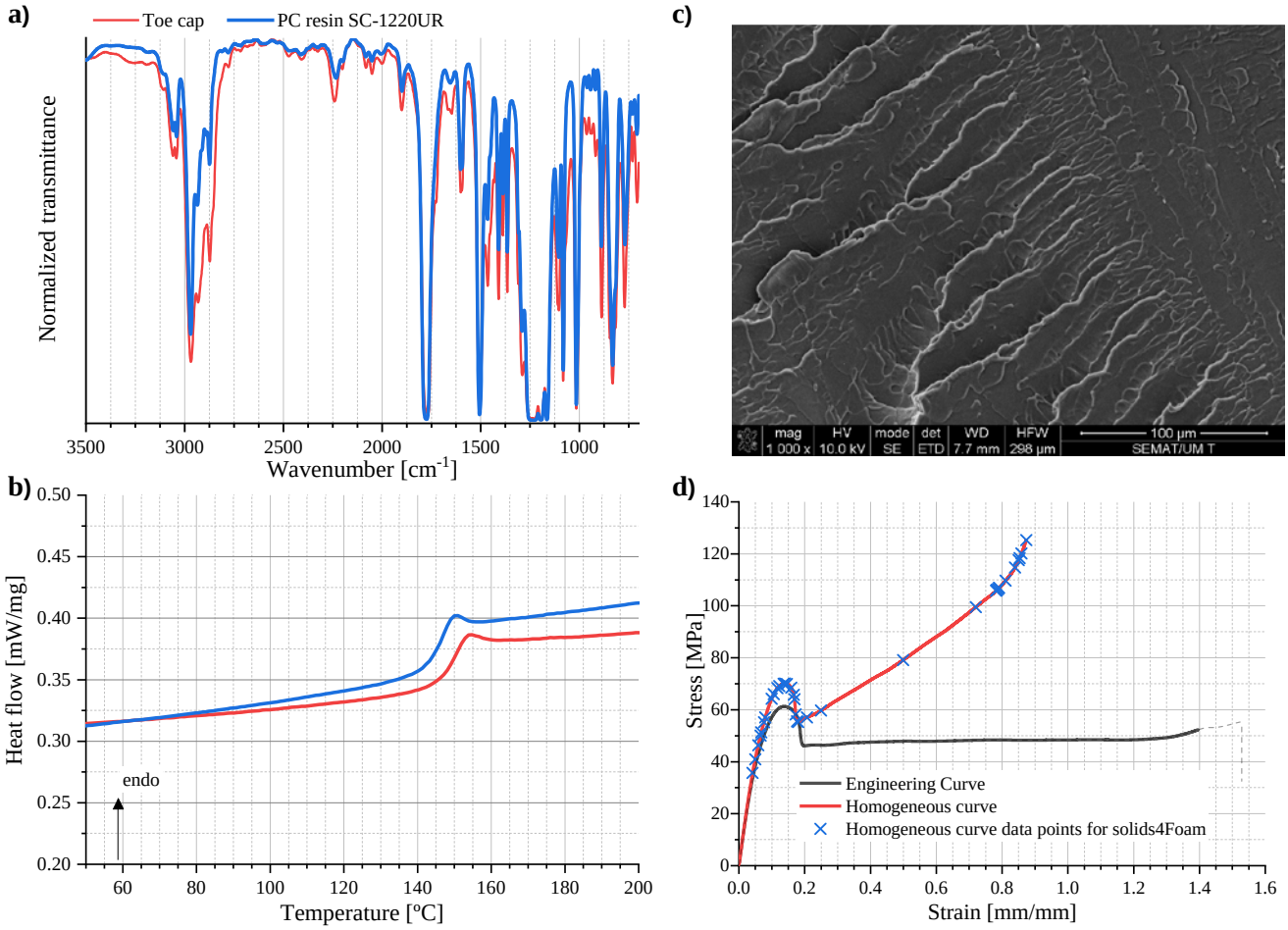

Figure 5.5: Toe cap material characterization: a) FT-IR spectrum, b) DSC thermogram, c) tensile test curve, and d) SEM image.

Additional data for the constitutive model employed on the simulations are presented in Table 5.5, together with the linear elastic model data considered for the plates and striker parts.

Table 5.5: Mechanical properties of the materials used for simulation.

	Toe cap	**Plate/striker**	
Elastic Modulus	2.5	200	*GPa*
Poisson ratio	0.3	0.3	-
Density	1 200	7 850	kg/m^3
1st nonlinear stress point	35.66	-	*MPa*

5.3.2 Mesh sensitivity analysis

The mesh quality information regarding the setup cases for impact and compression simulations using the M4 toe cap mesh are presented in Table 5.6 and Figure 5.6. As discussed in Subsection 2.2.4, the toe cap mesh is mainly comprised of hexahedral cells, where meshes M4 and M5 have the lowest average

non-orthogonality value. Additionally, due to its simple (cubic) geometry both plates (bottom and top) are comprised of just hexahedral cells. The local refinement of the striker mesh at the impact zone leads to a high level of non-orthogonality, with more than 15% of non-hexahedral cells. Despite the high non-orthogonality value for the metallic parts, simulation errors are not expected, since both the striker and plates have a substantial higher elastic modulus than the toe cap, which substantially reduces these parts deformation. Figure 5.7 displays the setup cases with the generated meshes for the M4 mesh.

Table 5.6: Quality parameters of the used meshes.

Mesh size and additional information				
Component		**Striker**	**M4**	**Plates**
Nr. of elements		8 168	670 640	8 208
Max aspect ratio		7.49	7.13	1.56
Non orthogonality	*Max*	62.81	57.11	2.16
	Average	18.42	3.15	0.56
Max skewness		0.63	1.86	0.04

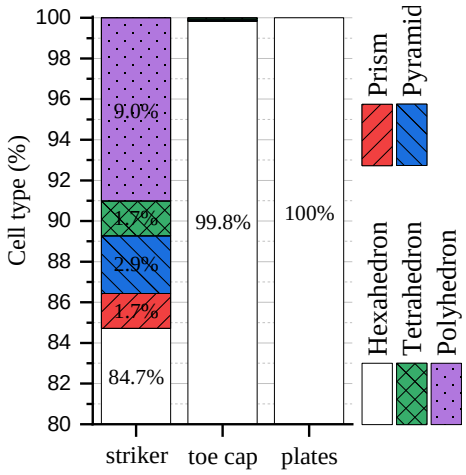

Figure 5.6: Percentage of cell type distribution.

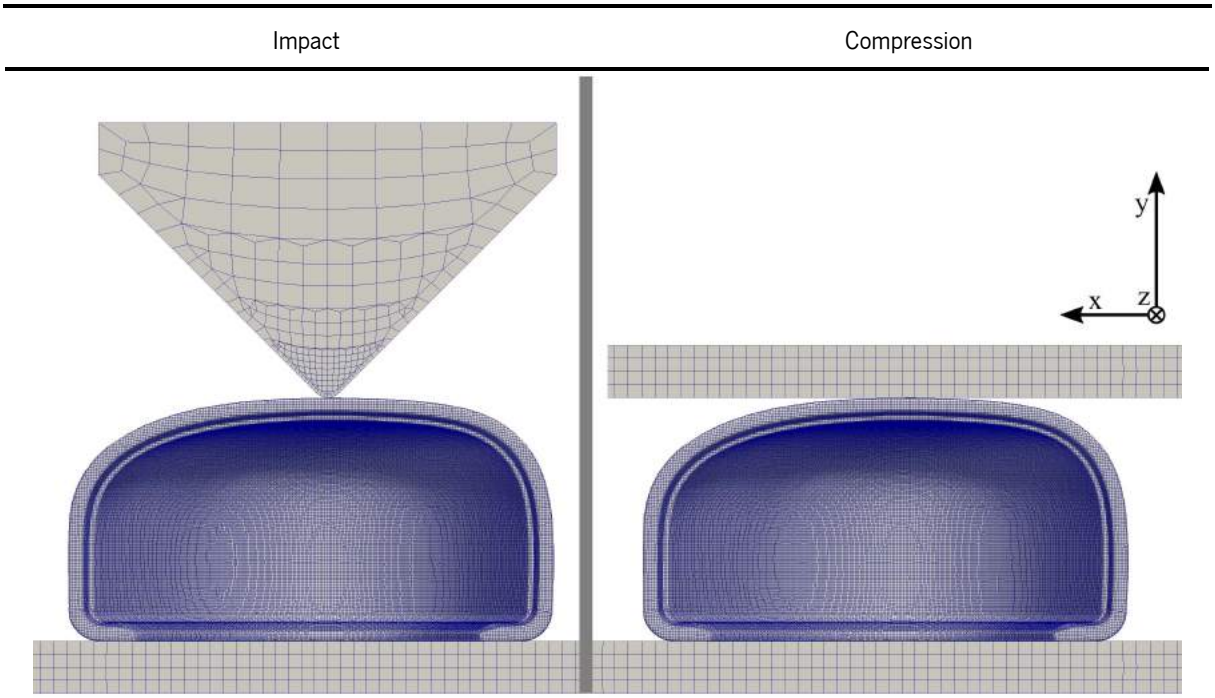

Figure 5.7: Back view of impact and the compression simulation cases using M4 mesh.

Figure 5.8 shows an overview of the mesh sensitivity study, an expected exponential increase in computational time with increasing number of cells is shown. While for the coarsest mesh (M1), it takes around one hour to complete each simulation, for the finer mesh (M5) almost two days are required. It is also visible that, until the simulation reaches the interest point, the compression simulation is a little bit more time consuming for the same hardware resources.

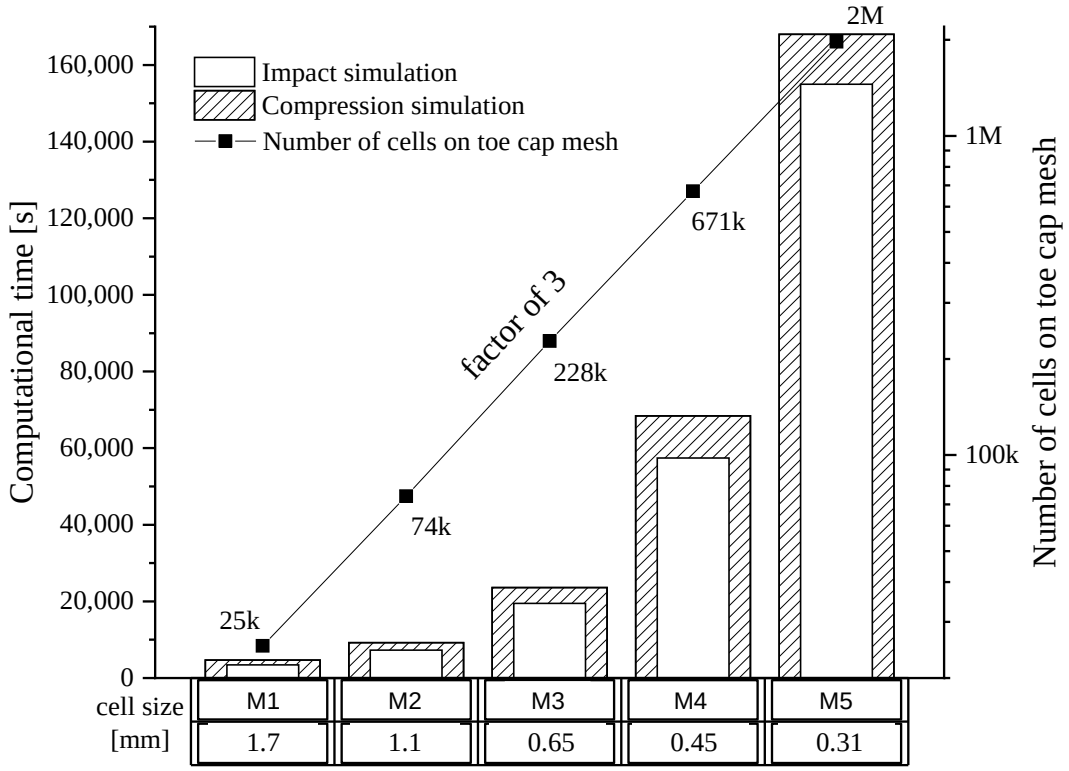

Figure 5.8: Details of the mesh study for both mechanical analyses.

To check for grid convergence, the overall domain variables distribution was averaged by the ratio between a property ϕ and the cell volume. The results for the compression and impact tests are presented in Figure 5.9. In both cases, the weighted (Equation (5.8) and (5.9)) von Mises Stress and displacement along the *y*-axis are plotted. As expected, when the mesh is refined the results converge. For coarse meshes it is also visible a huge variation in values for the initial time steps. In geometries with round edges, the mesh generation can create vertices that might be outside the geometry boundaries. In this case, for meshes M1 and M2 there were some cells from the bottom of the toe cap that intersect the bottom plate cells (Figure 5.10), resulting in induced stresses at the beginning of the simulation. The resultant induced stresses were in the elastic domain of the toe cap material. Therefore, no plastic deformation is induced due to cell crossover. From these results, it is also clear that the weighted values do not have a significant variation between meshes M4 and M5.

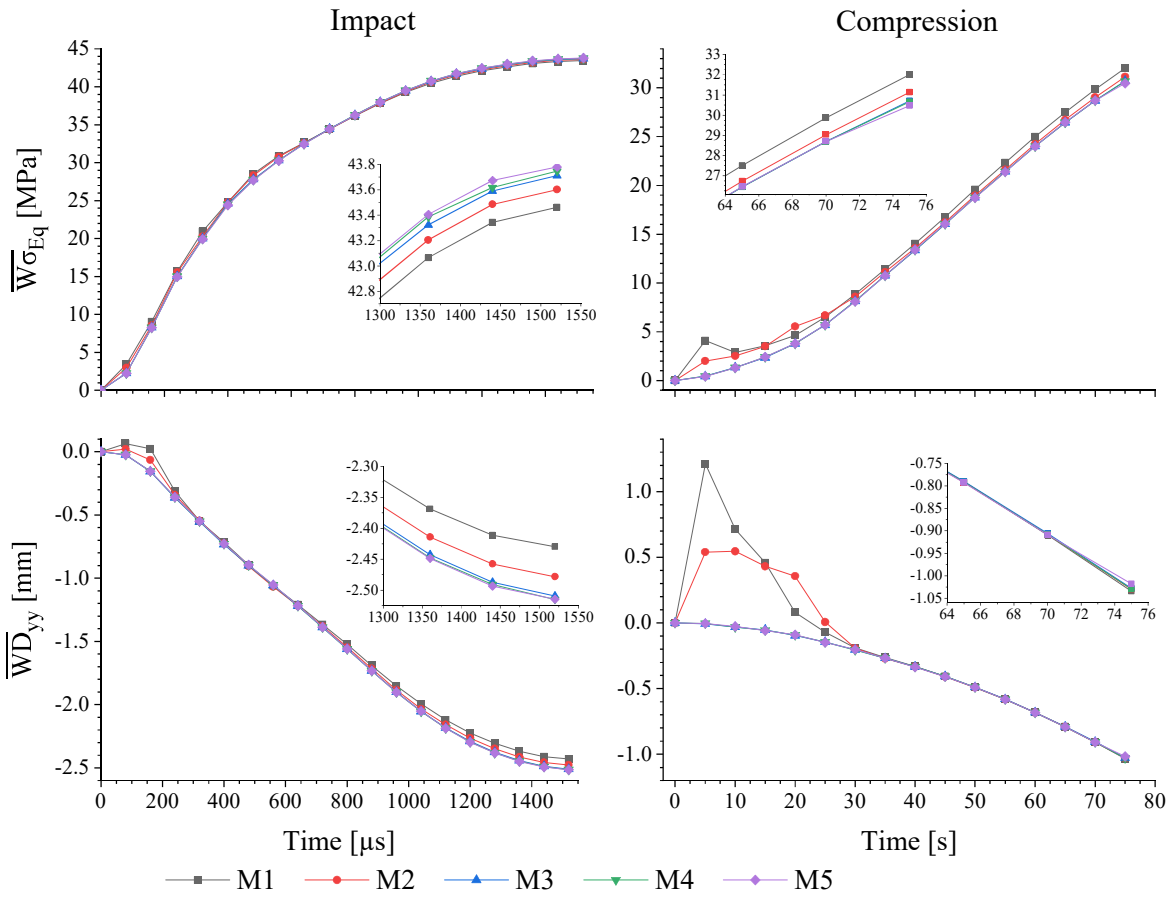

Figure 5.9: Analysis of the average von Mises stress and y-displacement evolutions as a function of mesh size for impact and compression simulations.

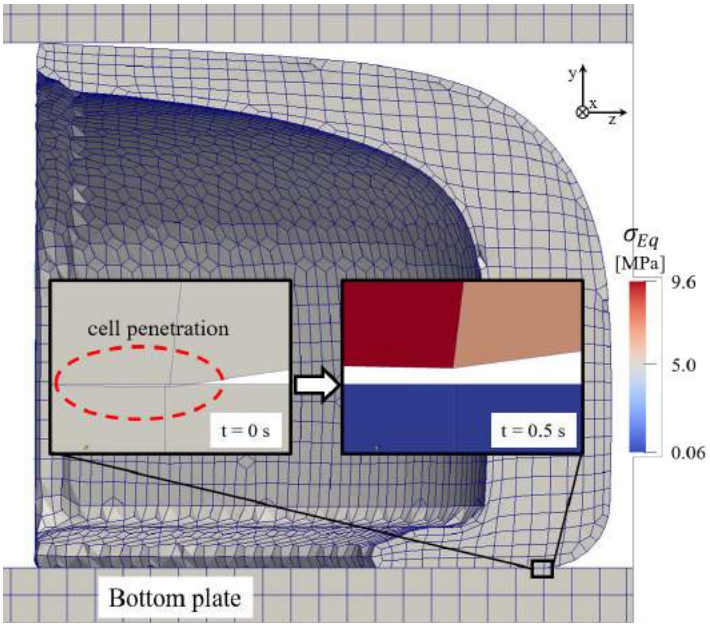

Figure 5.10: Induced stress due to cell penetration with M1 toe cap mesh in compression simulation for 0s and 0.5s.

The compressive simulation results of Δh_i and top plate displacement (Dy_{plate}) as a function of the top plate *y*-resultant force (Fy_{plate}) are depicted in Figure 5.11 The insert shows that Δh_i is a little bit more sensitive to mesh refinement than Dy_{plate}. Between the coarsest and finer meshes, a 0.2 mm difference of Δh_i value is reported.

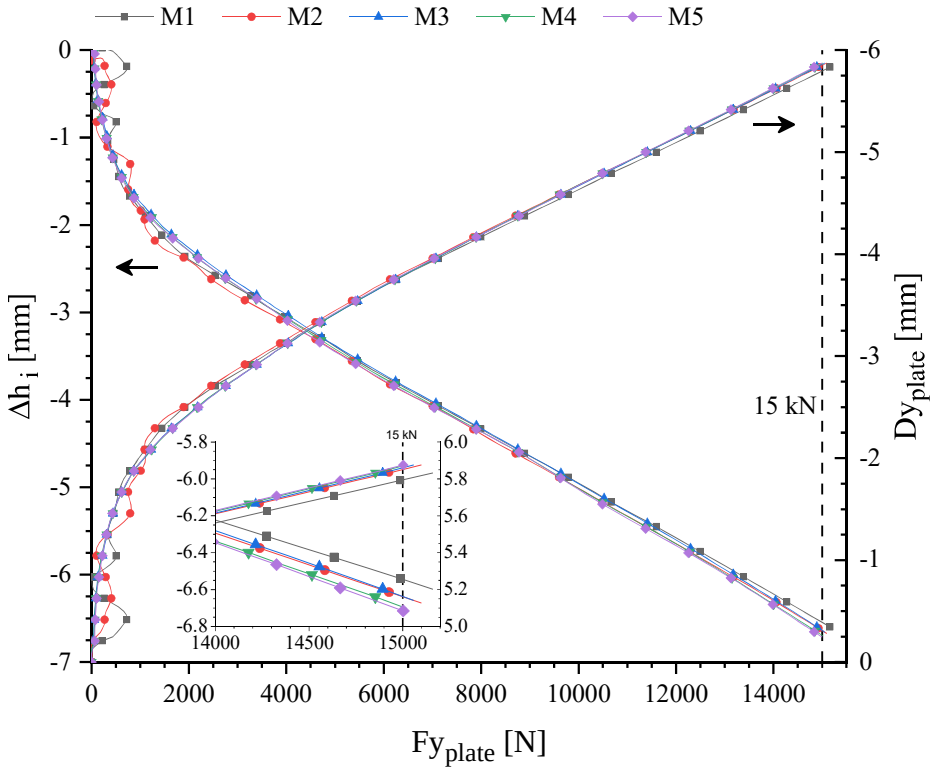

Figure 5.11: Inner toe cap y-variation and top plate y-displacement plot over plate y-force, for compression simulation.

Figure 5.12 exhibits the effect of mesh refinement over the inner toe cap wall displacement as a function of the striker velocity in the *y*-direction. There is a tendency for convergence in the maximum $\boldsymbol{\Delta h_i}$ value when the impact stops (Uy = 0 m/s). Moreover, for the M5 mesh predictions are similar to the ones of the M4 mesh. A difference of 0.13 mm is seen between the M1 and M5 for the final $\boldsymbol{\Delta h_i}$. This results also show that the cell crossover at the initial time steps just affect the compression simulation, on the impact counterpart there are no visible effects.

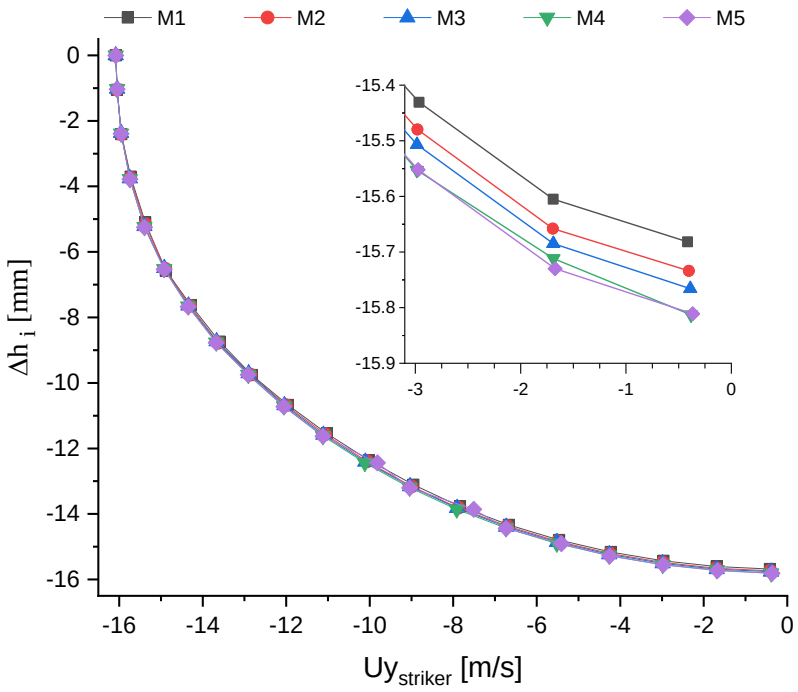

Figure 5.12: Inner toe cap y variation vs striker velocity, for impact simulation.

To quantify the practical impact of mesh refinement in the estimated clay height values, the graph shown in Figure 5.13 plots the h_{clay} value for impact (left axis) and compression (right axis) simulations as a function of the total toe cap cell number. For the impact simulation there is no value variation between M4 and M5, while for the compression simulation a lower value of variation is seen for the two most refined meshes.

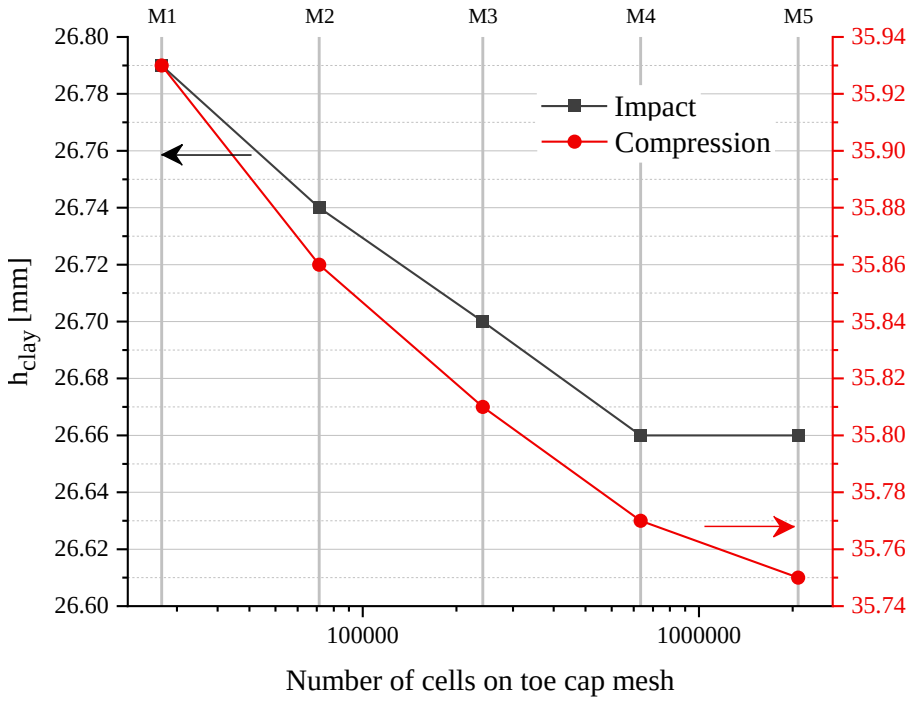

Figure 5.13: Clay height for impact (left) and compression (right) simulations as a function of number of cells on toe cap mesh.

Based on these results, for the remainder analysis it was decided to use mesh M4 since it is the one that presents the best balance between precision and computational cost.

5.3.3 Quasi-Static compression test

During the compression loading simulation, the force on the loading plate was monitored until reaching a value of 15 kN. Afterwards, Paraview v5.6.2 [46] was used for post-processing of the simulation data. The results from the normal stress field along the *y*-axis (σ_{yy}), von Mises Stress (σ_{Eq}), and *y*-displacement (D_{yy}) are depicted in Figure 5.14. Analysis of the contour plots indicates the existence of a complex state of stress within the part. A maximum compressive stress around 100 MPa is located at the top and bottom of the toe cap, at the contact regions between the toe cap and the top and bottom plates, whilst a tensile stress closely to 40 MPa is identified at the top front of the toe cap. The top back of the toe cap is where the negative *y*-displacement is higher, which contributes to the final value of h_{clay}, while the rest of the toe cap is pushed up as a result of the resultant force on the bottom plate. The von Mises Stress on the cross-section is displayed in Figure 5.14 exhibiting that the contact points are critical areas where the material will have a higher plastic deformation. Also, the inner material seems to be more protected from the resultant stresses than the outer material. Consequently, a higher degree of permanent deformation at the top region of the toe cap is expected, where σ_{Eq} is higher than 70 MPa. Also, σ_{yy} shows that the toe cap presents some bending, stretching at the toe cap surface (positive values), and compressing at the inner side (negative values).

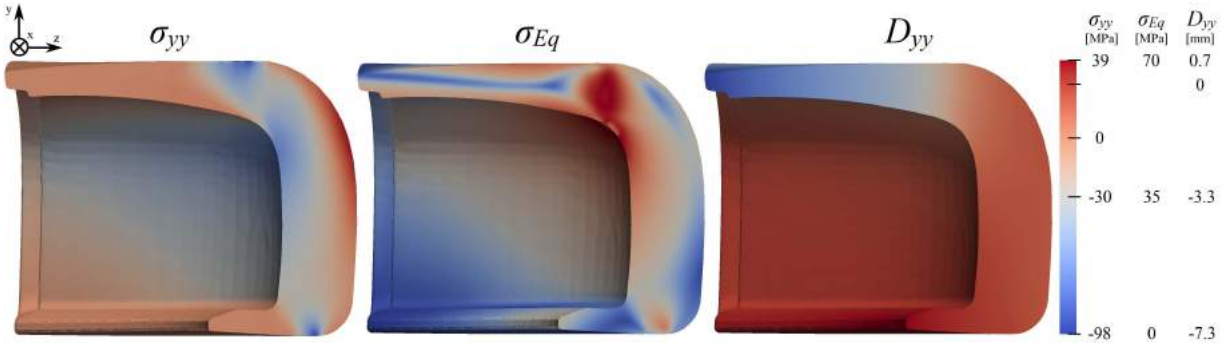

Figure 5.14: Normal stress (σ_{yy}), von Mises Stress (σ_{Eq}) and cell y-displacement (D_{yy}) distribution inside the toe cap for compressive simulation, when $Fy_{plate} = 15kN$.

For a better understanding of how the von Mises stresses evolves inside the toe cap, Figure 5.15 demonstrate the distribution on some slices at different critical regions. It is possible to notice that the thickest region (A) of the toe cap presents a uniform stress distribution along the thickness, whose

magnitude increases with the thickness reduction, which is typical of axial stress loading, in this case compressive. Progressing to the top, the stress distribution along the thickness changes to bending, with a stress magnitude higher near the surface (B) and a lower at the core region (C). These results indicate that in terms of compression the thicker region could be thinner, since the stress magnitude at the thickest region is always lower than the one induced by bending.

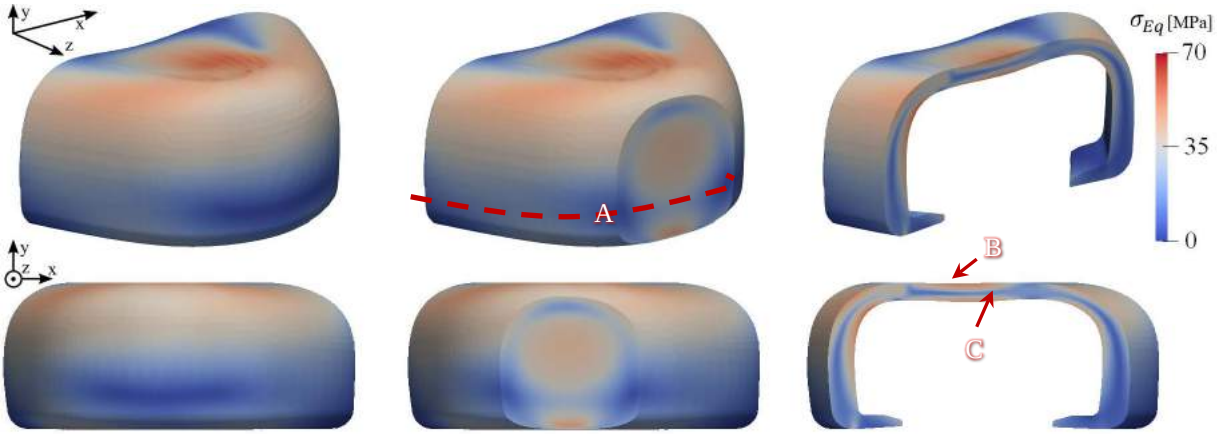

Figure 5.15: Von Mises stress distribution on compressive simulation computed with the M4 toe cap mesh.

A comparison between the Force – displacement ($F - d$) curve resulting from the compression test and the one obtained numerically is made in Figure 5.16. In the $F - d$ curve of the tested toe cap, the maximum loading displacement recorded at 15 kN was 6.12 mm and for the simulation curve was 5.79 mm. As it can be seen, the computational and experimental curves have a very good correlation, exhibiting a maximum error of 5.4%. The results showed grate simulation accurately on the behavior the toe cap.

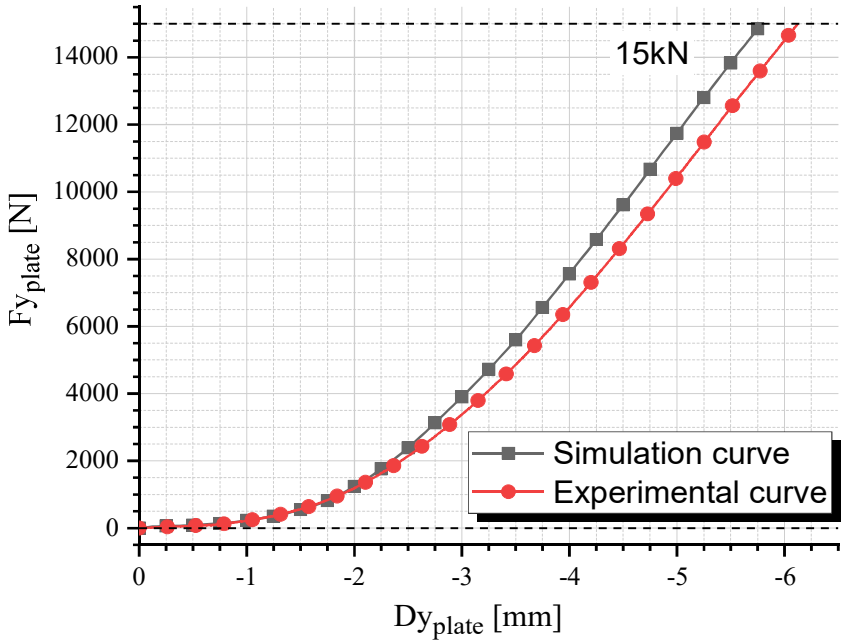

Figure 5.16: Comparison of the compression behavior of the tested and simulated toe cap.

5.3.4 Impact Tests

Figure 5.17 presents the stress and displacement fields along the *y*-axis obtained on the impact test, at the moment of maximum displacement of the striker (where it reaches a null velocity). The highest compressive stresses (negative σ_{yy}) are located at the bottom contact regions of the toe cap, between the striker and the bottom plate, with a maximum value of approximately 200 MPa. The remainder of the part is mainly under compression (negative σ_{yy}), with certain regions presenting tensile stress (red zones at Figure 5.17 for σ_{yy}) near the surface. It is possible to infer a complex state of stress along the cross section of the toe cap, where a strong compressive behavior is observed at the top of the toe cap and propagates in a wave-like form from the point of impact to the base support (Figure 5.17 σ_{Eq}). This behavior is more perceptible in Figure 5.18, where slices at some critical regions are shown with von Mises stress values to better identify yielding spots. From these, one can conclude that the impact zone (region where the striker hits the toe cap) is clearly the most severely affected region and will be the zone with the highest plastic deformation. When compared to the compression test simulation, the impact event is far more aggressive causing higher von Mises stresses distributed throughout toe cap, reaching a maximum value of 120 MPa at the impact region. From the images, it is possible to deduce that during the impact test that the main way for toe cap to accommodate the impact energy is through compression and bending. It is also visible a thin shell of higher stress values for the thinner parts of the toe cap.

Figure 5.19 displays the tension evolution in five points (inner, middle, outer, top and bottom) along the toe cap thickness and the height at the y-z plane, during simulation time, and the wave-like propagation visually observed in Figure 5.18, is shown in the chart with the oscillation of σ_{Eq} values. Bending is also detectable by the inner and outer points having negative and positive σ_{yy} values, respectively, while in the vertical direction all points have a negative value (compression). σ_{yy} and σ_{xx} are the stress components that contribute the most for the stress state of the toe cap, while the σ_{zz} contribution has a negligible effect at the analyzed zone.

Since no boundary was placed to restrict the movement of the base of the toe cap, due to the rebound that occurs in the test (which is also observed experimentally), it is possible to observe that the base presents a positive *y*-direction displacement of 1.7 mm (Figure 5.17 D_{yy}). The displacement of the top region of the toe cap is quite pronounced along the negative *y*-direction, as would be expected due to the nature of the test, reaching a maximum value of 17 mm. Based on the achieved results a large number of cells will be permanently deform due to the high stresses developed.

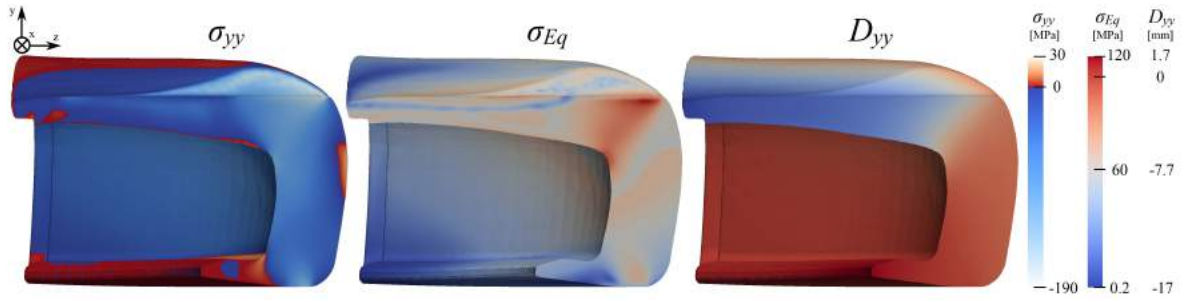

Figure 5.17: Normal stress (σ_{yy}), von Mises Stress (σ_{Eq}) and cell y-displacement (D_{yy}) distribution in the toe cap for the impact simulation, when $Uy_{striker} = 0m/s$.

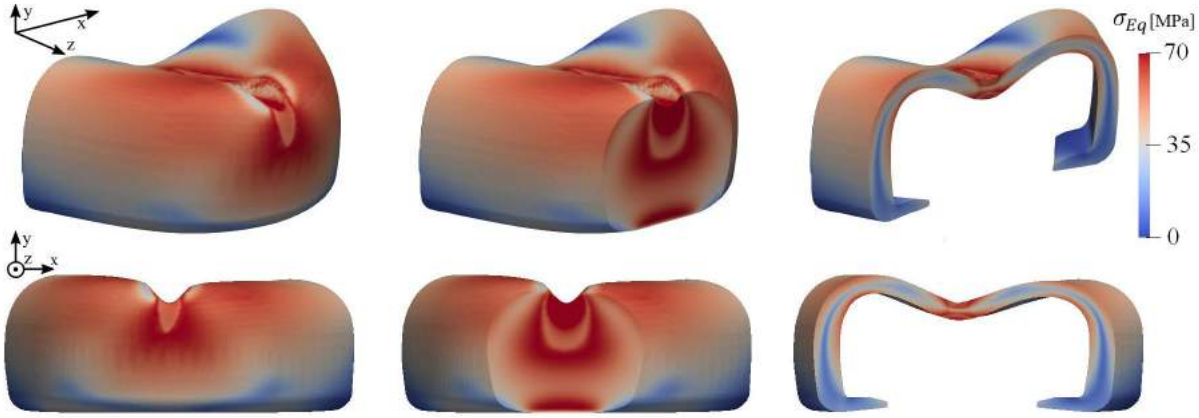

Figure 5.18: Von Mises stress distribution on impact simulation of M4 toe cap mesh.

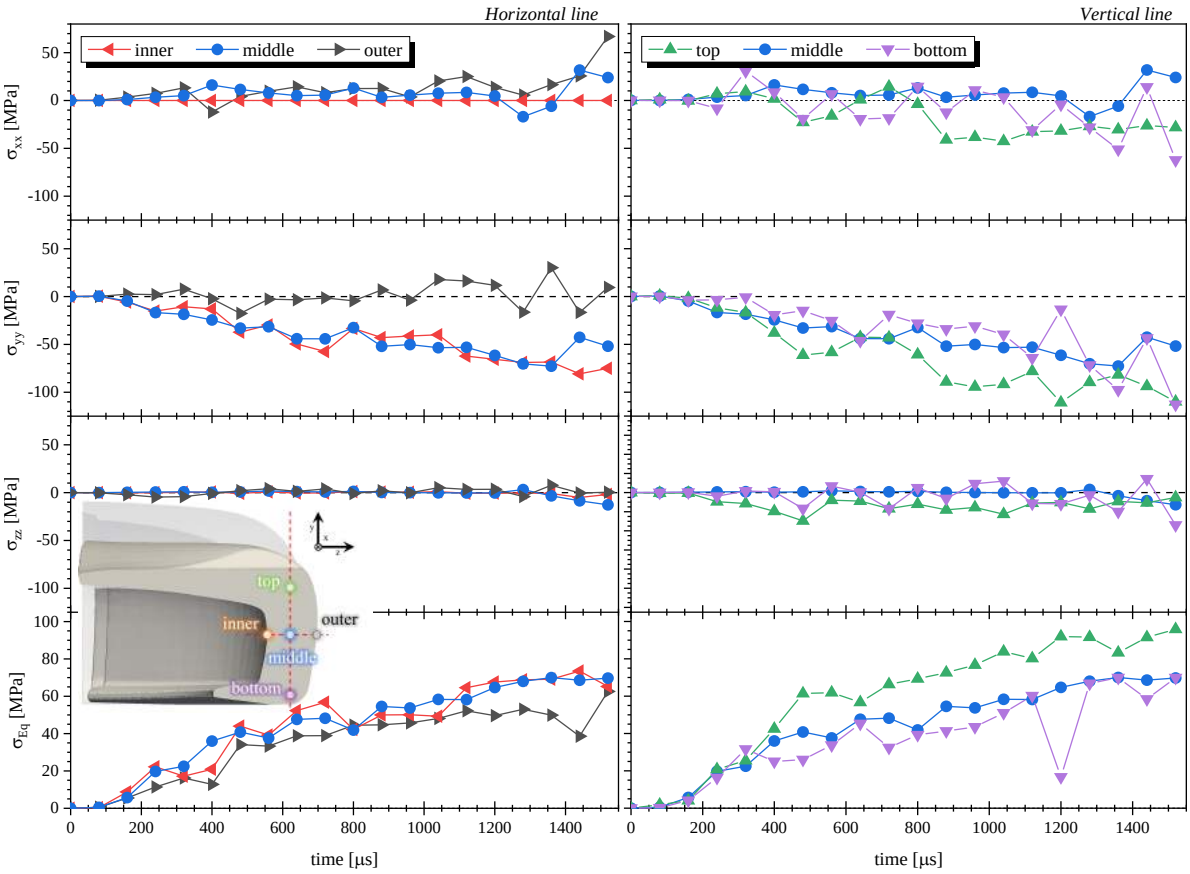

Figure 5.19: Stress at xx (σ_{xx}), yy (σ_{yy}) and zz (σ_{zz}) direction, and von Mises Stress (σ_{Eq}) evolution at the inner, middle and outer (left), top and bottom (right) of the toe cap horizontal and vertical y-z plane.

In Figure 5.20, a visibility filter based on σ_{Eq} was applied, to evidence: (a) the cells where plasticity criteria started to be applied (≥ 35 MPa) and (b) the critical cells which overpassed the yield stress (≥ 70 MPa). It is clear that the yielded region is located at the top of the toe cap, with the remaining areas just deforming in its quasi-elastic region (35 – 70 MPa). This is an indicator of the most critical zones that needs to be reinforced, and also the zones that are properly dimensioned. At the maximum strike displacement, where the velocity is null, there were a total of eleven cells where σ_{Eq} that had reached the stress at break given (125 MPa) for the characterized material, which could mean rupture. Since no rupture criterion was employed in this simulation, after reaching the maximum stress value defined in the constitutive model the solver clamps to the last stress value, imposing it for larger deformations.

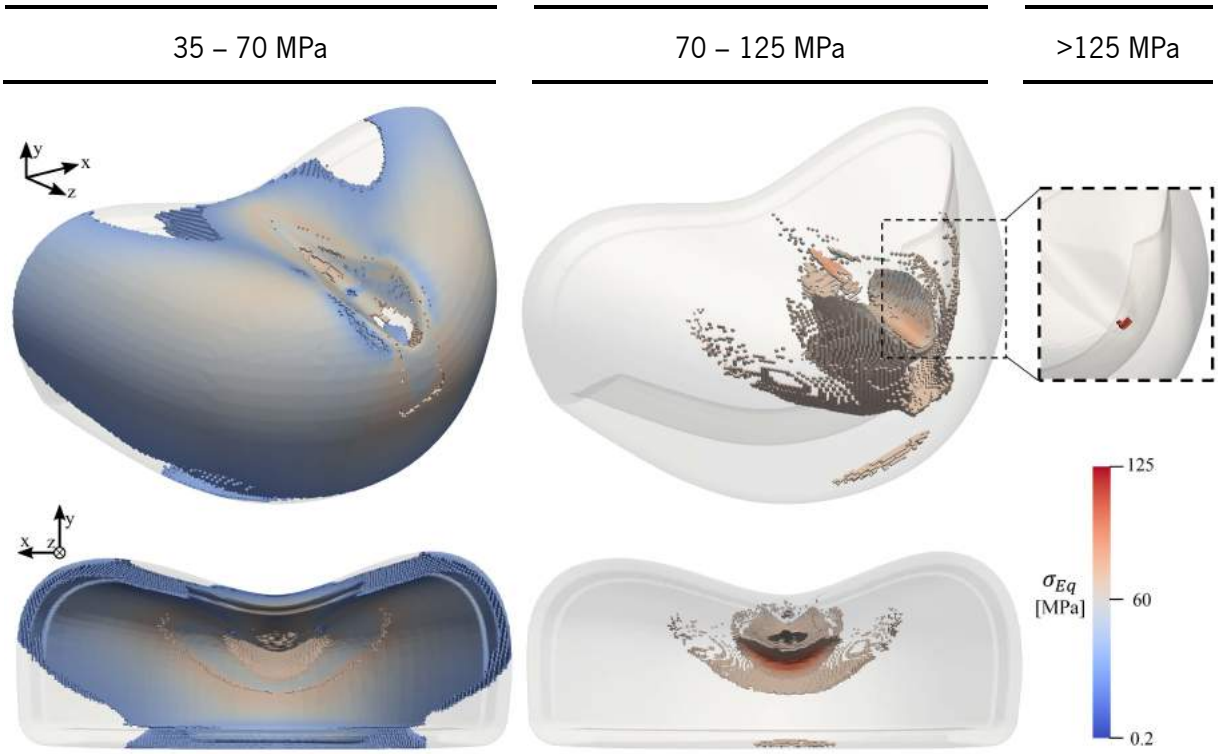

Figure 5.20: Von Misses stress distribution with applied threshold of left) 35 – 70 MPa, middle) 70 - 125 MPa, and right) cells with maximum stress, for the impact simulation.

Finally, on the impact simulation a value of 26.66 mm of toe cap clearance was obtained. Comparing with a value of 28.6 mm obtained experimentally, the simulation results have a difference of 6.8%, indicating also a very good agreement, for such a physical process like the impact test. This approach seems to validate the simulation tool with good agreement with experimental results, enabling its usage in the design of new toe cap solutions for safety footwear.

5.4 Conclusions

This work aimed at assessing the capability of using the *solids4Foam* toolbox, a free and open-source code developed in the framework of the OpenFOAM® computational library, to support the design of toe caps. For this purpose, a commercial toe cap supplied for this work had the material morphologically and mechanically characterized. These characterizations allowed to identify the material typology as a neat polycarbonate and describe the stress-strain behavior to be used as input in the numerical simulations of compression and impact tests used to validate the components in actual service conditions.

A mesh refinement study was carried out to obtain grid independent results, showing that the final deformation of the toe cap converges to a value by decreasing the cell size. The values obtained for compression and impact simulation revealed a very good agreement with the ones obtained in experimental testing, with an error of 5.5% and 6.8%, respectively. These simulations showed that the impact test is the most demanding (higher stress values) for this type of component. As such, it should be used for dimensioning. Critical zones were identified the contact point between the upper zone of the toe cap and the plate/striker. The stresses developed during the impact tests are very distinct from those in the compression tests, exhibiting a wave-like propagation form from the top to the bottom.

Given the obtained results, it was clearly demonstrated that *solids4Foam* toolbox can offer a significant support in future R&D in the footwear industry.

5.5 Acknowledgments

This work was funded by FEDER funds through the COMPETE 2020 Programme and National Funds through FCT - Portuguese Foundation for Science and Technology under the projects UIDB/05256/2020/UIDP/05256/2020 and FAMEST - Footwear, Advanced Materials, Equipment's and Software Technologies (POCI-01-0247-FEDER-024529). The authors also acknowledge the support of the computational clusters Search-ON2 (NORTE-07-0162-FEDER-000086) and Minho Advanced Computing Center (MACC).

5.6 References

[1] eurostat - Your key to European statistics, *Health and safety at work: Accidents at work by NACE Rev. 2 activity and part of body injured.* [Online]. Available: https://ec.europa.eu/eurostat/web/health/data/database (accessed: Feb. 24 2020).

[2] *Personal protective equipment - Safety footwear*, ISO 20345:2011(E), 2011.

[3] *Personal protective equipment - Protective footwear*, ISO 20346:2014, 2014.

[4] *Personal protective equipment - Occupational footwear*, ISO 20347:2012, 2012.

[5] J. Y. Kwon, J. T. Campbell, M. S. Myerson, and C. L. Jeng, "Effect of a Steel Toe Cap on Forefoot Injury Pattern in a Cadaveric Model," *Foot & Ankle International*, vol. 32, no. 4, pp. 443–447, 2011, doi: 10.3113/FAI.2011.0443.

[6] S. S. Chiou, N. Turner, J. Zwiener, D. L. Weaver, and W. E. Haskell, "Effect of boot weight and sole flexibility on gait and physiological responses of firefighters in stepping over obstacles," *Human factors*, vol. 54, no. 3, pp. 373–386, 2012, doi: 10.1177/0018720811433464.

[7] M. J. Abreu, P. Mendonça, C. S. Pereira, and A. Abreu, Eds., *Design of Innovative Protective Insoles for Safety Footwear*. International Conference on Engineering, Technology and Innovation (ICE/ITMC): IEEE, 2017.

[8] A. Goldcher and D. Acker, "Chaussures de sécurité, de protection et de travail," *EMC - Podologie*, vol. 1, no. 1, pp. 12–23, 2005, doi: 10.1016/j.emcpol.2005.01.002.

[9] S. Marr and S. Quine, "Shoe concerns and foot problems of wearers of safety footwear," *Occupational Medicine*, vol. 43, no. 2, pp. 73–77, 1993, doi: 10.1093/occmed/43.2.73.

[10] F. J. Wojcik, "Foot shield," U.S. Patent 1,626,489, Apr 26, 1927.

[11] A. W. Hauer, "Toe protector," U.S. Patent 2,002,662, May 28, 1935.

[12] A. R. Allard, "Safety shoe," U.S. Patent 2,079,237, May 4, 1937.

[13] W. J. Richards, "Safety show," U.S. Patent 2,836,909, Jun 3, 1958.

[14] S. L. Costa, J. P. Mendonça, and N. Peixinho, "Numerical Simulation of Quasi-Static Compression Behavior of the Toe Cap Component for Safety Footwear," *International Journal of Computer Theory and Engineering*, vol. 6, no. 4, pp. 285–291, 2014, doi: 10.7763/IJCTE.2014.V6.876.

[15] C. Frulla, "Protective toecap, particularly for safety shoes," WO 03/037127 A1, May 8, 2003.

[16] F. Fron, "Plastic foot protector," U.S. Patent 4,103,438, Aug 1, 1978.

[17] Y. Tanaka, M. Hirota, and T. Ishida, "Resin safety shoe toe cap," European Patent 1 380 221 A1, Jan 14, 2004.

[18] C. C. Yang, M. Duhovic, R. J. T. Lin, and D. Bhattacharyya, "Finite element modelling and analysis of composites toecaps," *IOP Conference Series: Materials Science and Engineering*, vol. 4, pp. 1–6, 2009, doi: 10.1088/1757-899X/4/1/012010.

[19] S. Erden and M. Ertekin, "Mechanical Evaluation of a Composite Overshoe Protector," *TEKSTIL VE KONFEKSIYON*, vol. 27, pp. 414–420, 2017.

[20] S. M. Lee, T. S. Lim, and D. G. Lee, "Damage tolerance of composite toecap," *Composite Structures*, vol. 67, no. 2, pp. 167–174, 2005, doi: 10.1016/j.compstruct.2004.09.009.

[21] J. L. Dykeman, "Protective toe cap for footwear," U.S. Patent 4,735,003, Apr 5, 1988.

[22] S. L. Costa, J. V. Silva, N. Peixinho, and J. P. Mendonça, "Advanced Metallic Solution for Toe Cap Component," *Proceedings of the ASME 2013 International Mechanical Engineering Congress and Exposition*, pp. 1–9, 2013.

[23] C.-C. Yang, "Development of High Strength Composite Toecaps Using LS-DYNA," Master of Engineering, Centre for Advanced Composite Materials / Department of Mechanical Engineering, The University of Auckland, New Zealand, 2010.

[24] V. Jankauskaitė, T. ŽUKAS, K. ŽUKIENĖ, and M. MALCIUS, "Low-weight Impact Behaviour of Carbon Fibre Reinforced Methyl Methacrylate Nanocomposites," *Materials Science*, vol. 21, no. 2, 2015, doi: 10.5755/j01.ms.21.2.7075.

[25] S. Costa, N. Peixinho, and J. P. Mendonça, "Design and Testing of a New Metallic Solution for Toecap Component on Safety Footwear," *Applied Mechanics and Materials*, 44-47, pp. 1460–1464, 2011, doi: 10.4028/www.scientific.net/AMM.44-47.1460.

[26] N. Peixinho, S. Costa, and J. Mendonça, "Impact Behaviour of Safety Shoe High Strength Steel Parts," *Engineering Transactions*, vol. 66, no. 2, pp. 175–185, 2018.

[27] S. L. Costa, J. P. Mendonça, and N. Peixinho, "Study on the impact behaviour of a new safety toe cap model made of ultra-high-strength steels," *Materials & Design*, vol. 91, pp. 143–154, 2016, doi: 10.1016/j.matdes.2015.11.082.

[28] R. C. F. Soares, "Simulação numérica do comportamento ao impacto de componentes para calçado de segurança," Dissertação de mestrado integrado em Engenharia Mecânica, Universidade do Minho, Departamento de Engenharia Mecânica, 2015.

[29] N. Dirksen, P. Deters, and K. Peikenkamp, "Numerical simulation of compression testing according to DIN EN 12568 of steel toe caps for safety footwear," *Footwear Science*, vol. 11, sup1, S182-S184, 2019, doi: 10.1080/19424280.2019.1606321.

[30] E. Schamp, P. Shaw, J. Vernon, E. Kantor, and H. Bertram, "In-depth assessment of the situation of the European footwear sector and prospects for its future development: Task 7 : synthesis report - Study," Revised Final Report, Risk & Policy Analysts Ltd, Publications Office of the European Union, 2012. Accessed: Feb. 21 2020. [Online]. Available: https://op.europa.eu/en/publication-detail/-/publication/daf8fc79-394f-4157-996d-829b63b916dc

[31] P. Cardiff *et al.,* "An open-source finite volume toolbox for solid mechanics and fluid-solid interaction simulations," *arXiv e-prints*, arXiv:1808.10736, 2018.

[32] *Foot and leg protectors - Requirements and test methods for toecaps and penetration resistant inserts*, EN 12568:2010, 2010.

[33] *Foam-extend.* Accessed: Oct. 21 2020. [Online]. Available: https://sourceforge.net/projects/foam-extend/

[34] Z. Tukovic, A. Karač, P. Cardiff, H. Jasak, and A. Ivankovic, "OpenFOAM Finite Volume Solver for Fluid-Solid Interaction," *Transactions of FAMENA XLII-3*, vol. 42, pp. 1–31, 2018, doi: 10.21278/TOF.42301.

[35] T. Tang, O. Hededal, and P. Cardiff, "On finite volume method implementation of poro-elasto-plasticity soil model," *Int. J. Numer. Anal. Meth. Geomech.*, vol. 39, no. 13, pp. 1410–1430, 2015, doi: 10.1002/nag.2361.

[36] P. Cardiff, Ž. Tuković, P. de Jaeger, M. Clancy, and A. Ivanković, "A Lagrangian cell-centred finite volume method for metal forming simulation," *Int. J. Numer. Meth. Engng*, vol. 109, no. 13, pp. 1777–1803, 2017, doi: 10.1002/nme.5345.

[37] *cfMesh.* Accessed: Oct. 23 2020. [Online]. Available: https://sourceforge.net/projects/cfmesh/

[38] B. Fabritius and G. Tabor, "Improving the quality of finite volume meshes through genetic optimisation," *Engineering with Computers*, vol. 32, no. 3, pp. 425–440, 2016, doi: 10.1007/s00366-015-0423-0.

[39] S. E. Norris, *Finite Volume Methods for Non-Orthogonal Meshes - Chapter 5, in "A Parallel Navier Stokes Solver for Natural Convection and Free Surface Flow"*. University of Sydney, 2000. [Online]. Available: http://hdl.handle.net/2123/376

[40] H. Jasak, "Error analysis and estimation for the finite volume method with applications to fluid flows," PhD dissertation, Imperial College London (University of London), London, England, 1996. Accessed: Oct. 28 2020. [Online]. Available: http://hdl.handle.net/10044/1/8335

[41] *Personal protective equipment - Test methods for footwear*, ISO 20344:2011 (E), 2011.

[42] J. H. Lee, G. H. Xu, and H. Liang, "Experimental and numerical analysis of friction and wear behavior of polycarbonate," *Wear*, vol. 251, no. 1, pp. 1541–1556, 2001, doi: 10.1016/S0043-1648(01)00788-8.

[43] PDL Staff, *Fatigue and Tribological Properties of Plastics and Elastomers*. Morris, NY: Plastics Design Library, 1995.

[44] M. Abbate, E. Martuscelli, P. Musto, G. Ragosta, and G. Scarinzi, "Toughening of a highly cross-linked epoxy resin by reactive blending with bisphenol A polycarbonate. I. FTIR spectroscopy," *J. Polym. Sci. B Polym. Phys.*, vol. 32, no. 3, pp. 395–408, 1994, doi: 10.1002/polb.1994.090320301.

[45] M. C. Delpech, F. M. Coutinho, and M. E. S. Habibe, "Bisphenol A-based polycarbonates: characterization of commercial samples," *Polymer Testing*, vol. 21, no. 2, pp. 155–161, 2002, doi: 10.1016/S0142-9418(01)00063-0.

[46] *ParaView - v5.6.2.* Accessed: Oct. 23 2020. [Online]. Available: https://www.paraview.org/

CHAPTER 6

6 CONCLUSIONS AND FUTURE WORK

The final chapter presents the general conclusions and major accomplishments of this PhD work. Afterwards, a subchapter is presented with suggestions of some topics to be explored in future works.

6.1 General Conclusions

The research presented in this thesis aimed to develop new materials systems (**Chapter 3 and 4**) for the manufacture of a key protection component used in safety footwear as well as to define a simulation methodology for assessment of toe cap's performance according to the tests defined in European standards (**Chapter 5**). Polycarbonate blend/(nano)composite systems were prepared by two melt processing routes: batch mixing and twin-screw extrusion. Material characterization was performed with tensile tests at quasi-static and high-speed conditions, impact tests, dynamic mechanical analysis, differential scanning calorimetry, infra-red spectroscopy, and optical and electronic microscopy. Also, the development of a numerical methodology was presented by using an open-source software, OpenFOAM®, able to simulate the impact and compression tests as defined by the European standards for safety footwear.

Chapter 3 describes the preparation of blends using three different PC grades with different MVR at a small scale. The results show that the mechanical properties of PC are highly affected by melt processing due to thermo-oxidative degradation, and the addition of elastomeric materials help to diminish this effect, increasing the toughness of the processed PC. Also, the addition of only 1wt.% of SEBS–*g*-MA has a huge positive effect on toughening and prevents the fracture tendency of the ABS-*g*MA phase in the PC/ABS-*g*MA blends during cryogenic fracture. Also, higher melt viscosity was essential to provide better dispersion of nanoclay. SEBS-*g*MA improved the compatibility between PC/nanoclay and PC/cotton fiber, but no improvement on the toughening was noticed. **Chapter 4** deals with the scale up production of PC systems blended with elastomeric materials prepared on a twin-screw extruder. Grafting maleic anhydride onto ABS improved the adhesion to PC matrix, lowering slightly the T_g value and providing better mechanical properties at higher ABS content. SEBS-*g*-MA and COPE proved to be more promising at improving the toughness of PC at tensile and impact events, with cavitation and crazing with fibrils as the main toughening mechanism, respectively. It was demonstrated that COPE reacts with PC by a transesterification mechanism and the performance of PC/COPE blends were not affected by the induced stress distribution of the injection molding process. According to the results of both chapters, blending PC with different elastomeric polymers allows the tailoring of PC properties, such as, increasing the elastic modulus in tensile solicitations when blended with ABS–*g*-MA, or enhancing the toughness when blended with SEBS–*g*-MA and COPE. Regarding thermomechanical properties, COPE has a substantial impact in decreasing T_g value and damping factor.

Chapter 5 presented a new methodology to support the design of toe caps, using the capabilities of an opensource computational library, OpenFOAM®. The mechanical characterization of the material retrieved from a commercial toe cap was used to feed the numerical simulations of compression and impact tests required to certificate this component for use in safety footwear. Both simulations revealed good agreement with the experimental results, with a maximum error of 5.5% and 6.8% for compression and for impact tests, respectively. This approach enables the study of the stress distribution and total deformation to be used as support for new design developments.

Overall, this work shows that blending PC with elastomeric materials might be a promising alternative way to improve the mechanical resistance of currently available thermoplastic toe caps. Combining these findings with the numerical methodology developed, it encourages the development of new toe caps designs with optimized dimensions, in order to be create more compact and appealing safety shoes. The licensed free character of OpenFOAM® enables the majority of small-medium sized Portuguese footwear companies to use this tool in their processes of R&D.

6.2 Future Work

The research present in this dissertation showed that is possible to tailor the mechanical properties of PC with potential for safety footwear applications. Also, the numerical methodology developed can aid the design of new toe cap components. Although, there is a lack of knowledge on the mechanical behavior of toe caps and the usage of different materials to increase their resistance. Taken in consideration the results and conclusions of the present research, some future work can be recommended:

- To investigate the effect of different wt.% of COPE and SEBS-*g*MA on PC mechanical response, and if the combination of both elastomers promotes a synergetic effect.
- To investigate new toughening systems for PC matrixes.
- To understand if the developed materials can improve the toe cap performance.
- To use the numerical methodology on the design of a new toe cap design.
- To explore alternative thermoplastic materials that better meet the European standard requirements.
- To explore new design concepts that provide better energy dissipation from compressive forces and impact events, and to provide permeability capabilities in order to provide better thermal comfort.